Numerical solution of the Hartree-Fock equation by multilevel tensor-structured methods

vorgelegt von Diplom-Physikerin
Venera Khoromskaia
Stadt Kazan, Russland

Von der Fakultät II - Mathematik und Naturwissenschaften
der Technischen Universität Berlin
zur Erlangung des akademisches Grades
Doktor der Naturwissenschaften
Dr.rer.nat.
genehmigte Dissertation

Promotionausschuss:

Vorsitzender: Prof. Dr. J. Blath

Berichter/Gutachter: Prof. Dr. Reinhold Schneider
Berichter/Gutachter: Prof. Dr. Dr. h.c. Wolfgang Hackbusch
zusätzlicher Gutachter: Prof. Dr. Eugene Tyrtyshnikov

Tag der mündlichen Prüfung: 10 December 2010

Berlin 2011
D 83

Acknowledgements

I would like to express my gratitude to Prof. Dr. Reinhold Schneider for supervising my PhD project, for fruitful discussions and his friendly encouragement during the work on this project. His interest and expertise in the research topics related to the Hartree-Fock equation and the density functional theory motivated much of the recent progress in the algebraic tensor methods in electronic structure calculations.

I would like to thank Prof. Dr. Dr. h.c. Wolfgang Hackbusch for valuable discussions and excellent conditions for performing research at the Max-Planck-Institute for Mathematics in the Sciences.

This work is done due to fruitful collaboration with Dr. Heinz-Jürgen Flad. I appreciate very much his kind encouragement and support of my work and always beneficial and stimulating discussions owing to his thorough expertise in modern quantum chemistry.

Professional assistance of PD DrSci. Boris Khoromskij in the research on tensor numerical methods helped me to make an active start in a new field. I acknowledge him for the statement of some research problems and for proofreading the manuscript.

I kindly acknowledge Prof. Eugene Tyrtyshnikov, Prof. Dr. Christian Lubich and Prof. Dr. Lars Grasedyck, for their interest to my work and for the opportunity to give talks at recent conferences and seminars on tensor methods.

I am very much appreciative to Prof. Dr. Ivan Gavrilyuk for his encouragement and interest to my work.

I would like to thank my colleagues at the Max-Planck-Institute in Leipzig, Dr. Ronald Kriemann, Dr. Jan Schneider, Dr. Kishore Kumar Naraparaju, Dr. Sambasiva Rao Chinnamsetty, Dr. Hongjun Luo, Dr. Thomas Blesgen, Dr. Lehel Banjai, Dipl.-Math. Konrad Kaltenbach, Dipl.-Math. Stephan Schwinger, Dipl.-Math. Florian Drechsler and colleagues at the TU Berlin, Prof. Dr. Harry Yserentant, Dipl.-Math. Fritz Krüger and Dipl.-Math. André Ushmaev for interesting discussions. I would like to acknowledge the colleagues from the Institute of Numerical Mathematics of the Russian Academy of Science in Moscow, Dr. Ivan Oseledets and Dr. Dmitrij Savostyanov for stimulating discussions.

I would like to thank Prof. Vikram Gavini (University of Michigan) for productive collaboration and for the data on electron density of large Aluminium clusters.

Kind assistance of the librarians Mrs. Britta Schneemann and Mrs. Katarzyna Baier was very helpful during my work. I would like to thank cordially the

secretaries at the Max-Planck-Institute and TU Berlin, Mrs. Valeria Hünniger and Mrs. Susan Kosub for their helpful technical support.

Numerische Lösung der Hartree-Fock-Gleichung mit mehrstufigen Tensor-strukturierten Verfahren

Venera Khoromskaia

Abstract der PhD Dissertation

Die genaue Lösung der Hartree-Fock-Gleichung (HFG), die ein nichtlineares Eigenwertproblem in $\mathbb{R}^3$ darstellt, ist infolge der nichtlokalen Intergraltransformationen und der scharfen Peaks in der Elektronendichte und den Molekülorbitalen eine herausfordernde numerische Aufgabe. Aufgrund der nichtlinearen Abhängigkeit der Hamilton-Matrix von den Eigenvektoren, ist das Problem nur iterativ lösbar. Die traditionelle Lösung der HFG basiert auf einer analytischen Berechnung der auftretenden Faltungsintegrale im $\mathbb{R}^3$ mit Hilfe von dem Problem angepassten Basen (so genannte Zwei-Elektron-Integrale). Die inhärenten Grenzen dieses Konzepts werden wegen der starken Abhängigkeit der numerischen Effizienz von der Größe und den Eigenschaften der analytisch separablen Basis sichtbar.

In dieser Dissertation wurden neue gitter-basierte mehrstufige Tensor-strukturierte Verfahren entwickelt und anhand der numerischen Lösung der HFG getestet. Diese Methoden beinhalten effiziente Algorithmen zur Darstellung diskretisierter Funktionen und Operatoren in $\mathbb{R}^3$ durch strukturierte Tensoren in den kanonischen, Tucker- und kombinierten Tensorformaten mit einer kontrollierbaren Genauigkeit sowie schnelle entsprechenden Operationen für multilineare Tensoren. Insbesondere wird die beschleunigte Mehrgitter-Rang-Reduktion des Tensors vorgestellt, die auf der reduzierten Singulärwertzerlegung höherer Ordnung basiert.

Der Kern der Anwendung dieser Verfahren für die Lösung der HFG ist die Verwendung strukturierter Tensoren zur genauen Berechnung der Elektronendichte und der nichtlinearen Hartree- und (nichtlokalen) Austauschoperatoren in $\mathbb{R}^3$, die in jedem Iterationsschritt auf einer Reihenfolge von $n \times n \times n$ kartesischen Gittern darstellt wurden. Somit wurden die entsprechenden sechs-dimensionalen Integrationen durch multilineare algebraische Operationen wie das Skalar- und Hadamardprodukt, die dreidimensionale Faltungstransformation und die Rang-Reduktion für Tensoren dritter Ordnung ersetzt, die annähernd mit $O(n)$-Komplexität implementiert wurden, wobei n die eindimensionale Gittergröße ist. Daher ist der wesentliche Vorteil unserer Tensor-strukturierten Verfahren, dass die gitterbasierte Berechnung von Integraloperatoren in $\mathbb{R}^d$, $d \geq 3$, lineare Komplexität in n hat. Man beachte, dass im Sinne der übliche Abschätzung mittels des Gittervolumens $N_{vol} = n^3$ die Operationen mit strukturierten Tensoren eine sublineare Komplexität haben, $O(N_{vol}^{1/3})$.

Das vorgestellte "'grey-box"'-Schema zur Lösung der HFG erfordert keine analytischen Vorberechnungen der Zwei-Elektron-Integrale. Weiterhin ist dieses

Schema sehr flexibel hinsichtlich der Wahl der gitter-orientierten Basisfunktionen.

Numerische Berechnungen am Beispiel des "all electron" Falls für H_2O, CH_4 und C_2H_6 und des Pseudopotentialfalls für CH_3OH and C_2H_5OH Moleküle zeigen die geforderte hohe Genauigkeit.

Die Tensor-strukturierten Verfahren können auch zur Lösung der Kohn-Sham-Gleichung angewandt werden, indem anstelle einer problem-unabhängigen Basis, wie die der ebenen Wellen oder einer großen Anzahl finiter Elemente im $\mathbb{R}^3$, eine geringe Anzahl problem-orientierter rang-strukturierter algebraischer Basisfunktionen verwendet werden, die auf einem Tensorgitter dargestellt sind.

Numerical solution of the Hartree-Fock equation by multilevel tensor-structured methods

Venera Khoromskaia

Abstract of PhD dissertation

An accurate solution of the Hartree-Fock equation, a nonlinear eigenvalue problem in $\mathbb{R}^3$, is a challenging numerical task due to the presence of nonlocal integral transforms and strong cusps in the electron density and molecular orbitals. In view of the nonlinear dependence of the Hamiltonian matrix on the eigenvectors, this problem can only be solved iteratively, by self-consistent field iterations. Traditionally, the solution of the Hartree-Fock equation is based on rigorous analytical precomputation of the arising convolution type integrals in $\mathbb{R}^3$ in the naturally separable basis (so-called two-electron integrals). Inherent limitations of this concept are evident because of the strong dependence of the numerical efficiency on the size and approximation quality of the problem adapted basis sets.

In this dissertation, novel grid-based multilevel tensor-structured methods are developed and tested by a numerical solution of the Hartree-Fock equation. These methods include efficient algorithms for the low-rank representation of discretized functions and operators in $\mathbb{R}^3$, in the canonical, Tucker and mixed tensor formats with a controllable accuracy, and fast procedures for the corresponding multilinear tensor operations. In particular, a novel multigrid accelerated tensor rank reduction method is introduced, based on the reduced higher order singular value decomposition.

The core of our approach to the solution of the Hartree-Fock equation is the accurate tensor-structured computation of the electron density and the nonlinear Hartree and the (nonlocal) exchange operators in $\mathbb{R}^3$, discretized on a sequence of $n \times n \times n$ Cartesian grids, at every step of nonlinear iterations. Hence, the corresponding six-dimensional integrations are replaced by multilinear algebra operations such as the scalar and Hadamard products, the 3D convolution transform, and the rank truncation for 3rd order tensors, which are implemented with an almost $O(n)$-complexity, where n is the univariate grid size. In this way, the basic advantage of our tensor-structured methods is the grid-based evaluation of integral operators in $\mathbb{R}^d$, $d \geq 3$, with linear complexity in n. Note that in terms of usual estimation by volume size $N_{vol} = n^3$, the tensor-structured operations are of sublinear complexity, $O(N_{vol}^{1/3})$.

The proposed "grey-box" scheme for the solution of the Hartree-Fock equation does not require analytical precomputation of two-electron integrals. Also, this scheme is very flexible to the choice of grid-based separable basis functions.

Numerical illustrations for all electron case of H_2O, CH_4, C_2H_6 and pseudopotential case of CH_3OH and C_2H_5OH molecules demonstrate the required high accuracy of calculations and an almost linear computational complexity in n.

The tensor-structured methods can be also applied to the solution of the Kohn-Sham equation, where instead of problem-independent bases like plane waves or a large number of finite elements in $\mathbb{R}^3$, one can use much smaller set of problem adapted basis functions specified on a tensor grid.

Contents

1 Introduction

All truths are easy to understand once they are discovered;
the point is to discover them.
Galileo Galilei

The classical Hartree-Fock equation is one of the basic *ab initio* models in electronic structure calculations. Accurate solution of the Hartree-Fock equation, a nonlinear eigenvalue problem (EVP) in $\mathbb{R}^3$, is a challenging numerical task due to the presence of nonlocal integral transforms and strong cusps in the electron density and molecular orbitals. This nonlinear problem of finding the eigenvectors (orbitals) of a molecular system is solved under the condition that also the electron correlation part of the Hamiltonian matrix, depending on orbitals is unknown. Therefore it is solved iteratively using the self-consistent field iteration (SCF) method.

Traditionally, the solution of the Hartree-Fock equation is based on the analytical precomputation of the arising convolution type integral transforms in $\mathbb{R}^3$ in the problem adapted naturally separable basis (the so-called two-electron integrals). This rigorous approach includes a number of efficient implementations which are widely used in computational quantum chemistry. The success of the analytical method stems from the big amount of precomputed physical information involved in the computational scheme including the problem adapted basis. Inherent limitations of this concept arise due to strong dependence of the numerical efficiency on the size and quality of the chosen GTO-type basis sets.

In this dissertation, novel multilevel grid-based tensor-structured methods are developed and tested by the *numerical solution of the Hartree-Fock equation*. These methods include efficient algorithms for the low-rank tensor representation of functions and operators in $\mathbb{R}^3$ in the canonical, Tucker and mixed tensor formats with a controllable accuracy, and fast procedures for the corresponding multilinear tensor operations. In particular, the novel multigrid accelerated tensor rank reduction method is proposed, based on the coarse-level reduced higher order singular value decomposition and selection of the most significant fibers. A beneficial feature of this method is the employment of the interpolated orthogonal basis functions on finer grid levels.

The core of our approach to the solution of the Hartree-Fock equation is the accurate tensor-structured computation of the electron density and the nonlin-

ear Hartree and nonlocal exchange operators in $\mathbb{R}^3$, discretized on $n \times n \times n$ Cartesian grids, at all steps of iterations on nonlinearity. Within the solution process, the six-dimensional integrations are replaced by the multilinear algebra operations such as the scalar and Hadamard products, the three-dimensional convolution transform, and rank truncation, which are implemented with almost $O(n)$-complexity. Efficient "formatted" separable tensor representations of functions and operators enable fast algebraic transforms with multidimensional data arrays. The grid-based solution of the Hartree-Fock equation also benefits from the multilevel arrangement of the conventional SCF iteration on a sequence of refined grids.

In this way, the basic advantage of the tensor-structured methods is the grid-based evaluation of the *integral operators in* $\mathbb{R}^d$, $d \geq 3$, with linear complexity in the *univariate grid size* n, see [61, 68]. Note that the commonly used notation as "linear in the problem size" for the problems with $d = 3$, often means linear complexity with respect to the volume size $\mathcal{N}_{vol} = n^3$. From this point of view the tensor-structured operations are of sublinear complexity, that is $O(\mathcal{N}_{vol}^{1/3})$.

High accuracy is achieved due to efficient rank optimization algorithms for 3rd order tensors, which enable computations over the 3D Cartesian grids with up to 10^{12} (16384^3) grid nodes, using MATLAB on a SUN station. In electronic structure calculations, this implies a fine resolution with the mesh size $h \approx 10^{-4}$ $\mathring{A}$, providing possibility for arbitrary space orientation of a molecule in the computational box (like in the analytical approaches).

The proposed "grey-box" scheme for the solution of the Hartree-Fock equation does not require an analytical precomputation of two-electron integrals. Also, this scheme is very flexible to the choice of grid-based separable basis functions. In the current implementation, the discretized Gaussians are used for the sake of convienient comparison of the intermediate results with the benchmark programs.

The tensor-structured methods can be also applied to the solution of the Kohn-Sham equation, where instead of problem-independent bases like plane waves or a large number of finite elements in $\mathbb{R}^3$, one can use much smaller set of problem adapted basis functions specified on a tensor grid.

1. Recent progress in multilinear algebra

Algebraic tensor algorithms for the low-rank approximation of multi-dimensional data have been originally developed for the problems of chemometrics and signal processing [112, 73, 97, 21, 22, 92], beginning from early papers [54, 55, 106, 17, 77, 18]. The higher order singular value decomposition (HOSVD) provides the generalization of the singular value decomposition (SVD) of matrices [37]. The

theoretical basis for the HOSVD, that is the principal ingredient for the best orthogonal Tucker[1] approximation of higher order tensors, have been introduced in [23, 24]. Comprehensive surveys on tensor decompositions with applications in computer science are presented in [74] and [97].

Recently, a number of numerical methods based on the separation of variables have been proposed for the multivariate problems of scientific computing [11, 41, 8, 94, 110, 111, 104, 102]. Extensive research on *tensor approximation* methods combined with the traditional numerical approaches, for example, wavelets, plane waves and sparse matrices have opened new perspectives for a feasible numerical solution of multi-dimensional problems arising in large scale electronic and molecular structure calculations [12, 27, 28, 40, 79, 13, 80, 93].

First results on theoretical approval of the extension of the basic tools in the traditional numerical linear algebra towards the modern multilinear algebra (MLA) have been presented in [104, 105, 47, 48]. Original works on the theory of sinc-approximation of the multivariate functions [35, 36] gave a significant impact for further development of the tensor methods in the problems of scientific computing. Validity and efficiency of the Tucker-type approximations and combined tensor formats to function related tensors in higher dimensions were demonstrated in [104, 47, 60, 59, 86]. In this way, the main principles and concepts of the representation of operators and functions in the rank-structured tensor formats as well as the methods of the algebraic tensor computations have been understood [34, 36, 46, 44, 45]. Nowadays this topic of research has attracted the interest of several groups from linear algebra, optimization theory and scientific computing communities, see [31, 19, 29, 85, 86, 87, 88] and [39, 7, 82, 66, 75, 71, 72].

Recent papers [60, 67, 68, 85, 70] demonstrated numerical efficiency of the Tucker and canonical tensor decompositions for a wide class of the problems of scientific computing in $\mathbb{R}^d$, ($d \geq 3$) which are not feasible for the treatment by conventional numerical methods due to their exponential complexity scaling in dimension d. These tensor approximations reduce dramatically the complexity of computations of the discretized multivariate operators and functions. Our main difficulties in establishing applicability of the tensor algorithms, earlier approved in chemometrics, for the treatment of higher order tensors in the problems of numerical analysis and scientific computing have been related to *accuracy* issues and to the challenge of *large spatial grids* required in the real-life applications.

This dissertation presents the tensor-structured methods[2] which were the topic of the author's work during 2006-2010, [67, 68, 69, 57, 70, 14]. Mostly, here

[1] Tucker-type decomposition, introduced by L. R. Tucker in 1966, see [106].

[2] We use the term "*tensor-structured methods*" as a common title to the numerical techniques based on the principles of algebraically separable rank-structured tensor representations.

the numerical applicability of the Tucker, canonical and mixed approximations is considered in application to the problems in $\mathbb{R}^3$, arising in electronic structure calculations. The numerical results described in these papers are based on the original algorithms implemented in MATLAB and tested in molecular computations.

[67] B. N. Khoromskij and V. Khoromskaia. *Low Rank Tucker-Type Tensor Approximation to Classical Potentials.*
Central European Journal of Mathematics v.5, N.3, 2007, pp.523-550,
(Preprint MPI MIS 105/2006).

[69] B. N. Khoromskij, V. Khoromskaia, S.R. Chinnamsetty, and H.-J. Flad. *Tensor Decomposition in Electronic Structure Calculations on 3D Cartesian Grids.* Journal of Comp. Physics, 228(2009), pp. 5749-5762, 2009,
(Preprint MPI MIS 65/2007).

[68] B. N. Khoromskij and V. Khoromskaia. *Multigrid Accelerated Tensor Approximation of Function Related Multi-dimensional Arrays.*
SIAM Journ. on Scient. Comp., vol. 31, No. 4, pp. 3002-3026, 2009,
(Preprint MPI MIS 40/2008).

[57] V. Khoromskaia. *Computation of the Hartree-Fock Exchange by the Tensor-structured Methods.*
Comp. Methods in Applied Math., Vol. 10(2010), No.2, pp.1-16.
(Preprint 25/2009, MPI MIS Leipzig, 2009).

[70] V. Khoromskaia, B. N. Khoromskij, and H.-J. Flad. *Numerical Solution of the Hartree-Fock Equation in the Multilevel Tensor-structured Format.*
SIAM Journ. on Scient. Comp., v.33, No.1, pp.45-65, 2011.
(Preprint 44/2009, MPI MIS Leipzig, 2009).

[58] V. Khoromskaia. *Multilevel Tucker Approximation of 3D Tensors.*
2010, in progress.

[14] T. Blesgen, V. Gavini and V. Khoromskaia. *Tensor Product Approximation of the Electron Density of Aluminium Clusters in OFDFT.*
Preprint 66/2009 MPI MIS Leipzig, 2009.

[52] E. Hayryan and V. Khoromskaia. *Low-rank Approximation of the Electrostatic Potentials of Proteins,* 2010, in progress.

The success of tensor methods based on the concept of the low-rank separable approximation of multivariate functions in $\mathbb{R}^d$, can be explained by their intrinsic nearly one-dimensional data structure organization. In fact, this allows us to relax the so-called "curse of dimensionality" inherent to traditional numerical methods. The idea of the tensor-structured techniques is based on the search and employment of normally hidden, well formatted data-sparse representations of large and highly redundant data arising in the conventional computer representation of physically relevant functions in $\mathbb{R}^d$. Hence, the rank-structured tensor methods enable an efficient "compact" approximation of multivariate functions and operators in $\mathbb{R}^d$, $d \geq 3$, represented on large tensor grids of size n^d.

Generally, the tensor methods employ the so-called orthogonal Tucker and canonical models. The main benefit of the orthogonal Tucker approximation is the robust construction of a problem adapted orthogonal basis that simultaneously resolves the peculiarities of the approximated data with an optimal tensor rank. In turn, the canonical tensor format is efficient in the bilinear rank-structured tensor operations.

2. Basic rank-structured formats

Section 2 of the dissertation begins with the description of the full format dth order tensors and respective bilinear operations necessary for the Tucker ALS minimization problem: the contracted product of a tensor with a matrix, matrix unfolding of tensors, and the scalar product. These operations can be understood as higher-order analogues of the standard linear algebra operations for vector-vector, matrix-vector and matrix-matrix calculations.

Discussion of the basic rank-structured tensor formats starts with the definitions of the rank-R canonical and the orthogonal rank-$(r_1, \ldots r_d)$ Tucker decompositions. The efficient tools for the rank-structured approximation of tensors cannot be derived via the straightforward extension of the algorithms of the classical numerical linear algebra, like the singular value decomposition (SVD). Instead, one arrives at the challenging nonlinear optimisation problems. As a starting point, we recall the seminal theorem in [21], asserting that the minimization problem of the Tucker approximation is equivalent to the dual maximization problem of finding vectors of the orthogonal mapping dominating subspaces, which provide the maximum norm of the Tucker core tensor over the product manifold of orthogonal matrices. We also remind the ALS iterative algorithm for the best Tucker tensor approximation (BTA) applied to the full format tensors (F2T) and the corresponding theorems on the *higher order singular value decomposition* (HOSVD) introduced in [21, 23, 24].

Our Theorem 2.14 on the canonical-to-Tucker decomposition (C2T) describes the reduced HOSVD (RHOSVD) applied to the canonical rank-R tensors and provides the error estimate with respect to the truncated SVD of the ℓ-mode side matrices, supplemented by the corresponding complexity bounds.

The general ALS based BTA algorithm [23] provides the complexity of the rank-$(r_1, \ldots, r_d)$ Tucker tensor decomposition of the order

$$W_{F2T} = O(n^{d+1}), \tag{1.1}$$

applied to full format target tensors, and, as we show in [67], it amounts to

$$W_{C2T} = O(Rn \min\{R, n\} + r^{d-1} n \min\{r^{d-1}, n\}), \tag{1.2}$$

operations with

$$r = \max_{\ell} r_\ell, \quad \ell = 1, \ldots, d,$$

in the case of canonical rank-R input tensors.

Next, we describe the two-level (mixed) tensor format, based on our Lemma 2.16, which proves that the Tucker-to-canonical (T2C) approximation applied to the Tucker decomposition of the full format tensor can be reduced to the canonical approximation of a small-size core tensor. We extensively use this format in electronic structure calculations, since the orthogonal Tucker decomposition is employed as the principle rank reduction technique, while the canonical representation is efficient in tensor product operations

In the numerical examples in Section 2, the standard collocation discretization has been used to represent the classical Newton potential, the Slater function, and the Yukawa and Helmholtz kernels on the $n \times n \times n$ 3D Cartesian grids. Figures demonstrate that for the function related tensors,
a) the error of the BTA decays *exponentially* in the Tucker rank,
b) the orthogonal vectors of the decomposition are of *special shapes* that resolve the peculiarities of a function,
c) the core tensor (coefficients of the orthogonal Tucker transform) is of *sparse character* (up to a certain threshold).
It is also shown, that for the tensors corresponding to the functions with periodic cells (with bumps or singularities) in $\mathbb{R}^d$, $d = 3$, the Tucker approximation error does not depend on a number of cells in a periodic structure. As examples, we consider cubic boxes with 27, 1000 and 4096 cells of the Slater function, see Figures 2.12 and 2.13. Next, the numerical examples on the electron densities ρ of some small organic molecules show that ρ can be efficiently approximated by the low-rank Tucker format.

In Section 2.4, the description of basic bilinear operations in the rank-structured tensor formats, including the scalar product, the Hadamard product and the convolution transform, is supplemented by the corresponding complexity estimates and bounds on required storage. This part is completed by the summary of tensor-structured operations in the canonical format which are of linear complexity scaling with respect to the parameters of the target tensors.

Note that for the full format tensors the complexity of basic bilinear operations vary from $W_{full} = O(n^d)$ to $W_{full} = O(n^{2d})$. Instead, for the canonical tensors with ranks R_1 and R_2, univariate grid size n and problem dimension d, the complexity of bilinear tensor operations is (up to $\log n$ factor)

$$W_{c\leftrightarrow c} = O(dnR_1R_2). \tag{1.3}$$

Notice that in evaluation of the Hartree potential, one should take into account large input ranks R_1 of the canonical tensor representing the electron density, see (4.4), (4.5), and possibly large n. Moreover, when using consequent tensor-to-tensor operations in the canonical format, tensor ranks are multiplied and hence increase enormously after several operations even with moderate initial ranks.

To reduce large canonical ranks with controllable accuracy, we introduce the C2T algorithm (see Algorithm C_BTA in subsection 2.2.3) with the consequent T2C transform. However, the conventional C2T and full-format-to-Tucker (F2T) algorithms are not computationally feasible in electronic structure calculations on large $n \times n \times n$ 3D Cartesian grids, since:

- For C2T case, the complexity is (see (1.2))

$$W_{C2T} = O(Rn \min\{R, n\} + dr^2 n \min\{r^2, n\}), \tag{1.4}$$

  i.e., polynomial (of degree at least 2) in r and either R or n. To resolve cusps due to core electrons in the electron density, both R and n are of the order 10^4.
  For simultaneously large R and n the SVD in the RHOSVD might be computationally unfeasible.

- For F2T case, the complexity of the general HOSVD based BTA algorithm,

$$W_{F2T} = O(n^4), \tag{1.5}$$

  restricts the size of the input tensor ($n^3 \sim 10^6$). Our goal is to reach the complexity (and resolution) corresponding to maximum size of the input tensor, $O(n^3)$, (that is, $n^3 \sim 10^8$).

3. Multigrid accelerated rank-structured approximation

To avoid above limitations, in Section 3 we introduce the *multigrid accelerated (MGA) Tucker decomposition*. The MGA tensor approximation method applied to discretised functions in $\mathbb{R}^3$, enables to relax the restrictions of the single grid Tucker model for large n and R.

The idea of the multilevel acceleration is based on the successive reiteration of the orthogonal Tucker tensor approximation on a sequence of nested refined grids. The HOSVD or RHOSVD are performed only on the coarsest grid representation of the target tensor, given in full or canonical formats, respectively. As the initial guess for the ALS iteration on finer grids, we apply the interpolated orthogonal side-matrices calculated on the coarser grid.

For the canonical target tensor, along with a good initial guess for the nonlinear ALS approximation, the MGA approach provides the transfer of the important data structure information from the coarse-to-fine grids, based on the introduced *maximum energy principle*. By using this principle, on the coarsest grid level, we extract the location of dominating columns – *most important fibers* of the ℓ-mode contracted unfolding matrices. This leads to the fast nonlinear ALS iteration on huge 3D Cartesian grids now performed over an almost minimal sufficient subset of directional fibers in the target tensor. Figures in Section 3 illustrate the mechanism of the choice of *most important fibers*.

The MGA technique exhibits the following benefits for the tensors related to functions in $\mathbb{R}^3$.

- For the rank-R canonical target tensors it is proved to have linear (instead of polynomial) scaling in all input parameters: n, R and the Tucker rank r,

  $$W_{C2T} = O(rRn),$$

  see Theorem 3.1 and Algorithm MG_C_BTA, in Section 3.2.

- For the full format tensors of size n^3, it leads to a nested F2T decomposition with the linear cost in the volume size of input data,

  $$W_{F2T} = O(n^3),$$

  (instead of $O(n^4)$-scaling for the standard Tucker approximation).

It should be emphasized that our technique is particularly efficient for the rank reduction of the canonical rank-R tensors with large R and n. Therefore, this algorithm is suitable for the functions with multiple strong singularities, such as electron densities of molecules in the Hartree-Fock equation.

Theorem 3.1 proves linear complexity with respect to the input parameters of a tensor, for the MGA BTA applied to the rank-R canonical input in $\mathbb{R}^3$.

Combination of C2T and T2C algorithms is successfully applied for rank reduction of the electron density of some organic molecules. This enables accurate computation of the Hartree potential (a convolution integral in $\mathbb{R}^3$), see Section 4, using remarkably fine $n \times n \times n$ grids with the size $n = 16384$ for all three dimensions. Figures present the comparison of elapsed times for the unigrid and multigrid schemes, as well as the cost for C2T transform in the MGA rank reduction of the electron density of H_2O and some small organic molecules. Parameters of the algorithms allow to choose the required accuracy level.

In the case of full format tensors, our multigrid accelerated Tucker algorithm enables usage of large grids up to $\mathcal{N}_{vol} = 512^3$. Computation time of this algorithm essentially outperforms the existing benchmark method based on the Newton-type scheme on the product Stiefel manifold [92]. The numerical examples on the MGA BTA of full size tensors related to functions in $\mathbb{R}^3$ include, for example, $\rho^{1/3}$, which is commonly used in the density functional theory. Notice that the alternative approach based on the cross approximation over the incomplete data set in 3D, is presented in [85]. Next, interesting numerical examples are presented on the Tucker approximation of the electron density of Aluminium clusters with 14, 172, and 365 atoms [14]. Along with the multicentered Slater functions considered in Section 2, they demonstrate that the rank of the Tucker representation of function related tensors with periodic multiple cusps (or bumps), is almost independent of the number of cells in the periodic structure. This indicates that the effective numerical complexity for solving larger grid-based quasi-periodic problems by the tensor-structured methods, for example in the orbital-free density functional theory [32, 33], may be expected to increase only linearly in the univariate grid size n.

4. The Hartree-Fock equation

In Section 4, the tensor-structured methods are applied for computation of the Galerkin matrices of the Coulomb and exchange operators in the Hartree-Fock model. The Hartree-Fock equation is the mean-field approximation of the electronic Schrödinger equation for computation of the ground state energy of many-electron systems. It is an eigenvalue problem (we consider a closed shell case) on finding N_{orb} lowest eigenvalues λ_i and respective pairwise L^2-orthogonal eigenfunctions (molecular orbitals) $\varphi_i : \mathbb{R}^3 \to \mathbb{R}$, $\varphi_i \in H^1(\mathbb{R}^3)$, from the equation

$$\mathcal{F}\varphi_i(x) = \lambda_i \varphi_i(x), \quad i = 1, ..., N_{orb}, \quad x \in \mathbb{R}^3, \tag{1.6}$$

with $\int_{\mathbb{R}^3} \varphi_i(x)\varphi_j(x)dx = \delta_{ij}$, $(i, j = 1, ..., N_{orb})$, where N_{orb} is the number of

electron pairs in a molecule. The *nonlinear* Fock operator $\mathcal{F}$ is given by

$$\mathcal{F} := -\frac{1}{2}\Delta + V_c + V_H - \mathcal{K}.$$

Here, an external nuclear potential V_c is defined by

$$V_c(x) = -\sum_{\nu=1}^{M} \frac{Z_\nu}{\|x - A_\nu\|}, \tag{1.7}$$

where M is the number of nuclei in a molecule, and Z_ν, $A_\nu \in \mathbb{R}^3$ denote the charge and spatial coordinates of the nuclei, respectively. The Hartree potential V_H determines the Coulomb interaction of every single electron with the field generated by all electrons of the system

$$V_H(x) := \int_{\mathbb{R}^3} \frac{\rho(y)}{\|x - y\|}\, dy, \quad x \in \mathbb{R}^3, \tag{1.8}$$

which corresponds to the convolution of the Coulomb potential with the electron density

$$\rho(y) = 2\sum_{i=1}^{N_{orb}} (\varphi_i(y))^2. \tag{1.9}$$

Calculation of the exchange Galerkin matrix in the Hartree-Fock equation is a challenging problem due to the *nonlocal* character of the exchange operator $\mathcal{K}$

$$(\mathcal{K}\varphi)(x) := \frac{1}{2}\int_{\mathbb{R}^3} \frac{\tau(x,y)}{\|x - y\|}\, \varphi(y) dy, \tag{1.10}$$

with the density matrix

$$\tau(x,y) = 2\sum_{i=1}^{N_{orb}} \varphi_i(x)\varphi_i(y).$$

Traditionally the Hartree and exchange potentials are computed by the analytical evaluation of two-electron integrals, using the separable Gaussian basis functions, or Gaussian type orbitals (GTOs), to represent the eigenfunctions,

$$\varphi_i(x) = \sum_{k=1}^{R_0} c_{i,k} g_k(x), \quad x = (x_1, x_2, x_3) \in \mathbb{R}^3. \tag{1.11}$$

Here basis functions g_k, $k = 1, \ldots, R_0$, are naturally separable Cartesian Gaussians represented in the rank-1 canonical tensor product form,

$$g_k(x) = g_k^{(1)}(x_1)\, g_k^{(2)}(x_2)\, g_k^{(3)}(x_3),$$

with 1, 2, 3 designating space dimensions. When using the traditional analytical-based approaches, computation of the Hartree and exchange potentials represents a major bottleneck for the numerical solution of the Hartree-Fock and Kohn-Sham equations.

5. Computation of the Hartree and exchange potentials

For grid-based agglomerated computation of (1.8) and the integral operator (1.10) on 3D Cartesian grids, we introduce an appropriate fixed computational box and apply a collocation discretization scheme for all involved multivariate functions and a projection (Galerkin) scheme for representation of operators. In particular, the collocation/projection scheme is used for representation of the Newton kernel in the discrete tensor-product convolution. The canonical rank-R_N representation of a tensor representing the projected Newton potential is computed using the sinc-quadratures in [10].

The fast tensor product convolution of the multivariate functions in $\mathbb{R}^d$ developed in [61] with complexity $O(dn \log n)$, is applied in the computation of the integral (1.8) and the integral operator (1.10). When applied in 3D case, it considerably outperforms the benchmark convolution based on the 3D Fast Fourier Transform (FFT) having the cost $O(n^3 \log n)$. Table 4.1 illustrates *linear* dependence of the CPU times for convolution (and preliminary rank reduction for the electron density) versus the univariate grid size n in the computation examples of V_H for H_2O, C_2H_6 and CH_4 molecules.

Accuracy of the tensor-structured computations on a fixed grid is $O(h^2)$, where $h = O(n^{-1})$ is the mesh-size. We achieve $O(h^3)$ accuracy in evaluation of the convolution integral operators by using the Richardson extrapolation on a couple of consequent equidistant grids. Notice that the tensor convolution on non-equidistant grids was described in [42, 43].

The size of the computational box for the considered molecules is in the range of $14 \div 20$ $\overset{\circ}{A}$. Our tensor-structured methods enable usage of large $n \times n \times n$ 3D Cartesian grids, and hence fine mesh sizes

$$h \approx 10^{-2} \overset{\circ}{A} \qquad \text{for } n = 1024,$$
$$h \approx 10^{-4} \overset{\circ}{A} \qquad \text{for } n = 16384.$$

In the calculation of the Hartree potential V_H, the electron density ρ is a square of a sum of Gaussians, see (1.9), (1.11), therefore it is expressed in terms of a larger number of Gaussians $R_{\rho_0} = \frac{R_0(R_0+1)}{2}$. As a result, the convolution operator with the rank R_N Newton kernel, applies to the canonical tensor for ρ, with large ranks $R_{\rho_0} \sim 10^4$. Moreover, the results of convolution with the ranks $R_C =$

$R_{\rho_0} R_N$, should be used further to compute the Galerkin projection of the Hartree potential in the Gaussian basis set, which can yield the total complexity of the order $O(R_{\rho_0}^2 R_N n \log n)$, to compute the Coulomb matrix in the Fock operator.

Hence, a rank reduction for the electron density is required, to enable evaluation of the Hartree potential V_H for both large R_{ρ_0} and n. We apply the multigrid accelerated C2T and T2C algorithms introduced in Sections 2, 3, to decrease R_{ρ_0} to much smaller value,

$$R_\rho \ll R_{\rho_0}, \quad \text{with } R_\rho \le r^2,$$

where r is the Tucker rank (usually, we use equal ranks, $r = r_\ell$, $\ell = 1, 2, 3$).

In this way, we have linear scaling (up to lower order terms) in all parameters of the input canonical tensors, at every step of evaluation of the Coulomb matrix,

- Rank reduction scheme for the electron density. Complexity of C2T, $W_{C\to T} = O(rpR_{\rho_0} n)$, where $p \le r$ is the multigrid parameter. T2C complexity, $W_{T\to C} = O(R_\rho n)$, where $R_\rho \le r^2$.

- The Hartree potential V_H, is computed by the "agglomerated" tensor-product convolution, $W_{C*C} = O(R_\rho R_N n \log n)$.

- Tensor scalar product $W_{CC} = O(nR_{\rho_0} R_\rho R_N)$ to compute Coulomb matrix entries.

In the case of large molecules, the MGA rank reduction can be applied to the result of convolution, to reduce the rank of the tensor before computation of the Coulomb matrix entries.

Figures in Section 4 show linear scaling of the CPU times with respect to both R_{ρ_0}, and n, in the rank reduction and the tensor-product convolution. Figures illustrate the absolute error in calculations of V_H and the Coulomb matrix for CH_4, C_2H_6 and H_2O. Accuracy up to 10^{-6} hartree (absolute error) even for cusp areas in ρ is achieved due to huge $n \times n \times n$ Cartesian grids with n up to 10^4.

Next, in Section 4, the tensor-structured evaluation of the nonlocal (integral) exchange operator $\mathcal{K}$ in the Hartree-Fock equation is considered. Note that computation of the Hartree-Fock exchange leads to integration in six dimensions, see (4.17). Mostly, analytical evaluation of these six-dimensional integrals was considered in the literature (two-electron integrals), and many efforts have been devoted to solution of this problem (see [109, 78] and references therein).

We introduce the "agglomerated" scheme for the computation of the exchange matrix entries by "dividing" the integration into the following steps.

- Tensor-product convolutions of the Newton kernel with the rank-R_0 canonical tensors representing the Hadamard product of the corresponding molecular orbital with every Gaussian.

- Computation of the Galerkin projection of the convolution result with respect to the GTO basis set (by tensor scalar products), to obtain contribution to the entries of the exchange matrix from the corresponding orbital.

- Summation over all N_{orb} orbitals completes the matrix computation.

This tensor-product algorithm for evaluation of (4.16) has the complexity

$$W = O(n_{eff}\, R_0^4\, N_{orb}),$$

where N_{orb} is the number of orbitals in a molecule, $n_{eff} \ll n$ is the "effective" univariate grid size, and R_0 is the number of Galerkin basis functions. To reduce the R_0-asymptotics to $O(R_0^3)$, we apply the C2T algorithm to reduce the ranks after the convolution step.

Note, that in the traditional *ab initio* electronic structure calculations, many years have been devoted to the development of the rigorous schemes for the analytical evaluation of the two-electron integrals inherent to this approach, which yielded state-of-the-art packages like GAUSSIAN, Abinit and MOLPRO [5, 108]. In analytical-based programs, elaborated by large scientific groups, essential parts of calculations use precomputed parameters and additional "non-zero" initial approximations for accelerating the iterative solution of the eigenvalue problem (1.6).

6. Description of the Hartree-Fock solver

In Section 5 of this dissertation we introduce the *novel multilevel scheme* for the numerical solution of the Hartree-Fock equation (1.6) using the *grid-based tensor-structured methods* to represent basic operators as described in previous sections. The new concept for the numerical solution of the Hartree-Fock equation is a "grey box" scheme based on a moderate number of the problem-adapted Galerkin basis functions $\{\overline{g}_k\}$ *represented on 3D Cartesian grid*, which are used as "global elements" with the low separation rank[3].

We solve the nonlinear EVP obtained by the Galerkin-type discretisation of the Hartree-Fock equation (1.6), with respect to this "global element basis",

$$\mathbf{F}C_i = \lambda_i \mathbf{S}C_i \quad \text{with } \mathbf{F} = H_0 + J(C) - K(C), \quad i = 1, ..., N_{orb}, \tag{1.12}$$

[3]Here, the grid-based GTO basis is chosen for the reasons of convenient comparison of the intermediate results of computations with the MOLPRO output. Any appropriate algebraically separable basis with the rank larger than 1 can be used instead.

where the eigenvectors $C_i \in \mathbb{R}^{R_0}$ form a matrix $C = \{c_{ki}\} = [C_1 C_2 \dots C_{N_{orb}}] \in \mathbb{R}^{R_0 \times N_{orb}}$, representing the Galerkin expansion coefficients of orbitals in the given basis set, $\varphi_i = \sum_{k=1}^{R_0} c_{ki} \overline{g}_k$. Here, $J(C)$, and $K(C)$, correspond to the Galerkin matrices of the Hartree and exchange operators, respectively.

The discrete Hartree-Fock equation is solved by the *self-consistent field* (SCF) iteration on a sequence of refined grids. To enhance the convergence, the SCF iteration is supplemented by the *direct inversion in the iterative subspace* (DIIS) scheme commonly used in the physical literature [89, 53, 16]. The multilevel acceleration of DIIS iteration described in Section 5.2.3 leads to stable and fast convergence on fine grid levels. We begin the iterative solution of the EVP with the initial zero approach for the matrices J, K, ($J(C) = 0$, $K(C) = 0$), i.e., only with the given core Hamiltonian part of the Fock operator, H_0, which contains the contribution of the nuclear external potential and the kinetic energy of the electrons in a molecule (linear part of $\mathbf{F}$).

The core of our method is the tensor-structured computation of the electron density and Galerkin matrices of the Hartree and exchange operators $J(C)$, $K(C)$, with $O(n \log n)$-complexity using an updated matrix C, at every step of nonlinear iteration.

High accuracy is achieved due to 3D tensor-structured arithmetic, with rank truncation, enabling computations over huge $n \times n \times n$ tensor grids with up to 10^{12} entries at the finest level. In electronic structure calculations, this implies rather fine resolution discussed above, which enables an *arbitrary space orientation of a molecule in the computational box*, as in the case of analytically based methods[4].

Our multilevel tensor-structured scheme for the numerical solution of the *ab initio* Hartree-Fock equation includes the following ingredients.

- In current computations we use, for simplicity, the H_0 part of the Fock operator from MOLPRO (solution independent part).
- Computations involving the $n \times n \times n$ 3D grid, start with a coarse approximation (say, for $n_0 = 64$), and proceed using the dyadic grid refinement up to $n = 1024$ in the pseudopotential cases, and up to $n = 8192$ in all electron cases.
- Iterations for solving the EVP start with $J_{n_0}(C) = 0$, $K_{n_0}(C) = 0$.
- At every iteration step, the Hartree and exchange parts of the Fock matrix $\mathbf{F}$ are updated by the tensor-structured computations with $O(n \log n)$ complexity.

[4]Note that our algorithms are computationally feasible using MATLAB on a standard SUN station.

- A grid dependent termination criterion is used for switching iterations to the next level of grid refinement.

Specifically, as the termination criterion, we control the norms of the differences of the orbitals taken as the residual over subsequent iterations. Our multilevel strategy has a four-fold effect, since it

a) provides fast convergence of the SCF DIIS iterations on the coarse grids, in spite of zero initial guess for $J_{n_0}(C)$, $K_{n_0}(C)$,

b) ensures good initial guess for iterations on (time consuming) finer grids,

c) allows the improved asymptotical approximation $O(h^3)$, via the Richardson extrapolation over a sequence of grids.

d) allows to reduce considerably the number of recomputed entries in $K(C)$ at fine grid levels (much less than $R_0^2/2$), by using the filtering strategy on fine grid levels.

The discrete orbitals, represented by the respective coefficient vectors are updated by diagonalising the Galerkin stiffness matrix at each iteration of the solution of the nonlinear EVP problem, at the expense $O(R_0^3)$, where R_0 is the dimension of the Galerkin subspace. We observe that the multilevel DIIS iteration exhibits uniform linear convergence rate $q^{N_{it}}$, $q < 1$, where N_{it} is the number of iterations, while the overall computational time for one iteration on an $n \times n \times n$ 3D Cartesian grid scales as $O(n \log n)$ in the univariate grid size n (under fixed rank parameters).

The current version of our method still scales cubically in the size of the approximating basis. Hence, any *algebraic optimisation of this basis set* may give new opportunity to high accuracy *ab initio* computations for large molecules. The quadratic scaling in the size of the approximating basis might be possible for the iterative solution of the discrete spectral problem, or in the framework of direct minimization algorithms, see [95, 93] for the detailed discussion on the direct minimization methods.

The numerical illustrations for the SCF iteration are presented for the all electron case of H_2O, and the pseudopotential case of CH_4, CH_3OH and C_2H_5OH molecules. Figures demonstrate the exponential convergence of the residuals with respect to the number of iterations. The number of effective iterations, scaled with respect to the time-unit required for one iteration on the finest grid level, is fairly small. The uniform convergence rate $q \sim 0.4$ is observed for the multilevel iterations, and it turns out to be quite small, $q \sim 0.1$, in terms of effective iterations.

Numerical computations confirm almost linear scaling in n, and possibilities for the low-rank representation of the multivariate functions and operators, indicating attractive features of the multilevel tensor-truncated SCF iteration in the prospects of efficient *ab initio* and DFT computations for large molecules.

To summarize, we note that the novel tensor-structured methods considered in this dissertation address many interesting mathematical and algorithmic problems which need future rigorous theoretical and numerical analysis. Validity of these methods in molecular computations is verified by the numerical results discussed in this thesis, signifying their perspectives in application to computational problems in modern quantum chemistry.

Leipzig 2006-2010
Max-Planck Institute for Mathematics in the Sciences

2 Tensor structured (TS) methods for functions in $\mathbb{R}^d$, $d \geq 3$

During the last decades, the methods for the low-rank tensor approximation of multiway data, originating from the fundamental papers [54, 106, 77], have been intensively developed in application to the problems of chemometrics, psychometric, independent component analysis, signal processing and higher order statistics. A thorough mathematical approval and analysis of the Tucker decomposition algorithm has been presented in the seminal works on the higher order singular value decomposition [24] and the best rank-$(r_1, \ldots, r_d)$ orthogonal Tucker approximation of higher order tensors [23]. A comprehensive survey [74] summarized the results of the extensive research on tensor decomposition methods and applications in computer science.

In this section, we recall some of the results in [23, 24] and describe the new tensor decomposition methods especially designed for application to the problems of scientific computing. The validity of the Tucker model in scientific computing can be understood on the base of numerical results on low rank Tucker-type decomposition applied to classes of function related tensors in $\mathbb{R}^d$, $d = 3$, [67] that gainfully exploits the important analytical properties of a respective multivariate function.

We begin with the description of the full format dth order tensors and definitions of the basic rank-structured tensor formats: the rank-R canonical, the orthogonal rank-$(r_1, \ldots, r_d)$ Tucker and mixed type decompositions. As a starting point, we recall the important theorem in [21] that the minimization problem of the Tucker approximation is equivalent to the dual maximization problem of finding vectors of the orthogonal mapping dominating subspaces which provide the maximum norm of the Tucker core tensor over the product manifold of orthogonal matrices.

Our Theorem 2.14 on the canonical-to-Tucker decomposition describes the reduced higher order SVD (RHOSVD) applied to the canonical rank-R tensors and provides the error estimate in terms of the truncated SVD of the ℓ-mode side matrices, supplemented by the corresponding complexity bounds. This result is an analogue to the well known higher order SVD (HOSVD) approximation for the full format tensors in [24], but now applied to the case of rank-R targets.

We present numerical illustrations on the Tucker approximation of full format tensors on examples of the following discretized functions in $\mathbb{R}^3$: Newton, Yukawa and Helmholtz potentials, Slater and periodic multi-centered Slater-type functions, and electron densities of small-size organic molecules.

This section is concluded by the summary of linear and bilinear operations in the Tucker and canonical tensor formats with estimation of the required numerical complexity. In general, along with the consequent multigrid accelerated Tucker approximation techniques introduced in Section 3, the material of this section provides sufficient tools for the construction of efficient tensor-structured numerical methods in electronic structure calculations in $\mathbb{R}^3$ (see Sections 4, 5).

2.1 Definitions of rank-structured tensor formats

2.1.1 Full format dth order tensors

A tensor of order d is a multidimensional array of real (complex) numbers whose entries are referred by using a product index set $\mathcal{I} = I_1 \times \ldots \times I_d$. We use the common notation

$$A = [a_{i_1 \ldots i_d} : i_\ell \in I_\ell] \in \mathbb{R}^{\mathcal{I}}, \quad I_\ell = \{1, ..., n_\ell\}, \quad \ell = 1, ..., d, \tag{2.1}$$

to denote a dth order tensor, and $\mathbf{i}$ for the d-tuple $\mathbf{i} = (i_1, ..., i_d)$ of integers[1]. A tensor A is an element of the linear vector space $\mathbb{V}_{\mathbf{n}} = \mathbb{R}^{\mathcal{I}}$, where $\mathbf{n} = (n_1, ..., n_d)$, with the entrywise addition $(A+B)_{\mathbf{i}} = a_{\mathbf{i}} + b_{\mathbf{i}}$ and the multiplication $(c\,A)_{\mathbf{i}} = c\,a_{\mathbf{i}}$ ($c \in \mathbb{R}$). The linear vector space $\mathbb{V}_{\mathbf{n}}$ of tensors is equipped with the Euclidean *scalar product* $\langle \cdot, \cdot \rangle : \mathbb{V}_{\mathbf{n}} \times \mathbb{V}_{\mathbf{n}} \to \mathbb{R}$, defined as

$$\langle A, B \rangle := \sum_{(i_1 \ldots i_d) \in \mathcal{I}} a_{i_1 \ldots i_d} b_{i_1 \ldots i_d} \quad \text{for } A, B \in \mathbb{V}_{\mathbf{n}}. \tag{2.2}$$

We call the related norm $\|A\|_F := \sqrt{\langle A, A \rangle}$, the Frobenius norm, as for matrices. Notice that a vector is an order-1 tensor, while a matrix is an order-2 tensor, so the Frobenius tensor norm coincides with the Euclidean norm of vectors and the Frobenius norm of matrices, respectively.

In some cases when the tensor size should be specified explicitly, we use the equivalent notation for the linear space of tensors, $\mathbb{R}^{n_1 \times \ldots \times n_d}$, instead of $\mathbb{R}^{\mathcal{I}}$.

Some multilinear algebraic operations with tensors of order d ($d \geq 3$), can be reduced to the standard linear algebra by *unfolding of a tensor* into a matrix. Here, we recall the construction of matrix unfolding (or the so-called matricization) as given in the survey [74]. First, we recall the notion of *fibers* given in

[1]The alternative notation for the tensor entries $a_{i_1 \ldots i_d}$ is $a(i_1, \ldots, i_d)$.

[74], which are the higher order analogue of matrix rows and columns. A fiber is defined by fixing all indices of a tensor except one. In this way, a matrix column is a mode-1 fiber, and a matrix row is a mode-2 fiber. The ℓ-mode matricization of a tensor $A \in \mathbb{R}^{I_1 \times \ldots \times I_d}$ arranges the ℓ-mode fibers of a tensor to be the columns of the resulting matrix.

Definition 2.1 *([74]) The unfolding of a tensor along mode ℓ is a matrix of dimension $n_\ell \times (n_{\ell+1}...n_d n_1...n_{\ell-1})$, further denoted by*

$$A_{(\ell)} = [a_{ij}] \in \mathbb{R}^{n_\ell \times (n_{\ell+1}...n_d n_1...n_{\ell-1})}, \tag{2.3}$$

whose columns are the respective fibers of A along the ℓ-th mode, such that the tensor element $a_{i_1 i_2 \ldots i_d}$ is mapped into the matrix element $a_{i_\ell j}$ where

$$j = 1 + \sum_{k=1, k\neq\ell}^{d} (i_k - 1) J_k, \text{ with } J_k = \prod_{m=1, m\neq\ell}^{k-1} n_m.$$

An illustration of the tensor unfolding $A_{(\ell)}$, ($\ell = 1, 2, 3$) for the 3-rd order tensor is presented in Figure 2.3.

Another important tensor operation is the so-called *contracted product* of two tensors. In the following, we frequently use its special case of the *tensor-matrix multiplication* along mode ℓ.

Definition 2.2 *([21]) Given a tensor $A \in \mathbb{R}^{I_1 \times \ldots \times I_d}$ and a matrix $M \in \mathbb{R}^{J_\ell \times I_\ell}$, we define the respective mode-ℓ tensor-matrix product by*

$$B = A \times_\ell M \in \mathbb{R}^{I_1 \times \ldots \times I_{\ell-1} \times J_\ell \times I_{\ell+1} \ldots \times I_d}, \tag{2.4}$$

where

$$b_{i_1 \ldots i_{\ell-1} j_\ell i_{\ell+1} \ldots i_d} = \sum_{i_\ell=1}^{n_\ell} a_{i_1 \ldots i_{\ell-1} i_\ell i_{\ell+1} \ldots i_d} m_{j_\ell i_\ell}, \quad j_\ell \in J_\ell.$$

Notice that the order of indices $J_\ell \times I_\ell$ in Definition 2.2 corresponds to the traditional contracted product notations for the Tucker decomposition as in (2.10).

The tensor-matrix product can be applied successively along several modes, and it can be shown to be commutative

$$(A \times_\ell M) \times_m P = (A \times_m P) \times_\ell M = A \times_\ell M \times_m P, \quad \ell \neq m.$$

The repeated (iterated) mode-ℓ tensor-matrix product for matrices M and P of appropriate dimensions can be simplified as follows,

$$(A \times_\ell M) \times_\ell P = A \times_\ell (PM),$$

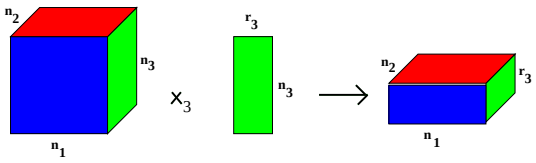

Figure 2.1: Contracted product of a 3rd order tensor with a matrix, see (2.4).

as discussed in [24].

For example, the contracted product of $A \in \mathbb{R}^{n_1 \times n_2 \times n_3}$ with a matrix $M \in \mathbb{R}^{r_3 \times n_3}$ yields the tensor $B \in \mathbb{R}^{n_1 \times n_2 \times r_3}$, see Figure 2.1.

An important property of the contracted product that resembles the matrix transpose is given in the following Lemma.

Lemma 2.3 *For any $B \in \mathbb{R}^{I_1 \times \ldots \times I_{\ell-1} \times J_\ell \times I_{\ell+1} \ldots \times I_d}$, we have*

$$\langle A \times_\ell M, B \rangle = \langle A, B \times_\ell M^T \rangle. \tag{2.5}$$

Proof: By definition,

$$\langle A \times_\ell M, B \rangle = \sum_{\mathbf{i} \in \mathcal{I} \setminus I_\ell,\, j_\ell \in J_\ell} \left(\sum_{i_\ell=1}^{n_\ell} a_{i_1,\ldots i_{\ell-1}, i_\ell, i_{\ell+1}, i_d} m_{j_\ell, i_\ell} \right) b_{i_1,\ldots,j_\ell,i_{\ell+1},\ldots,i_d}$$

$$= \sum_{\mathbf{i} \in \mathcal{I}} a_{\mathbf{i}} \left(\sum_{j_\ell \in J_\ell} b_{i_1,\ldots i_{\ell-1}, j_\ell, i_{\ell+1}, i_d} m_{j_\ell, i_\ell} \right) = \langle A, B \times_\ell M^T \rangle.$$

■

The number of entries in a full format tensor is $\prod_{\ell=1}^{d} \#I_\ell$. Assume for simplicity that $\#I_\ell = n$ for all $\ell = 1, ..., d$, then the number of entries in A amounts to n^d, hence growing exponentially in d.

2.1.2 Tucker, canonical and mixed (two-level) tensor formats

To get rid of exponential scaling in the dimension approximate representations in some classes $\mathcal{S} \subset \mathbb{V}_{\mathbf{n}}$ of "rank structured" tensors will be applied. To that end, the traditional concept of tensor-product Hilbert spaces (see, e.g. [91]) plays an important role. Specifically, the initial linear vector space of tensors $\mathbb{V}_{\mathbf{n}}$, is considered as the tensor-product Hilbert space $\mathbb{V}_{\mathbf{n}} = \otimes_{\ell=1}^{d} \mathbb{V}_\ell$ of real-valued d-th order tensors with $\mathbb{V}_\ell = \mathbb{R}^{I_\ell}$, where $\mathbb{R}^{I_\ell}$ $(\ell = 1, ..., d)$ is the standard Euclidean "univariate" vector space.

The tensor product of vector spaces $\mathbb{V}_\ell$ $(\ell = 1, ..., d)$ is defined by using the usual construction of the so-called rank-1 or elementary tensors: the *tensor product* of

vectors $u^{(\ell)} = \{u_{i_\ell}^{(\ell)}\}_{i_\ell \in I_\ell} \in \mathbb{V}_\ell$ $(\ell = 1, ..., d)$ forms the canonical *rank*-1 *tensor*

$$U \equiv [u_{\mathbf{i}}]_{\mathbf{i}\in\mathcal{I}} = u^{(1)} \otimes ... \otimes u^{(d)} \in \mathbb{V}_{\mathbf{n}} \quad \text{with entries} \quad u_{\mathbf{i}} = u_{i_1}^{(1)} \cdots u_{i_d}^{(d)}.$$

Now the tensor product of vector spaces $\mathbb{V}_\ell$ is defined by the span

$$\otimes_{\ell=1}^{d} \mathbb{V}_\ell := \text{span}\{u^{(1)} \otimes ... \otimes u^{(d)} : u^{(\ell)} \in \mathbb{R}^{I_\ell},\ 1 \le \ell \le d\}.$$

Taking all linear combinations of rank-1 tensors defined by the unit vectors in $\mathbb{R}^{I_\ell}$ $(\ell = 1, ..., d)$ shows that $\mathbb{V}_{\mathbf{n}} = \otimes_{\ell=1}^{d} \mathbb{R}^{I_\ell}$.

Notice that a rank-1 tensor requires only dn numbers to store it (now linear scaling in the dimension). Moreover, the scalar product of two rank-1 tensors U and V in $\mathbb{V}_{\mathbf{n}}$ can be represented by the componentwise univariate scalar products

$$\langle U, V \rangle := \prod_{\ell=1}^{d} \left\langle u^{(\ell)}, v^{(\ell)} \right\rangle,$$

that can be calculated in $O(dn)$ operations. When $d = 2$, the tensor product of two vectors $u \in \mathbb{R}^I$ and $v \in \mathbb{R}^J$ represents a rank-1 matrix,

$$u \otimes v = uv^T \in \mathbb{R}^{I\times J}.$$

As the simplest rank structured ansatz, we make use of rank-1 tensors. In the following, we consider the rank-structured representation of higher order tensors based on sums of rank-1 tensors. Specifically, we shall use the Tucker, canonical and mixed models.

Definition 2.4 *(The canonical format).*
Given a rank parameter $R \in \mathbb{N}$, we denote by $\boldsymbol{\mathcal{C}}_{R,\mathbf{n}} = \boldsymbol{\mathcal{C}}_R \subset \mathbb{V}_{\mathbf{n}}$ a set of tensors which can be represented in the canonical format,

$$U = \sum\nolimits_{\nu=1}^{R} \xi_\nu u_\nu^{(1)} \otimes \ldots \otimes u_\nu^{(d)}, \quad \xi_\nu \in \mathbb{R}, \tag{2.6}$$

with normalised vectors $u_\nu^{(\ell)} \in \mathbb{V}_\ell$ $(\ell = 1, ..., d)$. The minimal parameter R in (2.6) is called the rank (or canonical rank) of a tensor.

Introducing the side-matrices corresponding to representation (2.6),

$$U^{(\ell)} = [u_1^{(\ell)} ... u_R^{(\ell)}]$$

and the diagonal tensor $\boldsymbol{\xi} := diag\{\xi_1, ..., \xi_R\}$ such that $\xi_{\nu_1,...,\nu_d} = 0$ except when $\nu_1 = ... = \nu_d$ with $\xi_{\nu,...,\nu} = \xi_\nu$ $(\nu = 1, ..., R)$, we obtain the equivalent contracted product representation

$$U = \boldsymbol{\xi} \times_1 U^{(1)} \times_2 U^{(2)} ... \times_d U^{(d)}. \tag{2.7}$$

The canonical tensor representation is gainful for the multilinear tensor operations. In Section 2.4.2 it is shown that the linear tensor operations with tensors in the rank-R canonical format have linear complexity $O\left(\sum_{\ell=1}^{d} n_\ell\right)$ with respect to the univariate grid size n_ℓ of a tensor. The *disadvantage* of this representation is the lack of fast and stable algorithms for best approximation of arbitrary tensors in the fixed-rank canonical format.

The rank-$(r_1, \ldots, r_d)$ Tucker tensor format [106, 23] is based on a representation in subspaces

$$\mathbb{T}_{\mathbf{r}} := \otimes_{\ell=1}^{d} \mathbb{T}_\ell \quad \text{of} \quad \mathbb{V}_{\mathbf{n}} \quad \text{for certain} \quad \mathbb{T}_\ell \subset \mathbb{V}_\ell$$

with fixed dimension parameters $r_\ell := \dim \mathbb{T}_\ell \leq n$.

Definition 2.5 *(The Tucker format).*
For given rank parameter $\mathbf{r} = (r_1, ..., r_d)$, we denote by $\boldsymbol{\mathcal{T}}_{\mathbf{r},\mathbf{n}}$ (or shortly $\boldsymbol{\mathcal{T}}_{\mathbf{r}}$) the subset of tensors in $\mathbb{V}_{\mathbf{n}}$ represented in the so-called Tucker format

$$A_{(\mathbf{r})} = \sum\nolimits_{\nu_1=1}^{r_1} \cdots \sum\nolimits_{\nu_d=1}^{r_d} \beta_{\nu_1,\ldots,\nu_d}\, v_{\nu_1}^{(1)} \otimes \ldots \otimes v_{\nu_d}^{(d)} \in \mathbb{V}_{\mathbf{n}}, \tag{2.8}$$

with some vectors $v_{\nu_\ell}^{(\ell)} \in \mathbb{V}_\ell = \mathbb{R}^{I_\ell}$ $(1 \leq \nu_\ell \leq r_\ell)$, which form the orthonormal basis of r_ℓ-dimensional subspaces $\mathbb{T}_\ell = \operatorname{span}\{v_\nu^{(\ell)}\}_{\nu=1}^{r_\ell}$ $(\ell = 1, ..., d)$. With fixed $\mathbf{r}$ and $\mathbf{n}$, we can also write

$$\boldsymbol{\mathcal{T}}_{\mathbf{r},\mathbf{n}} := \{A \in \otimes_{\ell=1}^{d} \mathbb{T}_\ell \ \textit{for arbitrary}\ \mathbb{T}_\ell \subset \mathbb{V}_\ell, \ \textit{such that}\ \dim \mathbb{T}_\ell = r_\ell\}.$$

Here we call the parameter $r = \max\limits_{\ell}\{r_\ell\}$ the maximal Tucker rank.

In our applications, we usually apply the Tucker approximation with $r \ll n$, say $r = O(\log n)$. The coefficients tensor $\boldsymbol{\beta} = [\beta_{\nu_1,\ldots,\nu_d}]$, that is an element of a tensor space

$$\mathbb{B}_{\mathbf{r}} = \mathbb{R}^{r_1 \times \ldots \times r_d}, \tag{2.9}$$

is called the *core tensor*. Introducing the (orthogonal) side matrices $V^{(\ell)} = [v_1^{(\ell)} ... v_{r_\ell}^{(\ell)}]$, such that $V^{(\ell)T} V^{(\ell)} = I_{r_\ell \times r_\ell}$, we then use a tensor-by-matrix contracted product to represent the Tucker decomposition of $A_{(\mathbf{r})} \in \boldsymbol{\mathcal{T}}_{\mathbf{r}}$,

$$A_{(\mathbf{r})} = \boldsymbol{\beta} \times_1 V^{(1)} \times_2 V^{(2)} ... \times_d V^{(d)}. \tag{2.10}$$

Remark 2.6 *Notice that the representation (2.10) is not unique, since the tensor $A_{(\mathbf{r})}$ is invariant under directional rotations. In fact, for any set of orthogonal $r_\ell \times r_\ell$ matrices Y_ℓ $(\ell = 1, ..., d)$, we have the equivalent representation*

$$A_{(\mathbf{r})} = \widehat{\boldsymbol{\beta}} \times_1 \widehat{V}^{(1)} \times_2 \widehat{V}^{(2)} ... \times_d \widehat{V}^{(d)},$$

with

$$\widehat{\boldsymbol{\beta}} = \boldsymbol{\beta} \times_1 Y_1 \times_2 Y_2 ... \times_d Y_d, \quad \widehat{V}^{(\ell)} = V^{(\ell)} Y_\ell^T, \quad \ell = 1, ..., d.$$

Remark 2.7 *If the subspaces* $\mathbb{T}_\ell = \mathrm{span}\{v_\nu^{(\ell)}\}_{\nu=1}^{r_\ell} \subset \mathbb{V}_\ell$ *are fixed then the approximation* $A_{(\mathbf{r})} \in \boldsymbol{\mathcal{T}}_{\mathbf{r}}$ *of a given tensor* $A \in \mathbb{V}_{\mathbf{n}}$ *is reduced to the orthogonal projection of* A *onto the particular linear space* $\mathbb{T}_{\mathbf{r}} = \otimes_{\ell=1}^d \mathbb{T}_\ell \subset \boldsymbol{\mathcal{T}}_{\mathbf{r},\mathbf{n}}$*, that is*

$$\begin{aligned} A_{(\mathbf{r})} &= \sum_{\nu_1,\ldots,\nu_d=1}^{\mathbf{r}} \langle v_{\nu_1}^{(1)} \otimes \ldots \otimes v_{\nu_d}^{(d)}, A\rangle\, v_{\nu_1}^{(1)} \otimes \ldots \otimes v_{\nu_d}^{(d)} \\ &= \left(A \times_1 V^{(1)^T} \times_2 \cdots \times_d V^{(d)^T}\right) \times_1 V^{(1)} \times_2 \ldots \times_d V^{(d)}. \end{aligned}$$

This property plays an important role in the computation of the best orthogonal Tucker approximation, where the "optimal" subspaces $\mathbb{T}_\ell$ *are recalculated within a nonlinear iteration process.*

In the following, to simplify the discussion of complexity issues, we assume that $r_\ell = r$ ($\ell = 1, ..., d$). The storage requirements for the Tucker (resp. canonical) decomposition is given by $r^d + drn$ (resp. $R + dRn$), where usually r is noticably smaller than n. In turn, the maximal canonical rank of the Tucker representation is bounded by r^{d-1} (see Remark 2.17).

Since the Tucker core still presupposes r^d storage, we introduce further the approximation methods using a mixed (two-level) representation [60, 67] which gainfully combines the beneficial features of both the Tucker and canonical models.

Definition 2.8 *(The mixed (two-level) Tucker-canonical format).*
Given the rank parameters $\mathbf{r}, R$*, we denote by* $\boldsymbol{\mathcal{T}}_{\mathcal{C}_{R,\mathbf{r}}}$ *the subclass of tensors in* $\boldsymbol{\mathcal{T}}_{\mathbf{r},\mathbf{n}}$ *with the core* $\boldsymbol{\beta}$ *represented in the canonical format,* $\boldsymbol{\beta} \in \boldsymbol{\mathcal{C}}_{R,\mathbf{r}} \subset \mathbb{B}_{\mathbf{r}}$*. An explicit representation of* $A \in \boldsymbol{\mathcal{T}}_{\mathcal{C}_{R,\mathbf{r}}}$ *is given by*

$$A = \left(\sum_{\nu=1}^{R} \xi_\nu u_\nu^{(1)} \otimes \ldots \otimes u_\nu^{(d)}\right) \times_1 V^{(1)} \times_2 V^{(2)} \ldots \times_d V^{(d)}, \tag{2.11}$$

with some $u_\nu^{(\ell)} \in \mathbb{R}^{r_\ell}$*. Clearly, we have the embedding* $\boldsymbol{\mathcal{T}}_{\mathcal{C}_{R,\mathbf{r}}} \subset \boldsymbol{\mathcal{C}}_{R,\mathbf{n}}$ *with the corresponding (non-orthogonal) side-matrices* $U^{(\ell)} = [V^{(\ell)} u_1^{(\ell)} \ldots V^{(\ell)} u_R^{(\ell)}]$*, and scaling coefficients* ξ_ν *(*$\nu = 1, ..., R$*).*

A target tensor $A \in \mathbb{V}_{\mathbf{n}}$ can be approximated by a sum of rank-1 tensors as in (2.8), (2.6), or using the mixed format $\boldsymbol{\mathcal{T}}_{\mathcal{C}_{R,\mathbf{r}}}$ as in (2.11). More details on the mixed (two-level) tensor format are given in Sections 2.2.4 and 2.2.5.

In the next sections we discuss fast and efficient methods to compute the corresponding rank structured approximations in different problem settings.

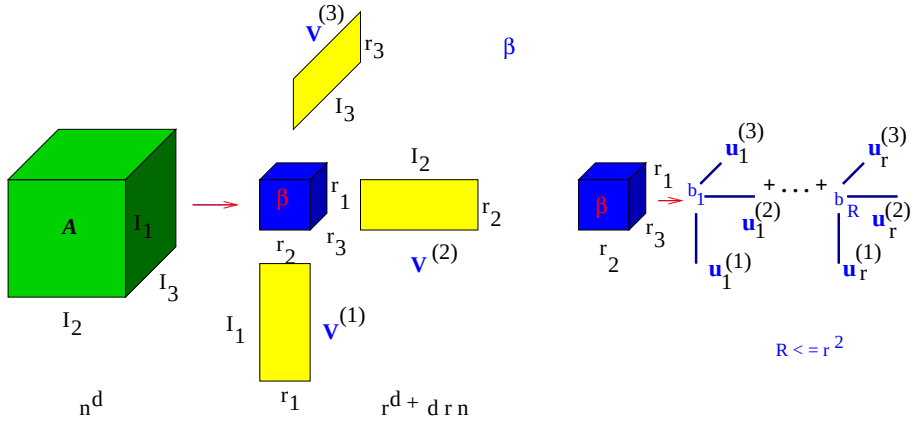

Figure 2.2: Mixed Tucker-canonical representation of the full format 3rd order tensor.

2.2 Best orthogonal Tucker approximation (BTA)

2.2.1 General discussion

The numerical Tucker-type approximation of dth order tensors is one of the most practically important MLA operations. This operation is, in fact, one of the possible higher order extensions of the best rank-r matrix approximation in linear algebra, based on the truncated SVD.

In our applications, we deal with the best Tucker approximation applied to the so-called function related tensors, whose entries are computed by sampling a given multivariate function in $\mathbb{R}^d$, $d = 3$ over an $n \times n \times n$ Cartesian tensor grid. Further, in the discussion of the numerical results in Section 2.3.2, we describe the particular construction of function related tensors and observe some useful properties of the Tucker format applied to these tensors.

In general, the target tensor A_0 to be approximated may belong itself to a certain class $\mathcal{S}_0 \subset \mathbb{V}_{\mathbf{n}}$ of data structured tensors. Since both $\boldsymbol{\mathcal{T}}_{\mathbf{r},\mathbf{n}}$ and $\boldsymbol{\mathcal{C}}_{R,\mathbf{n}}$ are not linear spaces we are led to the challenging *nonlinear approximation* problem

$$A_0 \in \mathcal{S}_0 \subset \mathbb{V}_{\mathbf{n}} : \quad f(A) := \|A_0 - A\|^2 \to \min \tag{2.12}$$

over all tensors $A \in \mathcal{S}$ with $\mathcal{S} \in \{\boldsymbol{\mathcal{T}}_{\mathbf{r},\mathbf{n}}, \boldsymbol{\mathcal{C}}_{R,\mathbf{n}}, \boldsymbol{\mathcal{T}}_{\mathcal{C}_{R,\mathbf{r}}}\}$. The target tensor A_0 might inherit a certain data-sparse structure like $\mathcal{S}_0 \subset \{\boldsymbol{\mathcal{C}}_{R_0,\mathbf{n}}, \boldsymbol{\mathcal{T}}_{\mathbf{r}_0,\mathbf{n}}\}$.

As the basic nonlinear approximation scheme, we consider the best orthogonal rank-$(r_1, ..., r_d)$ Tucker format corresponding to the choice $\mathcal{S} = \boldsymbol{\mathcal{T}}_{\mathbf{r},\mathbf{n}}$. Tensors $A \in \boldsymbol{\mathcal{T}}_{\mathbf{r}}$, are parametrised as in (2.10), with the orthogonality constraints

$$V^{(\ell)} \in \mathcal{V}_{n_\ell, r_\ell} \quad (\ell = 1, ..., d),$$

where

$$\mathcal{V}_{n,r} := \{Y \in \mathbb{R}^{n\times r} : Y^T Y = I_{r\times r} \in \mathbb{R}^{r\times r}\} \tag{2.13}$$

is the so-called Stiefel manifold of $n \times r$ orthogonal matrices. This minimisation problem on the product of Stiefel manifolds was first addressed in [76].

In the following we denote by $\mathcal{G}_\ell$ the Grassman manifold that is the factor space of the Stiefel manifold $\mathcal{V}_{n_\ell,r_\ell}$ $(\ell = 1, ..., d)$ in (2.13) with respect to all possible rotations, see Remark 2.6.

For a wide class of function related tensors, the quality of approximation via the minimisation (2.12) can be effectively controlled by the Tucker rank. In particular, for certain classes of function related tensors it is possible to prove exponential convergence (cf. [44, 60]),

$$\|A_{(\mathbf{r})} - A_0\| \le Ce^{-\alpha\hat{r}} \quad \text{with} \quad \hat{r} = \min_\ell r_\ell, \tag{2.14}$$

where $A_{(\mathbf{r})}$ is a minimizer in (2.12). As a consequence, the approximation error $\varepsilon > 0$ can be achieved with $\hat{r} = O(|\log\varepsilon|)$.

The following Lemma proves that the relative difference of norms of the best rank-$(r_1, \ldots, r_d)$ Tucker approximation $A_{(\mathbf{r})}$ and the target A_0 is estimated by the square of the relative Frobenius norm of $A_{(\mathbf{r})} - A_0$.

Lemma 2.9 *(quadratic convergence in norms). Let $A_{(\mathbf{r})} \in \mathbb{R}^{I_1\times\ldots\times I_d}$ solve the minimisation problem (2.12) over $A \in \boldsymbol{\mathcal{T}}_{\mathbf{r}}$. Then we have the "quadratic" relative error bound*

$$\frac{\|A_0\| - \|A_{(\mathbf{r})}\|}{\|A_0\|} \le \frac{\|A_{(\mathbf{r})} - A_0\|^2}{\|A_0\|^2}. \tag{2.15}$$

Moreover, it holds $\|\boldsymbol{\beta}\| = \|A_{(\mathbf{r})}\| \le \|A_0\|$.

Proof: First part of the proof is given for the completeness (cf. [23] for a short exposition). Letting $A_{(\mathbf{r})} = \boldsymbol{\beta} \times_1 V^{(1)} \times_2 V^{(2)} \ldots \times_d V^{(d)}$ and using Lemma 2.3, we easily obtain the identity

$$\|A_{(\mathbf{r})}\| = \|\boldsymbol{\beta}\|, \tag{2.16}$$

since orthogonal matrices $V^{(\ell)} \in \mathcal{V}_{n_\ell,r_\ell}$ do not effect the Frobenius norm. Furthermore, with fixed $V^{(\ell)}$ $(\ell = 1, ..., d)$, relation (2.12) is merely a linear least-square problem with respect to $\boldsymbol{\beta} \in \mathbb{R}^{r_1\times\ldots\times r_d}$,

$$g(\boldsymbol{\beta}) := \langle A_0, A_0\rangle - 2\langle A_0, \boldsymbol{\beta} \times_1 V^{(1)} \times_2 \ldots \times_d V^{(d)}\rangle + \langle \boldsymbol{\beta}, \boldsymbol{\beta}\rangle \to \min. \tag{2.17}$$

Hence, the corresponding minimisation condition

$$g(\boldsymbol{\beta} + \delta\boldsymbol{\beta}) - g(\boldsymbol{\beta}) \ge 0 \quad \forall\, \delta\boldsymbol{\beta} \in \mathbb{R}^{r_1\times\ldots\times r_d},$$

leads to the following equation for the minimiser,

$$-\langle A_0, \delta\boldsymbol{\beta} \times_1 V^{(1)} \times_2 \ldots \times_d V^{(d)} \rangle + \langle \boldsymbol{\beta}, \delta\boldsymbol{\beta} \rangle = 0 \quad \forall\, \delta\boldsymbol{\beta} \in \mathbb{R}^{r_1 \times \ldots \times r_d}.$$

This implies, using Lemma 2.3, that

$$\langle -A_0 \times_1 {V^{(1)}}^T \times_2 \ldots \times_d {V^{(d)}}^T + \boldsymbol{\beta}, \delta\boldsymbol{\beta} \rangle = 0, \quad \forall\ \delta\boldsymbol{\beta} \in \mathbb{R}^{r_1 \times \ldots \times r_d},$$

and we obtain

$$\boldsymbol{\beta} - A_0 \times_1 {V^{(1)}}^T \times_2 \ldots \times_d {V^{(d)}}^T = 0. \tag{2.18}$$

Next we readily derive

$$\begin{aligned} f(A_{(\mathbf{r})}) &= \|A_{(\mathbf{r})}\|^2 - 2\langle \boldsymbol{\beta} \times_1 V^{(1)} \times_2 \ldots \times_d V^{(d)}, A_0 \rangle + \|A_0\|^2 \\ &= \|A_{(\mathbf{r})}\|^2 + \|A_0\|^2 - 2\langle \boldsymbol{\beta}, A_0 \times_1 {V^{(1)}}^T \times_2 \ldots \times_d {V^{(d)}}^T \rangle, \\ &= \|A_0\|^2 - \|\boldsymbol{\beta}\|^2, \end{aligned}$$

hence it follows that

$$\|A_0\|^2 - \|A_{(\mathbf{r})}\|^2 = \|A_{(\mathbf{r})} - A_0\|^2. \tag{2.19}$$

The latter leads to the estimate (clearly (2.19) implies $\|A_0\| \geq \|A_{(\mathbf{r})}\|$)

$$\frac{\|A_0\| - \|A_{(\mathbf{r})}\|}{\|A_0\|} = \frac{\|A_{(\mathbf{r})} - A_0\|^2}{(\|A_{(\mathbf{r})}\| + \|A_0\|)\|A_0\|} \leq \frac{\|A_{(\mathbf{r})} - A_0\|^2}{\|A_0|^2},$$

that completes the proof. ∎

The key point for the efficient solution of the minimization problem (2.12) with $\mathcal{S} = \boldsymbol{\mathcal{T}}_{\mathbf{r},\mathbf{n}}$ is its equivalence to the *dual maximisation problem* [23],

$$[Z^{(1)}, ..., Z^{(d)}] = \operatorname{argmax} \left\| \left[\langle v_{\nu_1}^{(1)} \otimes ... \otimes v_{\nu_d}^{(d)}, A \rangle \right]_{\nu=\mathbf{1}}^{\mathbf{r}} \right\|_{\mathbb{B}_{\mathbf{r}}}^2 \tag{2.20}$$

over the set of side-matrices $V^{(\ell)} = [v_1^{(\ell)} \ldots v_{r_\ell}^{(\ell)}]$ in the Stiefel manifold $\mathcal{V}_{n_\ell, r_\ell}$, as in (2.13).

The following lemma reduces the minimisation of the original quadratic functional to the dual maximisation problem thus eliminating the core tensor $\boldsymbol{\beta}$ from the optimization process.

Lemma 2.10 *([23]) For given $A_0 \in \mathbb{R}^{I_1 \times \ldots \times I_d}$, the minimisation problem (2.12) on $\boldsymbol{\mathcal{T}}_{\mathbf{r}}$ is equivalent to the dual maximisation problem*

$$g(Y^{(1)}, ..., Y^{(d)}) := \left\| A_0 \times_1 {Y^{(1)}}^T \times_2 ... \times_d {Y^{(d)}}^T \right\|^2 \to max \tag{2.21}$$

over a set $Y^{(\ell)} \in \mathbb{R}^{n_\ell \times r_\ell}$ *from the Grassman manifold, i.e.,* $Y^{(\ell)} \in \mathcal{G}_\ell$ $(\ell = 1, ..., d)$. *For given maximizing matrices* $V^{(m)}$ $(m = 1, ..., d)$, *the tensor* $\boldsymbol{\beta}$ *minimising (2.12) is represented by*

$$\boldsymbol{\beta} = A_0 \times_1 V^{(1)^T} \times_2 ... \times_d V^{(d)^T} \in \mathbb{R}^{r_1 \times ... \times r_d}. \tag{2.22}$$

Proof: Inspecting the proof of Lemma 2.9 we find that substitution of $\boldsymbol{\beta}$ in (2.18) to (2.17) leads to the equivalent minimizing equation

$$\langle A_0, A_0 \rangle - \langle A_0 \times_1 V^{(1)^T} \times_2 ... \times_d V^{(d)^T}, A_0 \times_1 V^{(1)^T} \times_2 ... \times_d V^{(d)^T} \rangle \to \min, \tag{2.23}$$

that proves (2.21). Finally, (2.18) yields (2.22). ∎

In view of Remark 2.6, the rotational non-uniqueness of the maximizer in (2.20) can be avoided if one solves this maximisation problem in the so-called Grassmann manifold that is the factor space of $\mathcal{V}_{n_\ell, r_\ell}$ with respect to the rotational transforms [26]. The dual maximisation problem (2.21) posed on the compact manifold can be proven to have at least one global maximum (see [60, 26]). For the size consistency of the arising tensors, we require the natural compatibility conditions

$$r_\ell \le \bar{r}_\ell := r_1 ... r_{\ell-1} r_{\ell+1} ... r_d, \quad \ell = 1, ..., d. \tag{2.24}$$

2.2.2 BTA algorithm for full format tensors

The best (nonlinear) Tucker approximation (BTA) based on solving the dual maximization problem (2.20) is usually solved numerically by the ALS iteration with the initial guess computed by the higher order SVD [24].

The generalization of the SVD to the dth order tensors has been introduced in [24] in application to the multidimensional problems in signal processing. It is called the higher order SVD (HOSVD) or dth order SVD. We recall the theorem with the basic notations as in [23].

Theorem 2.11 *(dth order SVD, HOSVD, [23]).*

Every complex $n_1 \times n_2 \times ... \times n_d$*-tensor* A *can be written as the product*

$$A = \mathcal{S} \times_1 U^{(1)} \times_2 U^{(2)} ... \times_d U^{(d)},$$

in which

1. $U^{(\ell)} = [U_1^{(\ell)} U_2^{(\ell)} ... U_{n_\ell}^{(\ell)}]$ *is a unitary* $n_\ell \times n_\ell$*-matrix,*

2. $\mathcal{S}$ *is a complex* $n_1 \times n_2 \times ... \times n_d$*-tensor of which the subtensors* $\mathcal{S}_{i_\ell = \alpha}$*, obtained by fixing the* ℓ*th index to* α*, have the properties of*

(i) all-orthogonality: two subtensors $\mathcal{S}_{i_\ell=\alpha}$ and $\mathcal{S}_{i_\ell=\beta}$ are orthogonal for all possible values of ℓ, α, and β subject to $\alpha \neq \beta$:

$$\langle \mathcal{S}_{i_\ell=\alpha}, \mathcal{S}_{i_\ell=\beta} \rangle = 0 \quad when \quad \alpha \neq \beta,$$

(ii) ordering: $\|\mathcal{S}_{i_\ell=1}\| \geq \|\mathcal{S}_{i_\ell=2}\| \geq ... \geq \|\mathcal{S}_{i_\ell=n_\ell}\| \geq 0$ for all positive values of ℓ.

The Frobenius norms $\|\mathcal{S}_{i_\ell=i}\|$, symbolized by $\sigma_i^{(\ell)}$, are ℓ-mode singular values of $A_{(\ell)}$ and the vector $U_i^{(\ell)}$ is an ith ℓ-mode left singular vector of $A_{(\ell)}$.

Next theorem gives the error bound for the truncated HOSVD.

Theorem 2.12 *(approximation by HOSVD, [24]). Let the HOSVD of A be given as in Theorem 2.11 and let the ℓ-mode rank of A, rank$(A_{(\ell)})$, be equal to R_ℓ $(\ell = 1, ..., d)$. Define a tensor $\tilde{A}$ by discarding the smallest ℓ-mode singular values $\sigma_{r_\ell+1}^{(\ell)}, \sigma_{r_\ell+2}^{(\ell)}, ..., \sigma_{R_\ell}^{(\ell)}$ for given values of r_ℓ $(\ell = 1, ..., d)$, i.e., set the corresponding parts of $\mathcal{S}$ equal to zero. Then we have*

$$\|A - \tilde{A}\|^2 \leq \sum_{i_1=r_1+1}^{R_1} {\sigma_{i_1}^{(1)}}^2 + \sum_{i_2=r_2+1}^{R_2} {\sigma_{i_2}^{(2)}}^2 + \cdots + \sum_{i_d=r_d+1}^{R_d} {\sigma_{i_d}^{(d)}}^2.$$

Proof: We have

$$\begin{aligned}
\|A - \tilde{A}\|^2 &= \sum_{i_1=1}^{R_1}\sum_{i_2=1}^{R_2}\cdots\sum_{i_d=1}^{R_d} s^2_{i_1 i_2 \ldots i_d} - \sum_{i_1=1}^{r_1}\sum_{i_2=1}^{r_2}\cdots\sum_{i_d=1}^{r_d} s^2_{i_1 i_2 \ldots i_d} \\
&\leq \sum_{i_1=r_1+1}^{R_1}\sum_{i_2=1}^{R_2}\cdots\sum_{i_d=1}^{R_d} s^2_{i_1 i_2 \ldots i_d} + \sum_{i_1=1}^{R_1}\sum_{i_2=r_2+1}^{R_2}\cdots\sum_{i_d=1}^{R_d} s^2_{i_1 i_2 \ldots i_d} \\
&\quad + \cdots + \sum_{i_1=1}^{R_1}\sum_{i_2=1}^{R_2}\cdots\sum_{i_d=r_d+1}^{R_d} s^2_{i_1 i_2 \ldots i_d} \\
&= \sum_{i_1=r_1+1}^{R_1} \sigma_{i_1}^{(1)^2} + \sum_{i_2=r_2+1}^{R_2} \sigma_{i_2}^{(2)^2} + \cdots + \sum_{i_d=r_d+1}^{R_d} \sigma_{i_d}^{(d)^2},
\end{aligned}$$

that completes the proof. ∎

Next, we recall the method to solve the (local) maximization problem in Lemma 2.10 which is based on the alternating least squares (ALS) iteration. For the full format tensors, the sketch of ALS algorithm G_BTA reads as follows (see Algorithm 4.2 in [23] for more details).

Algorithm G_BTA ($\mathbb{V}_{\mathbf{n}} \to \boldsymbol{\mathcal{T}}_{\mathbf{r},\mathbf{n}}$). Given the input tensor $A \in \mathbb{V}_{\mathbf{n}}$, the Tucker rank $\mathbf{r}$, and the maximum number of ALS iterations $k_{max} \geq 1$.

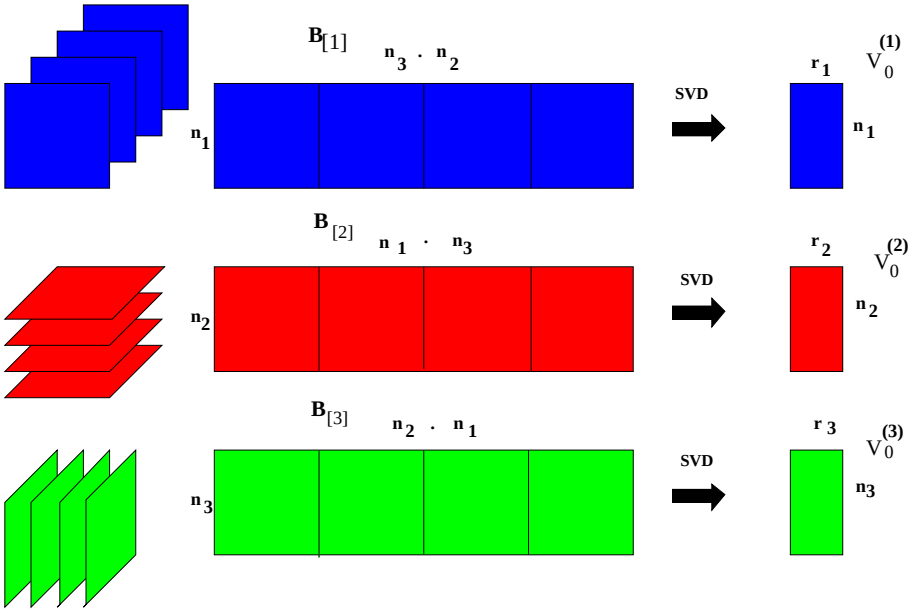

Figure 2.3: Truncated HOSVD of a tensor $A \in \mathbb{R}^{n_1 \times n_2 \times n_3}$ is computed by the truncated SVD of the ℓ-mode unfolding matrices, $\ell = 1, 2, 3$.

1. Compute the "truncated" HOSVD of A to obtain an initial guess $V_0^{(\ell)} \in \mathbb{R}^{n_\ell \times r_\ell}$ for the ℓ-mode side-matrices $V^{(\ell)}$ $(\ell = 1, ..., d)$ ("truncated" SVD applied to each matrix unfolding $A_{(\ell)}$). The complexity of HOSVD is bounded by
$$W = O(dn^{d+1}). \tag{2.25}$$

2. For $k = 1 : k_{max}$ perform:
for each $q = 1, ..., d$, and with fixed side-matrices $V_{k-1}^{(\ell)} \in \mathbb{R}^{n_\ell \times r_\ell}$, $\ell \neq q$, the ALS iteration optimises the q-mode matrix $V_k^{(q)}$ via computing the dominating r_q-dimensional subspace (truncated SVD) for the respective matrix unfolding
$$B_{(q)} \in \mathbb{R}^{n_q \times \bar{r}_q}, \quad \bar{r}_q = r_1 ... r_{q-1} r_{q+1} ... r_d = O(r^{d-1}), \tag{2.26}$$
corresponding to the tensor obtained by the q-mode contracted product
$$B = A \times_1 V_k^{(1)^T} \times_2 ... \times_{q-1} V_k^{(q-1)^T} \times_{q+1} V_{k-1}^{(q+1)^T} ... \times_d V_{k-1}^{(d)^T}.$$
Each iteration has the cost $O(dr^{d-1} n \min\{r^{d-1}, n\} + dn^d r)$, that represents the expense of SVDs and the computation of matrix unfoldings $B_{(q)}$.

3. Set $V^{(\ell)} = V_{k_{max}}^{(\ell)}$, and compute the core $\boldsymbol{\beta}$ as the representation coefficients of the orthogonal projection of A onto $\mathbb{T}_{\mathbf{n}} = \otimes_{\ell=1}^{d} \mathbb{T}_\ell$ with $\mathbb{T}_\ell = \text{span}\{v_\nu^{(\ell)}\}_{\nu=1}^{r_\ell}$

(see Remark 2.7),

$$\boldsymbol{\beta} = A \times_1 V^{(1)^T} \times_2 ... \times_d V^{(d)^T} \in \mathbb{B}_{\mathbf{r}},$$

at the cost $O(r^d n)$.

With fixed k_{max}, the overall complexity of the algorithm for $d = 3$, $n_\ell = n$, and $r_\ell = r$ ($\ell = 1, 2, 3$) (suppose that $r^2 \leq n$), is estimated by

$$W_{F\to T} = O(n^4 + n^3 r + n^2 r^2 + n r^3) = O(n^4),$$

where different summands denote the cost of initial HOSVD of A, computation of unfolding matrices $B_{(q)}$, related SVDs, and computation of the core tensor.

For the class of function related tensors we observe fast and robust local convergence of the ALS iteration (though it is not always the case in traditional applications of the Tucker decomposition in the independent component analysis and chemometrics). This fact can be, probably, illuminated by the exponential error bound in the Tucker rank for the rank-$\mathbf{r}$ orthogonal approximation (see (2.14)), which is often observed in applications to tensors representing the physically relevant functions [67].

However, notice that the Tucker model applied to the general fully populated tensor of size n^d requires $O(dn^{d+1})$ arithmetical operations due to the presence of complexity dominating higher-order SVD. Hence, in computational practice this algorithm applies only to small d and moderate n.

2.2.3 BTA for rank-R canonical input

In some applications, for example in electronic structure calculations, the target tensor is already presented in the rank-R canonical format, $A \in \boldsymbol{\mathcal{C}}_{R,\mathbf{n}}$, as in (2.6), but with relatively large R,

$$U_{(R)} = \sum\nolimits_{\nu=1}^{R} \xi_\nu u_\nu^{(1)} \otimes \ldots \otimes u_\nu^{(d)}, \quad \xi_\nu \in \mathbb{R}.$$

The complexity of tensor-structured operations, in spite of linear scaling with respect to the one-dimension grid size, is $O(R_1 R_2 n)$, is thus increasing also linearly with respect to the product of the ranks R_1 and R_2 of the input tensors. Hence, large parameters R_1 and R_2 may as well lead to substantial numerical cost.

In this case, to reduce the ranks of input tensors, we develop the two-level canonical-to-Tucker (C2T) approximation with the consequent Tucker-to-canonical (T2C) transform. The resulting computational cost of MLA operations supplemented by such a two-level method can be reduced essentially.

The corresponding canonical-to-Tucker-to-canonical approximation scheme [68] is presented as the following two-level chain,

$$\boldsymbol{\mathcal{C}}_{R,\mathbf{n}} \quad \stackrel{I}{\rightarrow} \quad \boldsymbol{\mathcal{T}}_{\mathcal{C}_{R},\mathbf{r}} \quad \stackrel{II}{\rightarrow} \quad \boldsymbol{\mathcal{T}}_{\mathcal{C}_{R'},\mathbf{r}}. \tag{2.27}$$

Here, on Level-I, we compute the best orthogonal Tucker approximation applied to the $\boldsymbol{\mathcal{C}}_{R,\mathbf{n}}$-type input, so that the resultant core is represented in the $\boldsymbol{\mathcal{C}}_{R,\mathbf{r}}$ format. On Level-II, the small-size Tucker core in $\boldsymbol{\mathcal{C}}_{R,\mathbf{r}}$ is approximated by a tensor in $\boldsymbol{\mathcal{C}}_{R',\mathbf{r}}$ with $R' < R$. Here we describe the Algorithm on Level-I (which is, in fact, the most laborious part in computational scheme (2.27)) that has a polynomial cost in the size of the input data in $\boldsymbol{\mathcal{C}}_{R,\mathbf{n}}$ (see Remark 2.15).

Next theorem gives the characterisation on the *solution structure* for the Level-I scheme in (2.27), and provides the key ingredients to construct its efficient numerical implementation provided that the target A is represented by (2.6).

It also presents the *error estimates* for the reduced rank-$\mathbf{r}$ HOSVD type approximation (RHOSVD), given in the definition below. Suppose for definiteness that $n \leq R$, so that an SVD of the side-matrix $U^{(\ell)}$ is given by

$$U^{(\ell)} = Z^{(\ell)} D_\ell {W^{(\ell)}}^T = \sum_{k=1}^{n} \sigma_{\ell,k} z_k^{(\ell)} \; {w_k^{(\ell)}}^T, \quad z_k^{(\ell)} \in \mathbb{R}^n, \; w_k^{(\ell)} \in \mathbb{R}^R,$$

with orthogonal matrices $Z^{(\ell)} = [z_1^{(\ell)}, ..., z_n^{(\ell)}]$, and $W^{(\ell)} = [w_1^{(\ell)}, ..., w_n^{(\ell)}]$, $\ell = 1, ..., d$. We use the following notations for the vector entries, $w_k^{(\ell)}(\nu) = w_{k,\nu}^{(\ell)}$ $(\nu = 1, ..., R)$.

Definition 2.13 *(RHOSVD).*
Introduce the truncated SVD of the side-matrices $U^{(\ell)}$, $Z_0^{(\ell)} D_{\ell,0} {W_0^{(\ell)}}^T$, $(\ell = 1, ..., d)$, *where* $D_{\ell,0} = diag\{\sigma_{\ell,1}, \sigma_{\ell,2}, ..., \sigma_{\ell,r_\ell}\}$ *and* $Z_0^{(\ell)} \in \mathbb{R}^{n \times r_\ell}$, ${W_0}^{(\ell)} \in \mathbb{R}^{R \times r_\ell}$, *represent the orthogonal factors being the respective submatrices of* $Z^{(\ell)}$ *and* $W^{(\ell)}$. *Then the RHOSVD approximation is given by*

$$A^0_{(\mathbf{r})} = \boldsymbol{\xi} \times_1 \left[Z_0^{(1)} D_{1,0} {W_0^{(1)}}^T \right] \times_2 \left[Z_0^{(2)} D_{2,0} {W_0^{(2)}}^T \right] \cdots \times_d \left[Z_0^{(d)} D_{d,0} {W_0^{(d)}}^T \right]. \tag{2.28}$$

Theorem 2.14 *(Canonical to Tucker approximation).*
(a) Let $A \in \boldsymbol{\mathcal{C}}_{R,\mathbf{n}}$ *be given by (2.6). Then the minimisation problem*

$$A \in \boldsymbol{\mathcal{C}}_{R,\mathbf{n}} \subset \mathbb{V}_{\mathbf{n}} : \quad A_{(\mathbf{r})} = \mathrm{argmin}_{T \in \mathcal{T}_{\mathbf{r},\mathbf{n}}} \|A - T\|_{\mathbb{V}_{\mathbf{n}}}, \tag{2.29}$$

is equivalent to the dual maximisation problem

$$[V^{(1)}, ..., V^{(d)}] = \underset{Y^{(\ell)} \in \mathcal{G}_\ell}{\mathrm{argmax}} \left\| \sum_{\nu=1}^{R} \xi_\nu \left({Y^{(1)}}^T u_\nu^{(1)} \right) \otimes ... \otimes \left({Y^{(d)}}^T u_\nu^{(d)} \right) \right\|^2_{\mathbb{B}_{\mathbf{r}}}, \tag{2.30}$$

over the Grassman manifolds $\mathcal{G}_\ell$, $Y^{(\ell)} = [y_1^{(\ell)}...y_{r_\ell}^{(\ell)}] \in \mathcal{G}_\ell$ $(\ell = 1, ..., d)$, *and where* $Y^{(\ell)^T} u_\nu^{(\ell)} \in \mathbb{R}^{r_\ell}$.

(b) The compatibility condition (2.24) is simplified to

$$r_\ell \leq rank(U^{(\ell)}) \quad with \quad U^{(\ell)} = [u_1^{(\ell)}...u_R^{(\ell)}] \in \mathbb{R}^{n\times R},$$

and we have the solvability of (2.30) assuming that the above relation is valid.

The maximizer is given by orthogonal matrices $V^{(\ell)} = [v_1^{(\ell)}...v_{r_\ell}^{(\ell)}] \in \mathbb{R}^{n\times r_\ell}$, *which can be computed similarly, as in Algorithm G_BTA, where the truncated HOSVD at Step 1 is now substituted by RHOSVD, see(2.28).*

(c) The minimiser in (2.29) is then calculated by the orthogonal projection

$$A_{(\mathbf{r})} = \sum_{\mathbf{k}=\mathbf{1}}^{\mathbf{r}} \mu_{\mathbf{k}} v_{k_1}^{(1)} \otimes ... \otimes v_{k_d}^{(d)}, \quad \mu_{\mathbf{k}} = \langle v_{k_1}^{(1)} \otimes \cdots \otimes v_{k_d}^{(d)}, A\rangle,$$

so that the core tensor $\boldsymbol{\mu} = [\mu_{\mathbf{k}}]$, *can be represented in the rank-R canonical format*

$$\boldsymbol{\mu} = \sum_{\nu=1}^{R} \xi_\nu (V^{(1)^T} u_\nu^{(1)}) \otimes \cdots \otimes (V^{(d)^T} u_\nu^{(d)}) \in \boldsymbol{\mathcal{C}}_{R,\mathbf{r}}. \tag{2.31}$$

(d) Let $\sigma_{\ell,1} \geq \sigma_{\ell,2}... \geq \sigma_{\ell,\min(n,R)}$ *be the singular values of the* ℓ*-mode side-matrix* $U^{(\ell)} \in \mathbb{R}^{n\times R}$ $(\ell = 1, ..., d)$. *Then the RHOSVD approximation* $A^0_{(\mathbf{r})}$, *as in (2.28), exhibits the error estimate*

$$\|A - A^0_{(\mathbf{r})}\| \leq \|\boldsymbol{\xi}\| \sum_{\ell=1}^{d} (\sum_{k=r_\ell+1}^{\min(n,R)} \sigma_{\ell,k}^2)^{1/2}, \tag{2.32}$$

where $\|\boldsymbol{\xi}\| = \sqrt{\sum_{\nu=1}^{R} \xi_\nu^2}$.

Proof: (a) The generic dual maximization problem (2.20) with A given by (2.6), now takes the form (2.30) due to the relation

$$\langle y_{k_1}^{(1)} \otimes ... \otimes y_{k_d}^{(d)}, A\rangle = \sum_{\nu=1}^{R} \xi_\nu \langle y_{k_1}^{(1)}, u_\nu^{(1)}\rangle ... \langle y_{k_d}^{(d)}, u_\nu^{(d)}\rangle.$$

(b) The compatibility condition ensures the size-consistency of all matrix unfoldings. Let us assume that $n_\ell \leq R$ for definiteness. To justify the choice of $Z_0^{(\ell)}$, we notice that using the contracted product representation (2.7) of the canonical tensors $A \in \boldsymbol{\mathcal{C}}_{R,\mathbf{n}}$,

$$A = \boldsymbol{\xi} \times_1 U^{(1)} \times_2 U^{(2)} \cdots \times_d U^{(d)},$$

we have expansion (2.28) for the RHOSVD. Now we start from the error representation

$$\begin{aligned} A - A^0_{(\mathbf{r})} &= \boldsymbol{\xi} \times_1 U^{(1)} \times_2 U^{(2)} \cdots \times_d U^{(d)} \\ &- \boldsymbol{\xi} \times_1 \left[Z_0^{(1)} D_{1,0} W_0^{(1)^T} \right] \times_2 \left[Z_0^{(2)} D_{2,0} W_0^{(2)^T} \right] \cdots \times_d \left[Z_0^{(d)} D_{d,0} W_0^{(d)^T} \right] \\ &= \boldsymbol{\xi} \times_1 \left[U^{(1)} - Z_0^{(1)} D_{1,0} W_0^{(1)^T} \right] \times_2 \left[Z_0^{(2)} D_{2,0} W_0^{(2)^T} \right] \cdots \times_d \left[Z_0^{(d)} D_{d,0} W_0^{(d)^T} \right] \\ &+ \boldsymbol{\xi} \times_1 U^{(1)} \times_2 \left[U^{(2)} - Z_0^{(2)} D_{2,0} W_0^{(2)^T} \right] \cdots \times_d \left[Z_0^{(d)} D_{d,0} W_0^{(d)^T} \right] + ... \\ &+ \boldsymbol{\xi} \times_1 U^{(1)} \times_2 U^{(2)} \cdots \times_d \left[U^{(d)} - Z_0^{(d)} D_{d,0} W_0^{(d)^T} \right]. \end{aligned}$$

To proceed, we introduce

$$\Delta^{(\ell)} = U^{(\ell)} - Z_0^{(\ell)} D_{\ell,0} W_0^{(\ell)^T}, \quad U_0^{(\ell)} = Z_0^{(\ell)} D_{\ell,0} W_0^{(\ell)^T},$$

then the ℓth summand in the right-hand side above takes the form

$$B_\ell = \boldsymbol{\xi} \times_1 U^{(1)} \cdots \times_{\ell-1} U^{(\ell-1)} \times_\ell \Delta^{(\ell)} \times_{\ell+1} U_0^{(\ell+1)} \cdots \times_d U_0^{(d)}.$$

This leads to the error bound (by the triangle inequality)

$$\begin{aligned} \|A - A^0_{(\mathbf{r})}\| \le \sum_{\ell=1}^{d} \|B_\ell\| &= \|\boldsymbol{\xi} \times_1 \Delta^{(1)} \times_2 U_0^{(2)} \cdots \times_d U_0^{(d)}\| \\ &+ \|\boldsymbol{\xi} \times_1 U^{(1)} \times_2 \Delta^{(2)} \cdots \times_d U_0^{(d)}\| + ... \\ &+ \|\boldsymbol{\xi} \times_1 U^{(1)} \times_2 U^{(2)} \cdots \times_d \Delta^{(d)}\|. \end{aligned}$$

Here the ℓth term B_ℓ can be represented by

$$\sum_{\nu=1}^{R} \xi_\nu \otimes u_\nu^{(1)} \cdots \otimes u_\nu^{(\ell-1)} \otimes \sum_{k=r_\ell+1}^{n} \sigma_{\ell,k} z_k^{(\ell)} w_{k,\nu}^{(\ell)} \otimes \sum_{k=1}^{r_{\ell+1}} \sigma_{\ell+1,k} z_k^{(\ell+1)} w_{k,\nu}^{(\ell+1)} \cdots \otimes \sum_{k=1}^{r_d} \sigma_{d,k} z_k^{(d)} w_{k,\nu}^{(d)},$$

providing the estimate (take into account that $\|u_\nu^{(\ell)}\| = 1$, $\ell = 1, ..., d$, $\nu = 1, ..., R$)

$$\|B_\ell\| \le \sum_{\nu=1}^{R} |\xi_\nu| \Big(\sum_{k=r_\ell+1}^{n} \sigma_{\ell,k}^2 {w_{k,\nu}^{(\ell)}}^2 \Big)^{1/2} \cdot \Big(\sum_{k=1}^{r_{\ell+1}} \sigma_{\ell+1,k}^2 {w_{k,\nu}^{(\ell+1)}}^2 \Big)^{1/2} \cdots \Big(\sum_{k=1}^{r_d} \sigma_{d,k}^2 {w_{k,\nu}^{(d)}}^2 \Big)^{1/2}.$$

Recall that $U^{(\ell)}$ ($\ell = 1, ..., d$) has normalised columns, i.e., $1 = \|u_\nu^{(\ell)}\| = \| \sum_{k=1}^{n} \sigma_{\ell,k} z_k^{(\ell)} w_{k,\nu}^{(\ell)} \|$, implying $\sum_{k=1}^{n} \sigma_{\ell,k}^2 {w_{k,\nu}^{(\ell)}}^2 = 1$ for $\ell = 1, ..., d$ and $\nu = 1, ..., R$.

Hence, we finalise the error bound as follows,

$$\begin{aligned}
\|A - A^0_{(\mathbf{r})}\| &\leq \sum_{\ell=1}^{d}\sum_{\nu=1}^{R}|\xi_\nu|\left(\sum_{k=r_\ell+1}^{n}\sigma^2_{\ell,k}{w^{(\ell)}_{k,\nu}}^2\right)^{1/2} \\
&\leq \sum_{\ell=1}^{d}\left(\sum_{\nu=1}^{R}\xi^2_\nu\right)^{1/2}\left(\sum_{\nu=1}^{R}\sum_{k=r_\ell+1}^{n}\sigma^2_{\ell,k}{w^{(\ell)}_{k,\nu}}^2\right)^{1/2} \\
&= \sum_{\ell=1}^{d}\|\boldsymbol{\xi}\|\left(\sum_{k=r_\ell+1}^{n}\sigma^2_{\ell,k}\sum_{\nu=1}^{R}{w^{(\ell)}_{k,\nu}}^2\right)^{1/2} \\
&= \|\boldsymbol{\xi}\|\sum_{\ell=1}^{d}\left(\sum_{k=r_\ell+1}^{n}\sigma^2_{\ell,k}\right)^{1/2}.
\end{aligned}$$

The case $R < n$ can be analysed along the same line. Now item (d) follows. ■

We notice that the error estimate (2.32) in Theorem 2.14 actually provides the control of the RHOSVD approximation error via the computable ℓ-mode error bounds since, by the construction, we have

$$\|U^{(\ell)} - Z^{(\ell)}_0 D_{\ell,0} W^{(\ell)}_0\|^2_F = \sum_{k=r_\ell+1}^{n}\sigma^2_{\ell,k}, \quad \ell = 1, ..., d.$$

This result is similar to the well-known error estimate for the HOSVD approximation (see Theorem 2.12 and Property 10 in [24]).

Based on Theorem 2.14 the corresponding algorithm C_BTA for the rank-R input data can be designed by respective modifications of Steps 1, 2 in the general G_BTA scheme. In this way we note that each column of the ℓ-mode unfolding matrix $A_{(\ell)}$ for the rank-R canonical tensor in (2.6) can be represented as the weighted sum of the ℓ-mode canonical vectors $u^{(\ell)}_\nu$ ($\nu = 1, ..., R$) implying $rank(A_{(\ell)}) \leq R$. Keeping this modification in mind, the sketch of the new algorithm C_BTA reads as follows.

Algorithm C_BTA ($\boldsymbol{\mathcal{C}}_{R,\mathbf{n}} \to \boldsymbol{\mathcal{T}}_{\mathcal{C}_R,\mathbf{r}}$). Given $A \in \boldsymbol{\mathcal{C}}_{R,\mathbf{n}}$ in the form (2.6), an iteration parameter k_{max}, and the rank parameter $\mathbf{r}$.

1. For $\ell = 1, ..., d$ compute the truncated SVD of $U^{(\ell)}$ to obtain orthogonal matrices $Z^{(\ell)}_0 \in \mathbb{R}^{n_\ell \times r_\ell}$, representing the rank-$r_\ell$ RHOSVD approximation of ℓ-mode dominating subspaces (cost $O(dRn\min\{R, n\})$).

2. Given an initial guess $Z^{(\ell)}_0$, ($\ell = 1, ..., d$) for ℓ-mode orthogonal matrices. Perform k_{max} ALS iterations as at Step 2 in the general **G_BTA** algorithm to obtain the maximizer $V^{(\ell)} \in \mathbb{R}^{n_\ell \times r_\ell}$, $\ell = 1, ..., d$ (cost $O(dr^{d-1}n\min\{r^{d-1}, n\})$ per iteration).

3. Calculate projections of $U^{(\ell)}$ onto the basis of orthogonal vectors of $W^{(\ell)}$ as the matrix product ${V^{(\ell)}}^T U^{(\ell)}$ $(\ell = 1, ..., d)$, at the cost $O(drRn)$.

4. Using the columns in ${V^{(\ell)}}^T U^{(\ell)}$ $(\ell = 1, ..., d)$, calculate the rank-R core tensor $\boldsymbol{\mu} \in \boldsymbol{\mathcal{C}}_{R,\mathbf{r}}$ as in (2.31), in $O(drRn)$ operations and with $O(drR)$-storage.

Notice that Step 2 in Algorithm C_BTA ($\boldsymbol{\mathcal{C}}_{R,\mathbf{n}} \to \boldsymbol{\mathcal{T}}_{\mathcal{C}_R,\mathbf{r}}$) above is not mandatory. It can be omitted if the initial guess $Z_0^{(\ell)}$ turns out to be "good enough" with respect to chosen threshold criterion (see estimate (2.32)). Our numerical study indicates that in the case of tensors related to the class of functions describing physical quantities in electronic structure calculations, Step 2 in the C2T transform is not required.

The following remark addresses the complexity issues.

Remark 2.15 *Algorithm C_BTA ($\boldsymbol{\mathcal{C}}_{R,\mathbf{n}} \to \boldsymbol{\mathcal{T}}_{\mathcal{C}_R,\mathbf{r}}$) exhibits polynomial cost in R, r, n,*

$$O(dRn \min\{n, R\} + dr^{d-1} n \min\{r^{d-1}, n\}),$$

with exponential scaling in d. In absence of Step 2 (if RHOSVD provides a satisfactory approximation), the algorithm does not contain iteration loops, and for any $d \geq 2$ it is a finite SVD-based scheme.

Numerical tests show that Algorithm C_BTA($\boldsymbol{\mathcal{C}}_{R,\mathbf{n}} \to \boldsymbol{\mathcal{T}}_{\mathcal{C}_R,\mathbf{r}}$) is efficient for moderate R and n, in particular, it works well in electronic structure calculations on 3D Cartesian grids for moderate grid size $n \lesssim 10^3$ and for $R \leq 10^3$. However, in real life applications the computations may require one-dimension grid sizes in the range $n_\ell \lesssim 3 \cdot 10^4$, $(\ell = 1, 2, 3)$ with canonical ranks $R \leq 10^4$. Therefore, to get rid of a polynomial scaling in R, n, r for 3D applications, we develop new generation of best Tucker approximation methods based on the idea of multigrid acceleration of the nonlinear ALS iteration, introduced in Section 3.

2.2.4 Mixed BTA for full format and Tucker tensors

A further reduction of numerical complexity for the Tucker model is based on the concept of the *mixed (two-level) Tucker-canonical* approximation [60, 67, 68], see Definition 2.8. The main idea of the mixed approximation consists of a rank-structured representation to the Tucker core $\boldsymbol{\beta}$ in certain tensor classes $\mathcal{S} \subset \mathbb{B}_{\mathbf{r}}$. In particular, we consider a class $\mathcal{S} = \boldsymbol{\mathcal{C}}_{R,\mathbf{r}}$ of rank-R canonical tensors, i.e., $\boldsymbol{\beta} \in \boldsymbol{\mathcal{C}}_{R,\mathbf{r}}$.

In the case of full format tensors, the two-level version of Algorithm G_BTA ($\mathbb{V}_{\mathbf{n}} \to \boldsymbol{\mathcal{T}}_{\mathbf{r},\mathbf{n}}$) can be described as the following computation chain,

$$\mathbb{V}_{\mathbf{n}} \overset{I}{\to} \boldsymbol{\mathcal{T}}_{\mathbf{r},\mathbf{n}} \overset{II}{\to} \boldsymbol{\mathcal{T}}_{\mathcal{C}_{R,\mathbf{r}}} \subset \boldsymbol{\mathcal{C}}_{R,\mathbf{n}},$$

where the Level-I is understood as application of Algorithm G_BTA ($\mathbb{V}_{\mathbf{n}} \to \boldsymbol{\mathcal{T}}_{\mathbf{r},\mathbf{n}}$) and the Level-II includes the rank-R canonical approximation to the small size Tucker core $\boldsymbol{\beta} \in \mathbb{B}_{\mathbf{r}}$. Figure 2.2 illustrates the computational scheme of the two-level Tucker approximation.

In the case of function related tensors, our goal is to compute the Level-I approximation with linear cost in the size of the input data (see Section 3.3).

If the input tensor A_0 is already presented in the rank-$\mathbf{r}$ Tucker format then one can apply the following Lemma 2.16. This lemma presents a simple but useful characterisation of the mixed (two-level) Tucker model (cf. [60, 67]) which allows to approximate the elements in $\boldsymbol{\mathcal{T}}_{\mathbf{r}}$ via the canonical decomposition applied to the small sized core tensor.

Lemma 2.16 *(Mixed Tucker-to-canonical approximation).*
Let the target tensor $A \in \boldsymbol{\mathcal{T}}_{\mathbf{r},\mathbf{n}}$ in (2.12) have the form $A = \boldsymbol{\beta} \times_1 V^{(1)} \times_2 ... \times_d V^{(d)}$ with the orthogonal side-matrices $V^{(\ell)} = [v_1^{(\ell)} \dots v_{r_\ell}^{(\ell)}] \in \mathbb{R}^{n \times r_\ell}$ and with $\boldsymbol{\beta} \in \mathbb{R}^{r_1 \times \dots \times r_d}$. Then, for a given $R \leq \min\limits_{1 \leq \ell \leq d} \overline{r}_\ell$ (see (2.37), (2.38)),

$$\min_{Z \in \boldsymbol{\mathcal{C}}_{R,\mathbf{n}}} \|A - Z\| = \min_{\boldsymbol{\mu} \in \boldsymbol{\mathcal{C}}_{R,\mathbf{r}}} \|\boldsymbol{\beta} - \boldsymbol{\mu}\|. \tag{2.33}$$

Assume that there exists a best rank-R approximation $A_{(R)} \in \boldsymbol{\mathcal{C}}_{R,\mathbf{n}}$ of A, then there is a best rank-R approximation $\boldsymbol{\beta}_{(R)} \in \boldsymbol{\mathcal{C}}_{R,\mathbf{r}}$ of $\boldsymbol{\beta}$, such that

$$A_{(R)} = \boldsymbol{\beta}_{(R)} \times_1 V^{(1)} \times_2 ... \times_d V^{(d)}. \tag{2.34}$$

Proof: Below we present the more detailed proof compared with the sketch in Lemma 2.5, [67]. Notice that the canonical vectors $y_k^{(\ell)}$ of any test element (see (2.6)) in the left-hand side of (2.33),

$$Z = \sum_{k=1}^{R} \lambda_k \, y_k^{(1)} \otimes ... \otimes y_k^{(d)} \in \boldsymbol{\mathcal{C}}_{R,\mathbf{n}}, \tag{2.35}$$

can be chosen in $span\{v_1^{(\ell)}, \dots, v_{r_\ell}^{(\ell)}\}$, i.e.,

$$y_k^{(\ell)} = \sum_{m=1}^{r_\ell} \mu_{k,m}^{(\ell)} v_m^{(\ell)}, \quad k = 1, \dots, R, \ \ell = 1, ..., d. \tag{2.36}$$

Indeed, assuming

$$y_k^{(\ell)} = \sum_{m=1}^{r_\ell} \mu_{k,m}^{(\ell)} v_m^{(\ell)} + E_k^{(\ell)} \quad \text{with} \quad E_k^{(\ell)} \perp span\{v_1^{(\ell)}, \dots, v_{r_\ell}^{(\ell)}\},$$

we conclude that $E_k^{(\ell)}$ does not effect the cost function in (2.33) because of the orthogonality of $V^{(\ell)}$. Hence, setting $E_k^{(\ell)} = 0$, and substituting (2.36) into (2.35), we arrive at the desired Tucker decomposition of Z,

$$Z = \boldsymbol{\beta}_z \times_1 V^{(1)} \times_2 \ldots \times_d V^{(d)}, \quad \boldsymbol{\beta}_z \in \boldsymbol{\mathcal{C}}_{R,\mathbf{r}}.$$

This implies

$$\|A - Z\|^2 = \|(\boldsymbol{\beta}_z - \boldsymbol{\beta}) \times_1 V^{(1)} \times_2 \ldots \times_d V^{(d)}\|^2 = \|\boldsymbol{\beta} - \boldsymbol{\beta}_z\|^2 \geq \min_{\mu \in \boldsymbol{\mathcal{C}}_{R,\mathbf{r}}} \|\boldsymbol{\beta} - \boldsymbol{\mu}\|^2.$$

On the other hand, we have

$$\min_{Z \in \boldsymbol{\mathcal{C}}_{R,\mathbf{n}}} \|A - Z\|^2 \leq \min_{\boldsymbol{\beta}_z \in \boldsymbol{\mathcal{C}}_{R,\mathbf{r}}} \|(\boldsymbol{\beta} - \boldsymbol{\beta}_z) \times_1 V^{(1)} \times_2 \ldots \times_d V^{(d)}\|^2 = \min_{\boldsymbol{\mu} \in \boldsymbol{\mathcal{C}}_{R,\mathbf{r}}} \|\boldsymbol{\beta} - \boldsymbol{\mu}\|^2.$$

Hence, we arrive at (2.33).

Likewise, for any minimizer $A_{(R)} \in \boldsymbol{\mathcal{C}}_{R,\mathbf{n}}$ in the right-hand side of (2.33), we obtain

$$A_{(R)} = \boldsymbol{\beta}_{(R)} \times_1 V^{(1)} \times_2 V^{(2)} \ldots \times_d V^{(d)}$$

with the respective rank-R core tensor

$$\boldsymbol{\beta}_{(R)} = \sum_{k=1}^{R} \lambda_k u_k^{(1)} \otimes \ldots \otimes u_k^{(d)} \in \boldsymbol{\mathcal{C}}_{R,\mathbf{r}},$$

where $u_k^{(\ell)} = \{\mu_{k,m_\ell}^{(\ell)}\}_{m_\ell=1}^{r_\ell} \in \mathbb{R}^{r_\ell}$, are calculated by using representation (2.36), and then changing the order of summation,

$$\begin{aligned} A_{(R)} &= \sum_{k=1}^{R} \lambda_k y_k^{(1)} \otimes \ldots \otimes y_k^{(d)} \\ &= \sum_{k=1}^{R} \lambda_k \left(\sum_{m_1=1}^{r_1} \mu_{k,m_1}^{(1)} v_{m_1}^{(1)} \right) \otimes \ldots \otimes \left(\sum_{m_d=1}^{r_d} \mu_{k,m_d}^{(d)} v_{m_d}^{(d)} \right) \\ &= \sum_{m_1=1}^{r_1} \ldots \sum_{m_d=1}^{r_d} \left\{ \sum_{k=1}^{R} \lambda_k \prod_{\ell=1}^{d} \mu_{k,m_\ell}^{(\ell)} \right\} v_{m_1}^{(1)} \otimes \ldots \otimes v_{m_d}^{(d)}. \end{aligned}$$

Now the relation (2.34) implies that

$$\|A - A_R\| = \|\boldsymbol{\beta} - \boldsymbol{\beta}_{(R)}\|,$$

since the ℓ-mode multiplication with orthogonal side matrices $V^{(\ell)}$ does not change the cost function. Using the already proven relation (2.33) this indicates that $\boldsymbol{\beta}_{(R)}$ is the minimizer in the right-hand side of (2.33). ■

Lemma 2.16 means that the corresponding low rank Tucker-canonical approximation of $A \in \boldsymbol{\mathcal{T}}_{\mathbf{r},\mathbf{n}}$ can be reduced to the canonical approximation of a small-size core tensor.

Lemma 2.16 suggests a two-level dimensionality reduction approach that leads to a better data structure compared with the standard Tucker model. Though $A_{(R)} \in \boldsymbol{\mathcal{C}}_{R,\mathbf{n}}$ can be represented in the mixed Tucker-canonical format, its efficient storage depends on further multilinear operations. In fact, if the resultant tensor is further used in scalar, Hadamard or convolution products with canonical tensors, it is better to store $A_{(R)}$ in the canonical format of the complexity rdn.

2.2.5 Remarks on the Tucker-to-canonical transform

In the rank reduction scheme for the canonical rank-R tensors, we use consequently the canonical-to-Tucker (C2T) transform and then the Tucker-to-canonical (T2C) tensor approximation. Next, we give two useful remarks which characterize the canonical representation of the full format tensors.

Remark 2.17 applied to the Tucker core tensor of the size $r \times r \times r$, indicates that the ultimate canonical rank of a large-size tensor in $\mathbb{V}_{\mathbf{n}}$ has the upper bound r^2. According to Remark 2.18, its canonical rank can be reduced to a smaller value using the SVD-based truncation procedure up to a fixed tolerance $\varepsilon > 0$.

Denote by $\overline{n}_\ell$ the single-hole product of ℓ-mode dimensions

$$\overline{n}_\ell = n_1 \cdots n_{\ell-1} n_{\ell+1} \cdots n_d. \tag{2.37}$$

Remark 2.17 *The canonical rank of a tensor $A \in \mathbb{V}_{\mathbf{n}}$ has the upper bound*

$$R \leq \min_{1 \leq \ell \leq d} \overline{n}_\ell. \tag{2.38}$$

Proof: First, consider the case $d = 3$. Let $n_1 = \max\limits_{1 \leq \ell \leq d} n_\ell$ for definiteness. We can represent a tensor A as

$$A = \sum_{k=1}^{n_3} B_k \otimes Z_k, \quad B_k \in \mathbb{R}^{n_1 \times n_2},\ Z_k \in \mathbb{R}^{n_3},$$

where $B_k = A(:,:,k)$ $(k = 1, \ldots, n_3)$ is the $n_1 \times n_2$ matrix slice of A and $Z_k(i) = 0$, for $i \neq k$, $Z_k(k) = 1$. Let $rank(B_k) = r_k \leq n_2$, $k = 1, \ldots, n_3$, then

$$rank(B_k \otimes Z_k) = rank(B_k) \leq n_2,$$

and we obtain

$$rank(A) \leq \sum_{n=1}^{n_3} rank(B_k) \leq n_2 n_3 = \min_{1 \leq \ell \leq 3} \overline{n}_\ell.$$

The general case of $d > 3$ can be proven similarly by induction argument. ■

The next remark shows that the maximal canonical rank of the Tucker core of 3rd order tensor can be easily reduced to the value $\leq r^2$ by the SVD-based procedure. Though, being not practically attractive for arbitrary high order tensors, the simple algorithm described in Remark 2.18 is proved to be useful for the treatment of small size 3rd order Tucker core tensors in the rank reduction algorithms described in the previous sections.

Remark 2.18 *Let $d = 3$ for the sake of clearness. There is a simple procedure based on SVD to reduce the canonical rank of the core tensor $\boldsymbol{\beta}$, within the accuracy $\varepsilon > 0$. Denote by $B_m \in \mathbb{R}^{r\times r}$, $m = 1, ..., r$ the two-dimensional slices of $\boldsymbol{\beta}$ in some fixed mode. Hence, we can represent*

$$\boldsymbol{\beta} = \sum_{m=1}^{r} B_m \otimes Z_m, \quad Z_m \in \mathbb{R}^r, \tag{2.39}$$

where $Z_m(m) = 1$, $Z_m(j) = 0$ for $j = 1, \ldots, r$, $j \neq m$ (there are exactly d possible decompositions). Let p_m be the minimal integer, such that the singular values of B_m satisfy $\sigma_k^{(m)} \leq \frac{\varepsilon}{r^{3/2}}$ for $k = p_m + 1, ..., r$ (if $\sigma_r^{(m)} > \frac{\varepsilon}{r^{3/2}}$, then set $p_m = r$). Then, denoting by

$$B_{p_m} = \sum_{k_m=1}^{p_m} \sigma_{k_m}^{(m)} u_{k_m} \otimes v_{k_m},$$

the corresponding rank-p_m approximation to B_m (by truncation of $\sigma_{p_m+1}^{(m)}, ..., \sigma_r^{(m)}$), we arrive at the rank-R canonical approximation to $\boldsymbol{\beta}$,

$$\boldsymbol{\beta}_{(R)} := \sum_{m=1}^{r} B_{p_m} \otimes Z_m, \quad Z_m \in \mathbb{R}^r, \tag{2.40}$$

providing the error estimate

$$\|\boldsymbol{\beta} - \boldsymbol{\beta}_{(R)}\| \leq \sum_{m=1}^{r} \|B_m - B_{p_m}\| = \sum_{m=1}^{r} \sqrt{\sum_{k_m=p_m+1}^{r} (\sigma_{k_m}^{(m)})^2} \leq \sum_{m=1}^{r} \sqrt{r\frac{\varepsilon^2}{r^3}} = \varepsilon$$

Representation (2.40) is a sum of rank-p_m terms so that the total rank is bounded by $R \leq p_1 + ... + p_r \leq r^2$.

This approach can be easily extended to arbitrary $d \geq 3$ with the bound $R \leq r^{d-1}$.

2.3 Numerics on BTA of function related tensors in $\mathbb{R}^3$

2.3.1 General description

Here we discuss the best rank-$\mathbf{r}$ Tucker decomposition of 3D tensors arising as discretization of classical potentials.

For a given continuous function $g : \Omega \to \mathbb{R}$, $\Omega := \prod_{\ell=1}^{d}[a_\ell, b_\ell] \subset \mathbb{R}^d$, $-\infty < a_\ell < b_\ell < \infty$, we introduce the collocation-type function related tensor of order d by

$$A_0 \equiv A_0(g) := [a_{i_1 \ldots i_d}] \in \mathbb{R}^{I_1 \times \ldots \times I_d} \text{ with } \; a_{i_1 \ldots i_d} := g(x_{i_1}^{(1)}, \ldots, x_{i_d}^{(d)}),$$

where $(x_{i_1}^{(1)}, \ldots, x_{i_d}^{(d)}) \in \mathbb{R}^d$ are grid collocation points, indexed by $\mathcal{I} = I_1 \times \ldots \times I_d$,

$$x_{i_\ell}^{(\ell)} = a_\ell + \left(i_\ell - \frac{1}{2}\right)\left(\frac{b_\ell - a_\ell}{n_\ell}\right), \quad i_\ell = 1, 2, \ldots, n_\ell, \; \ell = 1, \ldots, d, \tag{2.41}$$

which are the midpoints of n_ℓ equally spaced subintervals with the size $h_\ell = \frac{b_\ell - a_\ell}{n_\ell}$, in the intervals $[a_\ell, b_\ell]$, corresponding to mode ℓ. We are interested in the validity and the rank-dependence of the Tucker approximations to the function related tensors discretized on 3D Cartesian grid.

The initial tensor A_0 is approximated by a rank $\mathbf{r} = (r, ..., r)$ Tucker tensor, where the rank-parameter r increases from $r = 1, 2, ...$ to some predefined value, r_{max}. The orthogonal Tucker vectors and the core tensor of the size $r \times r \times r$ are then used for the construction of the approximating tensor $A_{(r)} \approx A_0$, for estimating the approximation properties of the tensor decomposition with the given rank. For every Tucker rank $\mathbf{r}$ in the respective range, we compute the relative error in the Frobenius norm as in (2.2)

$$E_{FN} = \frac{\|A_0 - A_{(r)}\|}{||A_0||}, \tag{2.42}$$

the relative difference of norms

$$E_{FE} = \frac{\|A_0\| - \|A_{(r)}\|}{||A_0||}, \tag{2.43}$$

as well as the relative maximum norm

$$E_C := \frac{\max_{i \in \mathcal{I}} |a_{0,i} - a_{r,i}|}{\max_{i \in \mathcal{I}} |a_{0,i}|}. \tag{2.44}$$

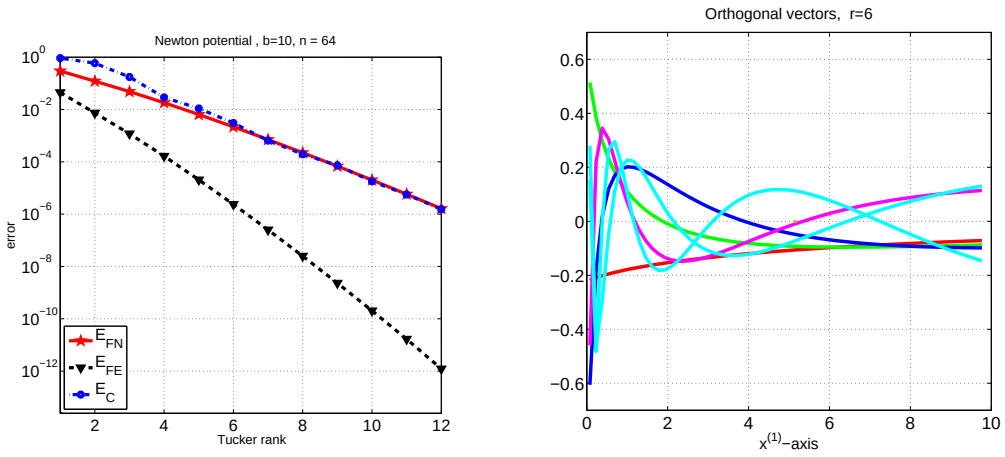

Figure 2.4: Convergence in the corresponding norms with respect to the Tucker rank r (left) and orthogonal vectors $v_k^{(1)}$, $k = 1, \ldots, 6$, (right) for the Tucker approximation to the Newton potential.

2.3.2 Numerics for classical potentials

We apply the numerical BTA algorithms to the full format tensors, and study the Tucker decomposition properties of the tensors generated by the Newton kernel, the Slater-type, Yukawa and Helmholtz functions in $\mathbb{R}^d$, $d = 3$.

1. Newton kernel

We apply the best rank-$\mathbf{r}$ Tucker decomposition algorithm with $\mathbf{r} = (r, ..., r)$ for approximating the Newton potential

$$g(x) = \frac{1}{\|x\|}, \quad x \in \mathbb{R}^3,$$

in the cube $[0, b]^3$ with $b = 10$, on the cell-centred uniform grid with $n = 64$. Here and in the following $\|x\| = \sqrt{\sum_{\ell=1}^{d} x_\ell^2}$ denotes the Euclidean norm of $x \in \mathbb{R}^d$. Due to spherical symmetry of the function, we consider the same sampling points $x_i^{(\ell)} = h/2 + (i-1)h$ for all space variables. Figure 2.4, left shows stable exponential convergence of the relative Frobenius, FE and maximum norms with respect to the Tucker rank up to $r = 12$. The right hand side of Figure 2.4 shows the orthogonal vectors $v_k^{(1)}$, $k = 1, \ldots, 6$, for the mode $\ell = 1$ ($x^{(1)}$-axis). The absolute error for the Tucker approximation with rank $r = 14$ in the cross-section $S := [h/2, b - h/2] \times [h/2, b - h/2] \times h/2$ is shown in Figure 2.5, where the maximum value is of the order $\sim 10^{-7}$. Figure 2.9 presents matrix slices $M_{\boldsymbol{\beta},\nu_r} \in \mathbb{R}^{9\times 9\times 1}$, $\nu_r = 1, \ldots 9$, of the core tensor $\boldsymbol{\beta} \in \mathbb{R}^{9\times 9\times 9}$ (see (2.8)), where the

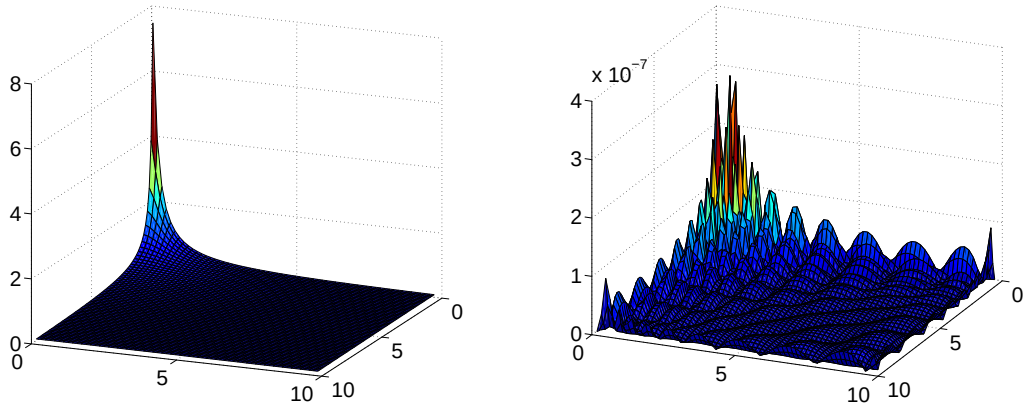

Figure 2.5: Left: the 3D Newton potential over cross-section $S = [h/2, b - h/2] \times [h/2, b - h/2] \times h/2$, right: the absolute approximation error for the Tucker decomposition with rank $r = 14$ ($\max \sim 10^{-7}$).

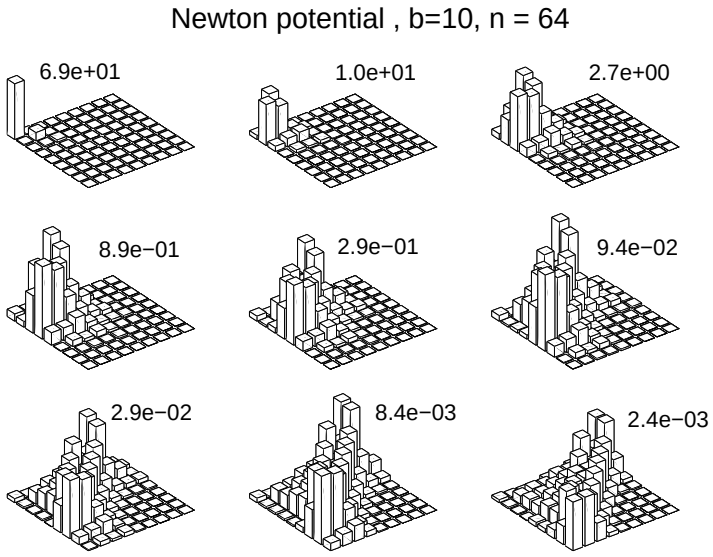

Figure 2.6: Coefficients of the core tensor $\boldsymbol{\beta} \in \mathbb{R}^{9\times9\times9}$ for the Tucker approximation of the Newton potential. We show the maximum values of $|\beta_{\boldsymbol{\nu}}|$ for every matrix slice $M_{\boldsymbol{\beta},\nu_r} \in \mathbb{R}^{9\times9\times1}$, $\nu_r = 1, \ldots, 9$, of $\boldsymbol{\beta}$.

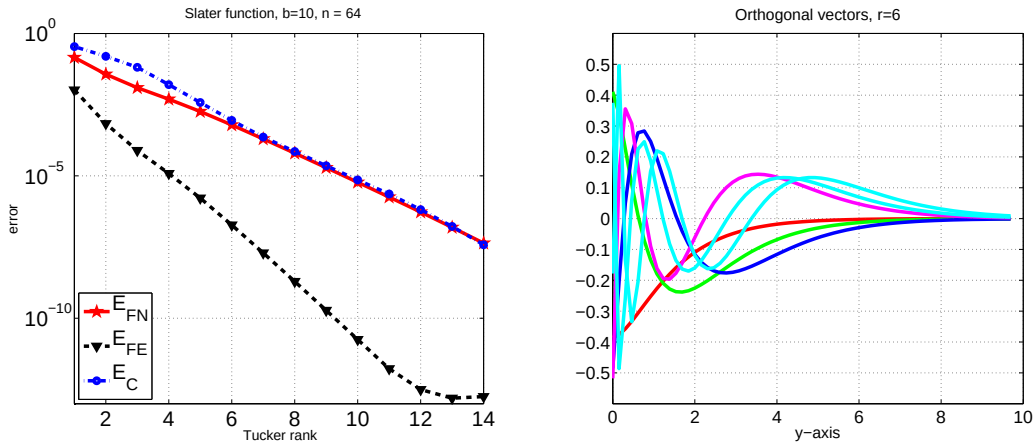

Figure 2.7: Convergence history and orthogonal vectors of the Tucker side matrix $V^{(1)} \in \mathbb{R}^{n \times r_1}$, $r_1 = 6$, for the Slater potential.

numbers indicate the maximum values of $|\beta_{\boldsymbol{\nu}}|$ at a given slice $M_{\boldsymbol{\beta},\nu_r}$ of $\boldsymbol{\beta}$.

Figure 2.6 shows the decay of the entries of the core tensor $\boldsymbol{\beta}$ for the Tucker decomposition with the rank $r = 9$ (smaller ranks are chosen for simplicity of visualization). We observe that for the particular class of function related tensors $A_0 \in \mathbb{V}_{\mathbf{n}}$, the core tensor $\boldsymbol{\beta} \in \mathbb{B}_{\mathbf{r}}$ turns out to be sparse (up to a certain threshold). We further demonstrate that the sparsity of the representation coefficients of the target tensor in the space $\mathbb{B}_{\mathbf{r}}$ will be even stronger for the physically relevant functions with strong singularities arising in electronic structure calculations.

2. Slater function

We are interested in the approximate low-rank representation of the Slater type functions which play significant role in electronic structure calculations.

The Slater function given by

$$g(x) = \exp(-\alpha\|x\|) \quad \text{with} \quad x = (x_1, x_2, x_3)^T \in \mathbb{R}^3,$$

presents the electron "orbital" ($\alpha = 1$) and the electron density function ($\alpha = 2$) corresponding to the Hydrogen atom. We compute the rank-(r, r, r) Tucker approximation to the function related tensor defined on the same grid as in the previous section, with $b = 10$.

Figure 2.7 shows that the Slater function can be efficiently approximated by low rank Tucker tensors. In fact, Tucker rank $r = 14$ provides a maximum absolute error of the approximation of order $\sim 10^{-8}$, see Figure 2.8.

Figure 2.9 presents the matrix slices $M_{\boldsymbol{\beta},\nu_r} \in \mathbb{R}^{9\times9\times1}$, $\nu_r = 1, \ldots, 9$, of the core tensor $\boldsymbol{\beta} \in \mathbb{R}^{9\times9\times9}$, where the numbers indicate the maximum values of the core entries at a given slice $M_{\boldsymbol{\beta},\nu_r} \in \mathbb{R}^{9\times9\times1}$ of $\boldsymbol{\beta}$. Figure shows that the "energy" of

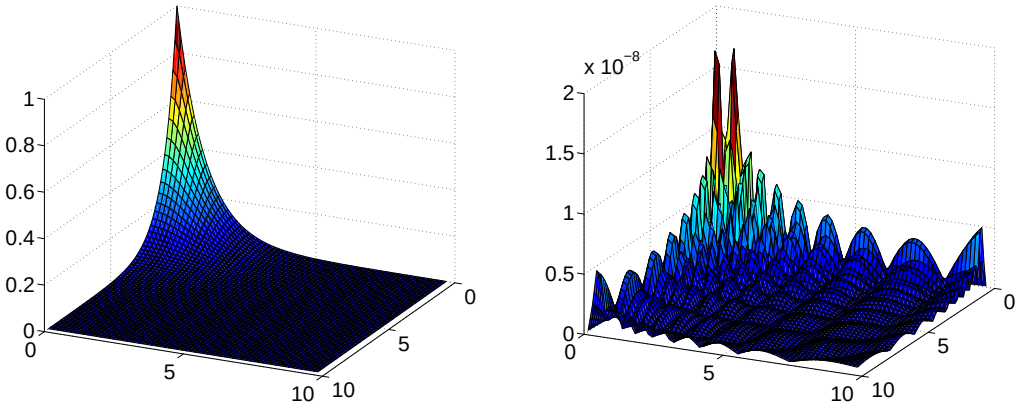

Figure 2.8: Left: the 3D Slater function in the cross-section $S = [0, b-h] \times [0, b-h] \times \{0\}$, right: the absolute approximation error for the Tucker decomposition with rank $r = 14$ (max $\sim 10^{-8}$), for the same section.

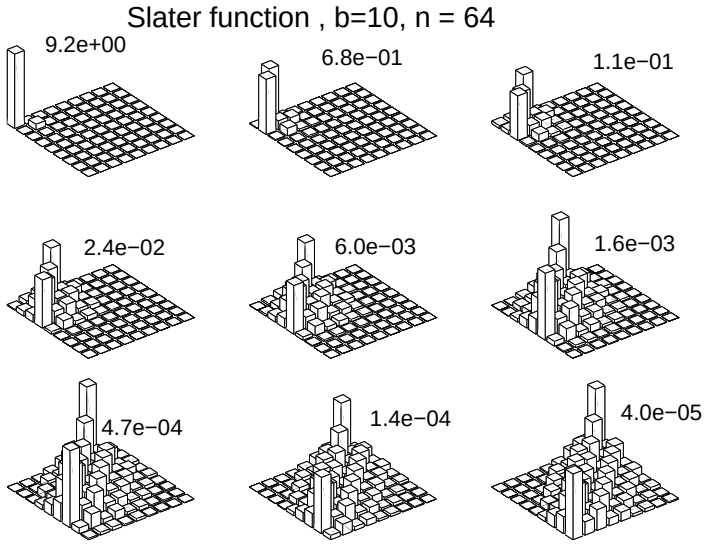

Figure 2.9: Coefficients of the core tensor $\boldsymbol{\beta} \in \mathbb{R}^{9\times9\times9}$ for the Tucker approximation of the Slater function. We show the maximum values of $|\beta_{\boldsymbol{\nu}}|$ for every matrix slice $M_{\boldsymbol{\beta},\nu_r} \in \mathbb{R}^{9\times9\times1}$, $\nu_r = 1, \ldots, 9$, of $\boldsymbol{\beta}$.

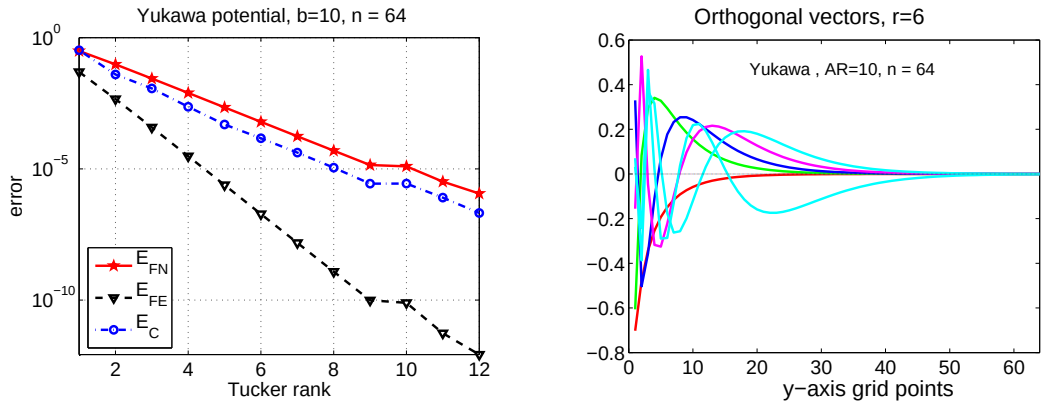

Figure 2.10: Tucker approximation of the Yukawa potential and an example of the Tucker orthogonal vectors $v_k^{(2)}$, $k = 1, \ldots, 6$, (right).

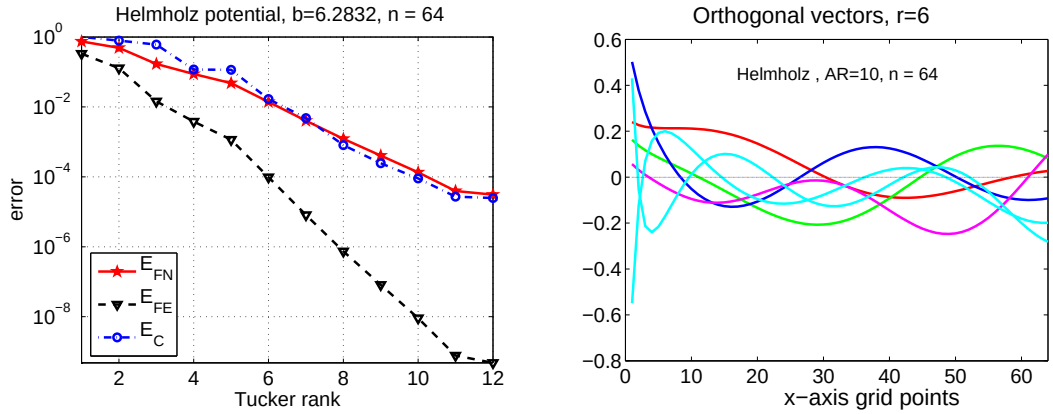

Figure 2.11: Convergence history (left) and orthogonal vectors $v_k^{(1)}$, $k = 1, \ldots, 6$, (right) for the Tucker approximation of the Helmholtz potential.

the decomposed function is concentrated in several upper slices of the core tensor. Our numerical experiments show that the dominating entries in $\boldsymbol{\mathcal{B}}$ are compactly concentrated in its "upper left corner". This feature of the Tucker decomposition will be employed further in Section 3.

3. Yukawa and Helmholtz Functions

In the next example, we consider a Tucker approximation of the third-order function-related tensor generated by the Yukawa potential

$$g(x) = \frac{e^{-\|x\|}}{\|x\|} \quad \text{with} \quad x = (x_1, x_2, x_3)^T \in \mathbb{R}^3.$$

We consider the function related tensor with the same "voxel-centred" collocation

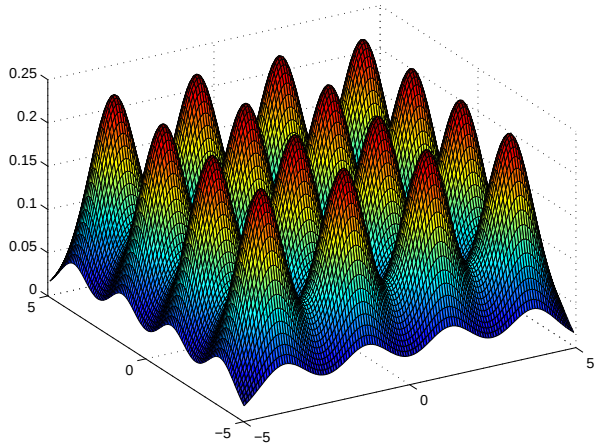

Figure 2.12: A slice of a 3D multi-centred Slater potential with 4^3 centers.

points with respect to the $n \times n \times n$-grid over $[0, b]^3$ with $b = 10$ as in previous examples.

Figure 2.10 shows the convergence history and the orthogonal vectors $v_k^{(2)}$, $k = 1, \ldots, 6$, of the Tucker decomposition of the Yukawa potential. These vectors represent the problem adaptive orthogonal basis. In almost all cases the ALS iteration to compute the Tucker approximation converges very fast and it is terminated at most after 5 iterations.

Fig. 2.11 provides computational results for the Helmholtz function given by

$$g(x) = \frac{\cos \|x\|}{\|x\|} \quad \text{with} \quad x = (x_1, x_2, x_3)^T \in \mathbb{R}^3,$$

indicating robust convergence in the considered applications.

5. Periodic structures of Slater functions

Finally, we analyse the "multi-centered Slater potential" obtained by displacing a single Slater function with respect to the $m \times m \times m$ spatial grid of step-size $H > 0$, specifying centers of Slater functions,

$$g(x) = c \sum_{i=1}^{m} \sum_{j=1}^{m} \sum_{k=1}^{m} e^{-\alpha \sqrt{(x_1 - iH + \frac{m+1}{2}H)^2 + (x_2 - jH + \frac{m+1}{2}H)^2 + (x_3 - kH + \frac{m+1}{2}H)^2}}. \quad (2.45)$$

Figure 2.12 shows the multi-centred Slater potential for $m = 4$, $H = 3$, $\alpha = 2$ and the corresponding approximation error in the cube $[-5, 5]^3$ on the $n \times n \times n$ grid with $n = 64$, the surface level corresponds to $x_3 = 2$. Convergence is shown in Figure 2.15 (left-top).

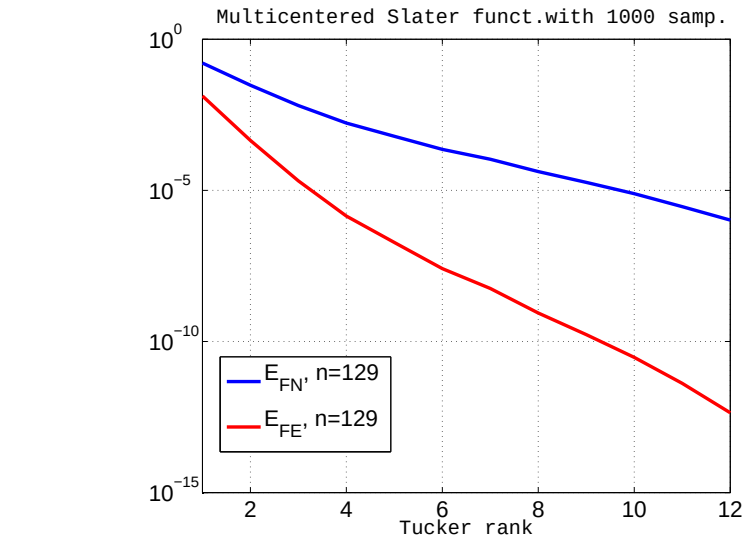

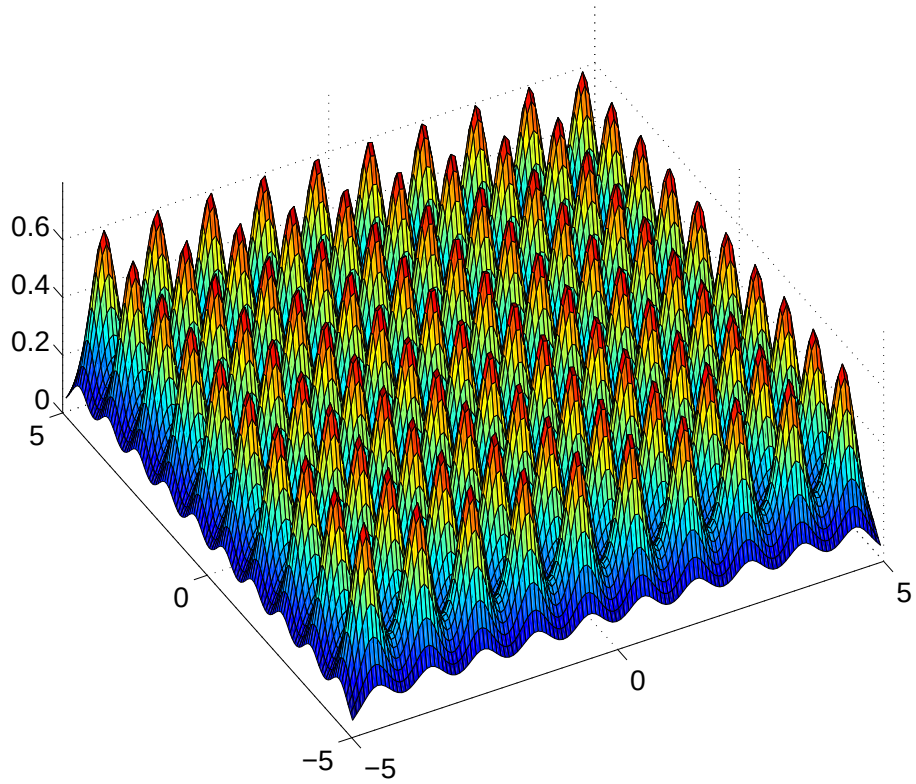

Figure 2.13: Top: rank-convergence of the Tucker approximation for the multi-centered Slater potential with 10^3 cells ; bottom: a 2D plane section of the 3rd order tensor representing the multi-centred Slater potential with 10^3 centers.

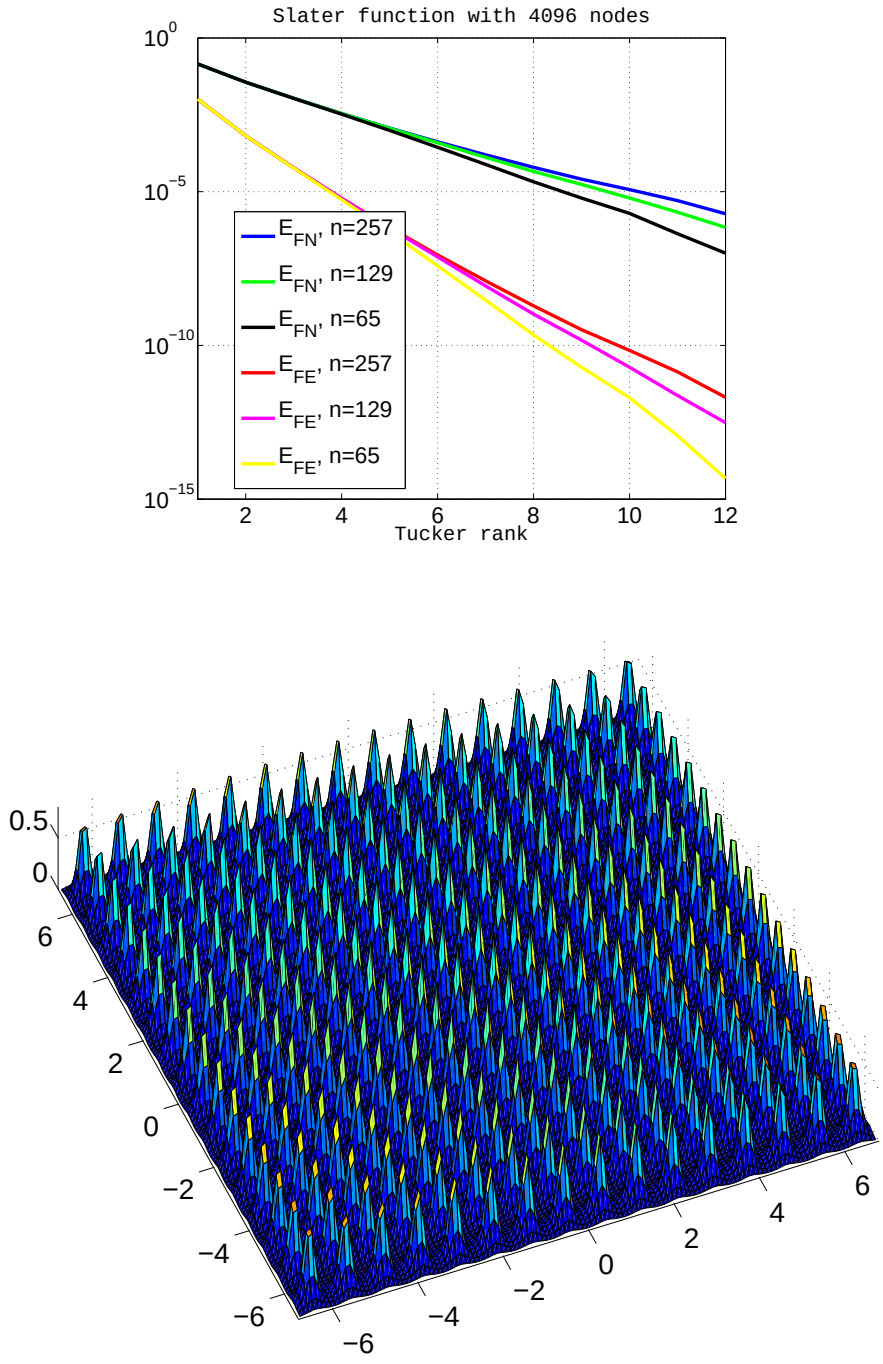

Figure 2.14: Top: convergence of G_BTA applied to the multi-centered Slater potential with 4096 cells with respect to the Tucker rank; bottom: a 2D plane section of the 3rd order tensor corresponding to the multi-centred Slater potential with 4096 centers.

Next, we consider function related tensors with a large number of periodic cells. Figure 2.13 (top) shows the convergence history for the tensor corresponding to the multicentered Slater function with 10^3 centers. Figure 2.13 (bottom) visualizes a 2D plane section of this 3rd order tensor. Figures 2.14 show the approximating error and a 2D plane section of a 3rd order tensor representing the multicentered Slater function with 4096 cells. Note, that the Tucker approximation using the grid size $n = 257$, is computationally feasible only when applying the MGA Tucker algorithm which we introduce in Section 3.

Investigation of these periodic structures show, that the convergence rate of the rank-(r, r, r) Tucker approximation practically does not depend on the number of cells in a considered structure. It is demonstrated that in all cases for the Slater function (see convergence of the multicentered Slater function in Figures 2.13, 2.14 and the convergence for a single Slater function in Figure 2.7), equal rank parameters imply equal accuracy of the Tucker approximation. For example, for the Tucker rank $r = 10$, it is exactly 10^{-5} for all versions of the single/multicentered Slater function. This feature can be valuable, in the grid-based modelling of periodic (or nearly periodic) structures in the density functional theory. It indicates that the Tucker decomposition can be helpful in constructing of a small number of problem-adapted basis functions for huge (almost) periodic clusters of atoms.

6. Multicentered Slater function with random perturbations

Results in the case of the Slater potential which entries are perturbed randomly are given in Figure 2.15. The random constituent equals to 1, 0.1 and 0.01 percents of the maximum amplitude. It is shown that the exponential convergence in the Tucker rank is observed only until the approximation level of the order of the random perturbation. Further increase in the Tucker rank does not improve essentially the approximation.

7. Conclusions to Section 2.3.2

The numerical examples for the function related tensors presented in Section 2.3.2 have led to further development of the Tucker-based algorithms for the problems in electronic structure calculations. Here we formulate some conclusions to above numerics.

Remark 2.19 *The Tucker approximation error for the considered class of function related tensors decays exponentially with respect to the Tucker rank.*

Remark 2.20 *The shape of the orthogonal vectors in the unitary matrices of the Tucker decomposition for the class of function related tensors is almost independent on n.*

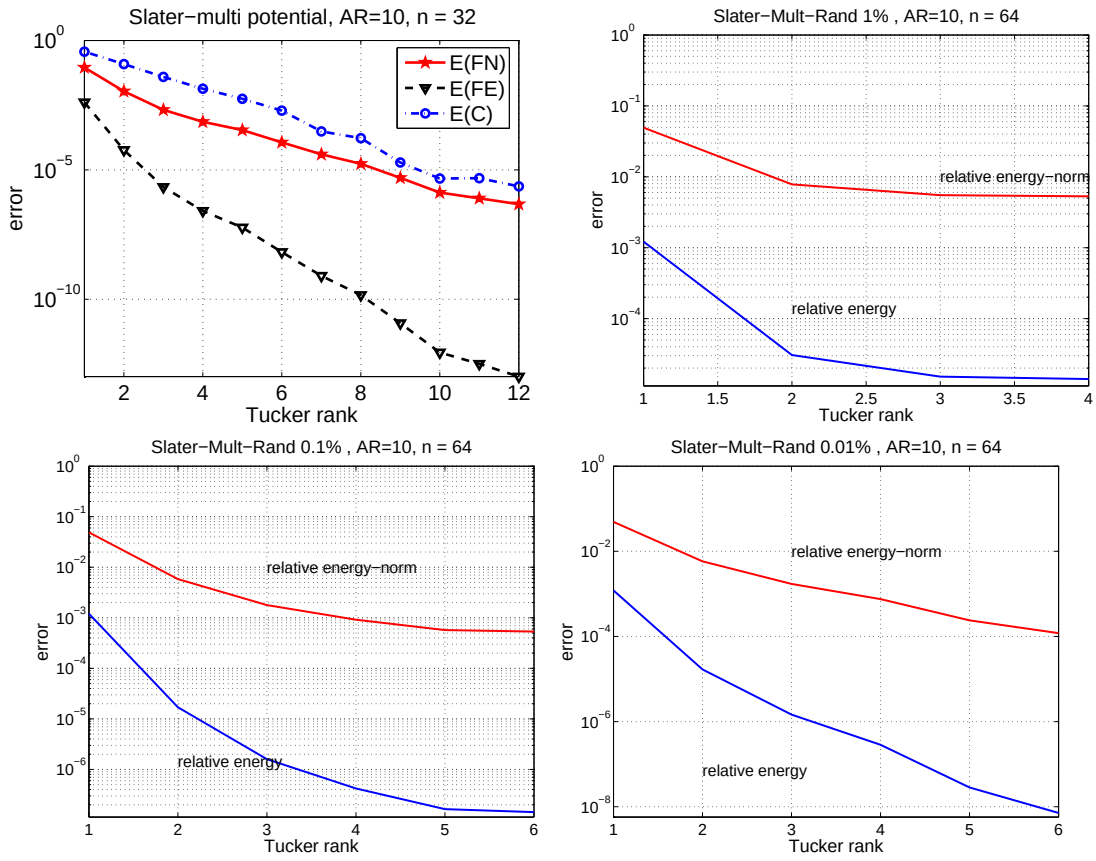

Figure 2.15: Convergence history for the multi-centered unperturbed (upper left figure) and randomly perturbed Slater potential.

Remark 2.21 *The entries of the core tensor of the Tucker decomposition for the considered function related tensors decay fast vs. index* $k_\ell = 1, \ldots, r$, $\ell = 1,\ 2,\ 3$.

Remark 2.22 *For a fixed approximation error, the Tucker rank of periodic structures practically does not depend on the number of cells included in the computational box (see also numerics in Section 3.3.2).*

Properties of the Tucker decomposition for the function related tensors described in Remarks 2.20 and 2.21 will be used further in the development of the multigrid accelerated BTA.

2.3.3 Application to functions in electronic structure calculations

Here, the approximating properties of the orthogonal Tucker-type representation (2.10) are studied for the 3D electron densities of some simple molecules. The ALS iterative scheme is applied to compute the low-rank tri-linear approximations for electron densities of the H atom, LiH, CH_4, C_2H_6 and H_2O molecules.

We assume that any particular molecule is embedded in a certain fixed computational box $[-b, b]^3$ with a suitable $b > 0$. Let $\omega_{\mathbf{3}} \subset [-b, b]^3$ be a uniform $n \times n \times n$ tensor grid of collocation points introduced in (2.41), and indexed by $\mathcal{I} = I_1 \times I_2 \times I_3$. The molecular orbitals and electron densities of the considered molecules are represented as

$$\varphi_a(x) = \sum_{k=1}^{R_0} c_{ka} g_k(x), \quad a = 1, ..., N_{orb}, \tag{2.46}$$

$$\rho(x) := 2 \sum_{a=1}^{N_{orb}} \varphi_a^2(x) = 2 \sum_{a=1}^{N_{orb}} \left(\sum_{k=1}^{R_0} c_{ka} g_k(x) \right)^2, \quad x \in \mathbb{R}^3, \tag{2.47}$$

where N_{orb} is the number of electron pairs in a molecule and R_0 is the number of Gaussians in the GTOs basis, of type

$$g_k(x) = \mu_k (x_1 - A_k)^{\ell_k} (x_2 - B_k)^{m_k} (x_3 - C_k)^{n_k} \exp(-\alpha_k \zeta_k^2) \tag{2.48}$$

with

$$\zeta_k^2 = (x_1 - A_k)^2 + (x_2 - B_k)^2 + (x_3 - C_k)^2, \quad x = (x_1, x_2, x_3)^T \in \mathbb{R}^3,$$

where the parameters for the Gaussians are taken from the standard quantum chemistry package MOLPRO [108]. For each particular molecule we use the following physically relevant parameters: $b = 10$ bohr, $R_0 = 10$ for H atom,

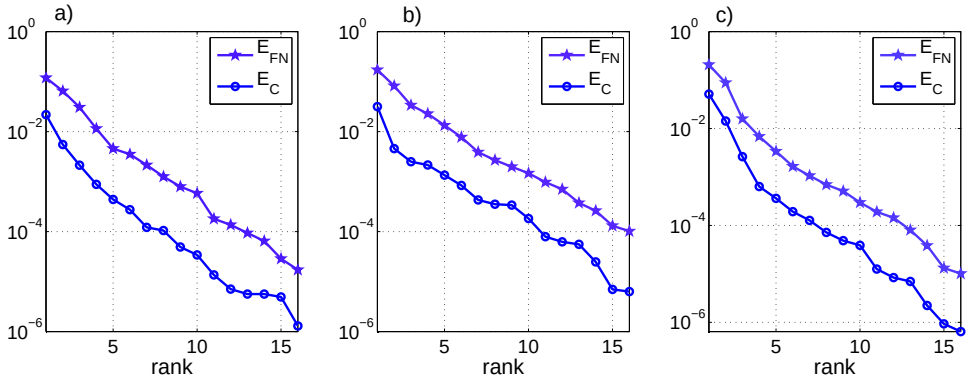

Figure 2.16: Approximation error in E_{FN} and E_C norms versus Tucker rank for the electron densities of a) CH_4, b) C_2H_6 and c) H_2O molecules with $n = 65$.

$b = 7$ bohr, $R_0 = 34$ for LiH, $b = 5$ bohr, $R_0 = 55$ for CH_4, $b = 5.8$ bohr, $R_0 = 96$ for C_2H_6 and $b = 10$ bohr, $R_0 = 41$ for H_2O.

We discretize $\rho : [-b, b]^3 \to \mathbb{R}$, by the function related tensor of order 3 by computing its entries according to relations (2.47), (2.48)

$$A_0 \equiv A_0(g) := [a_{i_1 i_2 i_3}]_{(i_1,i_2,i_3)\in\mathcal{I}} \in \mathbb{R}^{n\times n\times n} \text{ with } a_{i_1 i_2 i_3} := \rho(x^{(1)}_{i_1}, x^{(2)}_{i_2}, x^{(3)}_{i_3}),$$

where $(x^{(1)}_{i_1}, x^{(2)}_{i_2}, x^{(3)}_{i_3}) \in \omega_{\mathbf{3}}$ are the grid collocation points. In this way, we obtain the tensor representation A_0 of the corresponding density function, which is approximated by a rank $\mathbf{r} = (r, r, r)$ Tucker decomposition for a sequence of rank-parameters $r = 1, 2, \ldots, r_0$. The orthogonal matrices $V^{(\ell)} \in \mathbb{R}^{n\times r}$, $\ell = 1, 2, 3$, and the corresponding core tensor $\boldsymbol{\beta} \in \mathbb{R}^{r\times r\times r}$ are then used for the construction of the approximating tensor $A_{(\mathbf{r})} \approx A_0$. For every rank-$(r, r, r)$ Tucker approximation, we compute the relative error with respect to the Euclidean norm (2.42), as well as the relative maximum error (2.44).

The approximation errors shown in Figure 2.16 verify the exponential convergence of the orthogonal Tucker approximation (in the rank-parameter r) of electron densities reaching the relative accuracy $\sim 10^{-5}$ for CH_4, H_2O and C_2H_6 with $r = 16$. It is seen that the orthogonal vectors $v^{(\ell)}_{\nu_\ell}$ ($\nu_\ell = 1, ..., 4$, $\ell = 1, 3$) of the tensor-product decomposition for the H atom, LiH and C_2H_6 molecules shown in Figures 2.17 and 2.18 resemble the shape of the decomposed electron density along the corresponding spatial axis. Due to orthogonality of the decomposition, the Tucker model appears to be suitable for constructing a low dimensional problem-dependent orthogonal basis. The entries of the core tensor presented in Figure 2.18 are the weights $\beta_{\nu_1\nu_2\nu_3}$ of the corresponding tensor products of the orthogonal vectors $v^{(1)}_{\nu_1} \otimes v^{(2)}_{\nu_2} \otimes v^{(3)}_{\nu_3}$, which compose the summands of $A_{(\mathbf{r})}$ in (2.8) for $\nu_\ell \leq 6$. Figures 2.19 a) and c) visualise the electron density of CH_4 in a

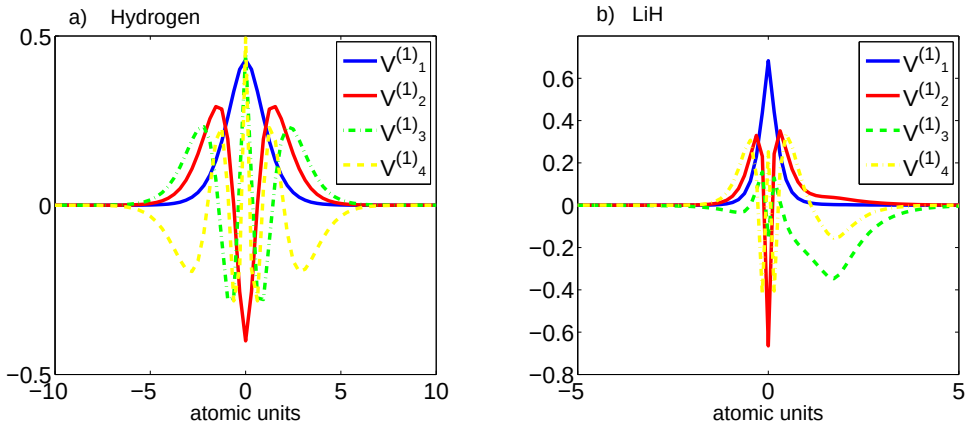

Figure 2.17: Orthogonal vectors $v^{(1)}_{\nu_1}$, $\nu_1 = 1, ..., 4$, for the rank-10 orthogonal Tucker approximation of the electron density for a) the H atom and b) for the LiH molecule.

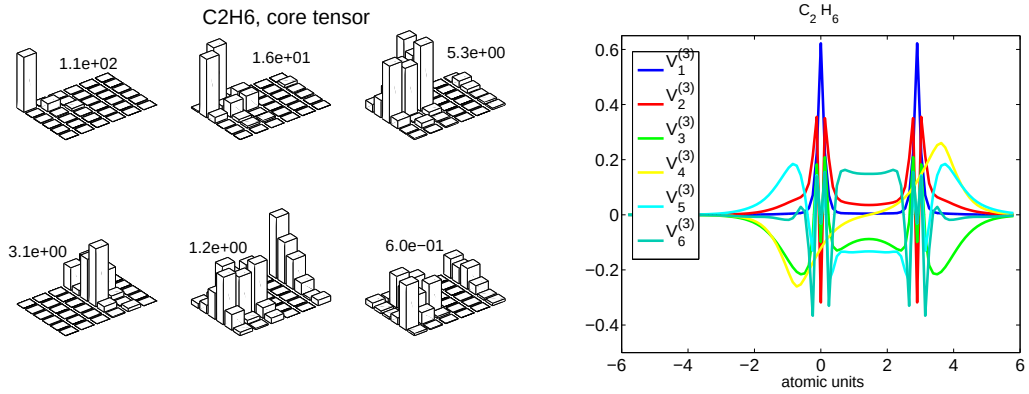

Figure 2.18: Slices $M_{\boldsymbol{\beta},\nu_r} \in \mathbb{R}^{6\times6\times1}$, $\nu_r = 1, \ldots, 6$ of the core tensor $\boldsymbol{\beta} \in \mathbb{R}^{6\times6\times6}$ and the orthogonal vectors $v^{(3)}_{\nu_3}$, $\nu_3 = 1, ..., 6$ of the rank-$(6, 6, 6)$ Tucker decomposition of the electron density of C_2H_6 molecule. Numbers correspond to the maxima of $|\beta_{\boldsymbol{\nu}}|$ for the corresponding slice of the core tensor.

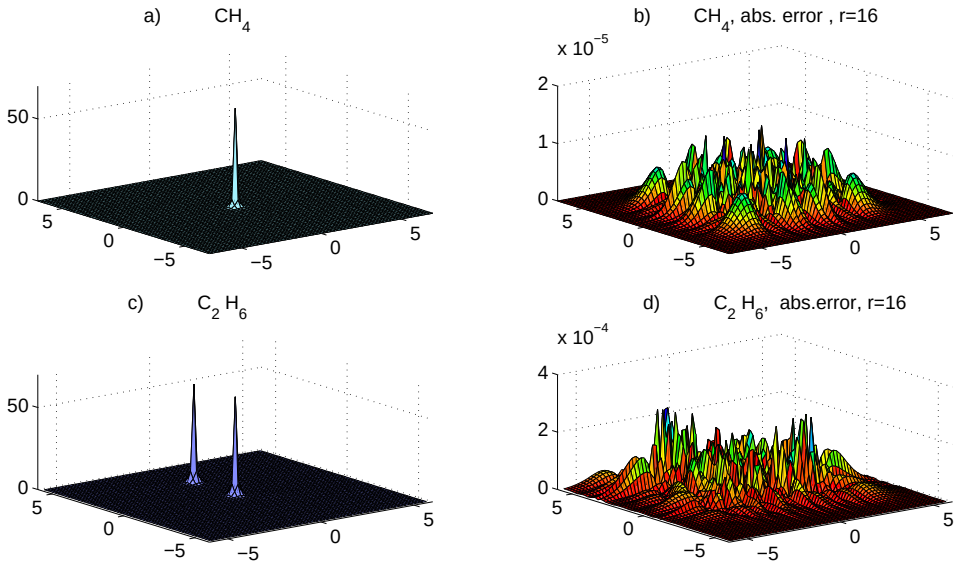

Figure 2.19: Electron densities and absolute errors of rank $r = 16$ Tucker approximation for CH_4 and C_2H_6 molecules.

plane containing the C atom and of C_2H_6 in a plane containing both C atoms, correspondingly. Figures 2.19 b) and d) visualise the absolute approximation error for the electron densities ρ of these molecules in the corresponding planes for $r = 16$. In spite of large values of ρ at the cusp regions (~ 60 units) we observe a rather uniform distribution of the absolute approximation error of the order $\sim 10^{-4} \div 10^{-5}$ in the computational domain. This is a typical feature of the orthogonal Tucker decomposition. For H_2O with even larger cusp (~ 148 units) at the origin, we see in Figure 2.16 c) that the Tucker approximation of ρ for this molecule yields the relative accuracy $\sim 10^{-5}$ for the Tucker rank $r = 16$. Finally, we present the convergence behaviour of the Tucker approximation applied to the tensor representation of the Hartree potentials of C_2H_6 and H_2O molecules, see Figure 2.20, indicating exponential convergence in the Tucker rank r. The numerical examples demonstrate efficiency of the low-rank Tucker tensor approximations for the electron densities and the Hartree potential of the considered molecules. This provides the background for further application of the Tucker model in low-complexity numerical evaluation of functionals and operators in the electronic structure calculations, see Sections 3, 4 and 5.

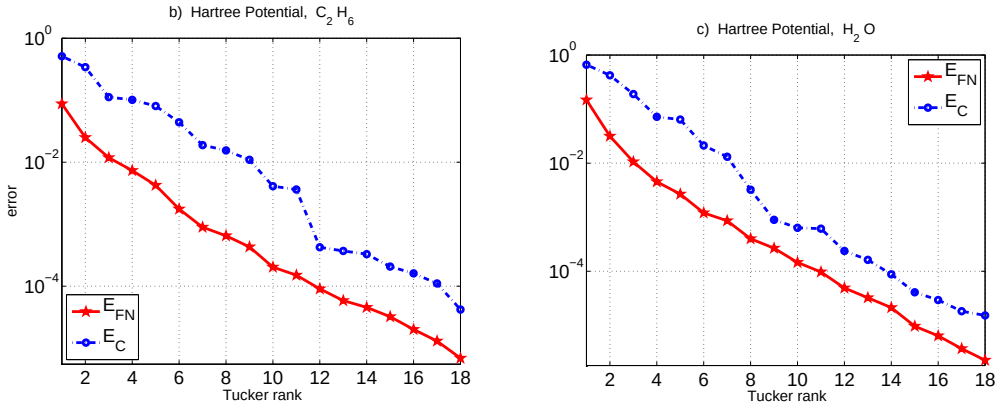

Figure 2.20: Approximation error in E_{FN} and E_C norms versus Tucker rank for the Hartree potentials of C_2H_6 (left) and H_2O (right).

2.4 Tensorisation of basic multilinear algebra (MLA) operations

For the sake of clarity (and without loss of generality) in this section we assume that $r = r_\ell$, $n = n_\ell$ $(\ell = 1, ..., d)$. If there is no confusion, the index $\mathbf{n}$ can be skipped. We denote by $\mathcal{N}$ the complexity of various tensor operations (say, $\mathcal{N}_{\langle\cdot,\cdot\rangle}$) or the related storage requirements (say, $\mathcal{N}_{st(\boldsymbol{\mathcal{B}})}$). We estimate the storage demands $\mathcal{N}_{st}$ and complexity of the following standard tensor-product operations: the scalar product, the so-called Hadamard (component-wise) product, and the convolution transform. We consider the MLA operations in $\boldsymbol{\mathcal{T}}_{\mathbf{r},\mathbf{n}}$, and $\boldsymbol{\mathcal{C}}_{R,\mathbf{n}}$ tensor classes.

The Tucker model requires

$$\mathcal{N}_{st,T} = drn + r^d \tag{2.49}$$

storage to represent a tensor.

The number of parameters in the rank-R canonical model scales linearly in R,

$$\mathcal{N}_{st,C} = dRn. \tag{2.50}$$

Setting $R = \alpha r$ with $\alpha \geq 1$, we can specify the range of parameters where the Tucker model is less storage consuming compared with the canonical one

$$r^{d-1} \leq d(\alpha - 1)n, \quad (\text{for } d = 3: \ r^2 \leq 3(\alpha - 1)n).$$

In general, the numerical Tucker decomposition leads to a fully populated core tensor, i.e., it is represented by r^d nonzero elements. However, the special data

structure of the Tucker core can be imposed which reduces the complexity of the corresponding tensor operations (cf. [60]). In particular, for the mixed (two-level) Tucker-canonical decomposition (see Definition 2.8), storage demands scale linearly in d,

$$\mathcal{N}_{st,TC} = dr(n + R).$$

2.4.1 Some bilinear operations in the Tucker format

For given tensors $A_1 \in \boldsymbol{\mathcal{T}}_{\mathbf{r}_1}, A_2 \in \boldsymbol{\mathcal{T}}_{\mathbf{r}_2}$ represented in the form (2.8), i.e.,

$$A_1 = \boldsymbol{\beta} \times_1 U^{(1)} \times_2 U^{(2)} \dots \times_d U^{(d)}, \quad A_2 = \boldsymbol{\zeta} \times_1 V^{(1)} \times_2 V^{(2)} \dots \times_d V^{(d)}, \tag{2.51}$$

the *scalar product* (2.2) is computed by

$$\langle A_1,\ A_2 \rangle := \sum_{\mathbf{k}=1}^{\mathbf{r}_1} \sum_{\mathbf{m}=1}^{\mathbf{r}_2} \beta_{k_1 \dots k_d} \zeta_{m_1 \dots m_d} \prod_{\ell=1}^{d} \left\langle u_{k_\ell}^{(\ell)}, v_{m_\ell}^{(\ell)} \right\rangle. \tag{2.52}$$

In fact, applying the definition of the scalar product in (2.2) to the rank-1 tensors (with $R = \mathbf{r} = 1$), we have

$$\begin{aligned} \langle A_1,\ A_2 \rangle &:= \sum_{\mathbf{i} \in \mathcal{I}} u_{i_1}^{(1)} \cdots u_{i_d}^{(d)} v_{i_1}^{(1)} \cdots v_{i_d}^{(d)} \\ &= \sum_{i_1=1}^{n_1} u_{i_1}^{(1)} v_{i_1}^{(1)} \cdots \sum_{i_d=1}^{n_d} u_{i_d}^{(d)} v_{i_d}^{(d)} = \prod_{\ell=1}^{d} \langle u^{(\ell)}, v^{(\ell)} \rangle. \end{aligned} \tag{2.53}$$

Then the above representation follows by combining all rank-1 terms in the left-hand side in (2.52).

We further simplify and suppose $\mathbf{r} = \mathbf{r}_1 = \mathbf{r}_2$. Then the calculation in (2.52) includes dr^2 scalar products of vectors of size n plus r^{2d} multiplications, leading to the overall complexity

$$\mathcal{N}_{\langle \cdot, \cdot \rangle} = O\left(dnr^2 + r^{2d}\right),$$

and the same for the respective norm.

Note that in the case of mixed Tucker-canonical decomposition (see Definition 2.8) the scalar product can be computed in $O\left(R^2 + dr^2 n + dR^2 r\right)$ operations (cf. [60], Lemma 2.8).

For given tensors $A, B \in \mathbb{R}^{\mathcal{I}}$, the *Hadamard product* $A \odot B \in \mathbb{R}^{\mathcal{I}}$ of two tensors of the same size $\mathcal{I}$ is defined by the componentwise product,

$$(A \odot B)_{\mathbf{i}} = a_{\mathbf{i}} \cdot b_{\mathbf{i}}, \quad \mathbf{i} \in \mathcal{I}.$$

Hence, for $A_1, A_2 \in \boldsymbol{\mathcal{T}}_{\mathbf{r}}$, as in (2.51), we tensorize the Hadamard product by

$$A_1 \odot A_2 := \sum_{k_1,m_1=1}^{r} \cdots \sum_{k_d,m_d=1}^{r} \beta_{k_1\ldots k_d}\zeta_{m_1\ldots m_d} \left(u_{k_1}^{(1)} \odot v_{m_1}^{(1)}\right) \otimes \ldots \otimes \left(u_{k_d}^{(d)} \odot v_{m_d}^{(d)}\right). \tag{2.54}$$

Again, applying definition (2.2) to the rank-1 tensors (with $\boldsymbol{\beta} = \boldsymbol{\zeta} = 1$), we obtain

$$\begin{aligned}(A_1 \odot\ A_2)_{\mathbf{i}} =& (u_{i_1}^{(1)} v_{i_1}^{(1)}) \cdots (u_{i_d}^{(d)} v_{i_d}^{(d)}) \\ =& \left(u^{(1)} \odot v^{(1)}\right) \otimes \cdots \otimes \left(u^{(d)} \odot v^{(d)}\right). \end{aligned} \tag{2.55}$$

Then (2.54) follows by summation over all rank-1 terms in $A_1 \odot A_2$. Relation (2.54) leads to the storage requirements

$$\mathcal{N}_{st(A\odot B)} = O(dr^2n + r^{2d}),$$

that includes the memory size for d modes $n \times r \times r$ Tucker vectors, and for the new Tucker core of size $(r^2)^d$.

The multi-dimensional *convolution product* is one of the basic integral transforms in the wide range of applications including many-particle models (see [27, 59, 65]). In this dissertation we apply the tensor-product convolution scheme corresponding to the discretisation by piecewise constant basis functions over uniform Cartesian grids. Methods to compute the multidimensional convolution on refined grids, by higher order elements and using the wavelet basis were considered in [42, 43].

For given tensors $F = [f_{\mathbf{i}}] \in \mathbb{R}^{\mathcal{I}}, G = [g_{\mathbf{i}}] \in \mathbb{R}^{\mathcal{I}}$, we define their discrete *convolution product* by

$$F * G := \left[\sum_{\mathbf{i}\in\mathcal{I}} f_{\mathbf{i}} g_{\mathbf{j}-\mathbf{i}+1}\right]_{\mathbf{j}\in\mathcal{J}}, \quad \mathcal{J} := \{1, ..., 2n-1\}^d,$$

where $\mathbf{j} - \mathbf{i} + 1 \in \mathcal{I}$ (equivalent to the assumption that G can be extended to the larger index set beyond $\mathcal{I}$ by zeros).

For given $A_1, A_2 \in \boldsymbol{\mathcal{T}}_{\mathbf{r}}$, see (2.51), we now tensorize the convolution product via

$$A_1 * A_2 := \sum_{\mathbf{k}=1}^{\mathbf{r}} \sum_{\mathbf{m}=1}^{\mathbf{r}} \beta_{k_1\ldots k_d}\zeta_{m_1\ldots m_d} \left(u_{k_1}^{(1)} * u_{m_1}^{(1)}\right) \otimes \ldots \otimes \left(u_{k_d}^{(d)} * v_{m_d}^{(d)}\right). \tag{2.56}$$

This relation again follows from the analysis for the case of rank-1 convolving tensors F and G, similar to the discussion for scalar product of tensors,

$$\begin{aligned}(F * G)_{\mathbf{j}} :=& \sum_{\mathbf{i}\in\mathcal{I}} f_{i_1}^{(1)} \cdots f_{i_d}^{(d)} g_{j_1-i_1+1}^{(1)} \cdots g_{j_d-i_d+1}^{(d)} \\ =& \sum_{i_1=1}^{n_1} f_{i_1}^{(1)} g_{j_1-i_1+1}^{(1)} \cdots \sum_{i_d=1}^{n_d} f_{i_d}^{(d)} g_{j_d-i_d+1}^{(d)} = \prod_{\ell=1}^{d} \left(f^{(\ell)} * g^{(\ell)}\right)_{j_\ell}. \end{aligned} \tag{2.57}$$

Assuming that "one-dimensional" convolutions of n-vectors, $u_{k_\ell}^{(\ell)} * v_{m_\ell}^{(\ell)} \in \mathbb{R}^{2n-1}$, can be computed in $O(n \log n)$ operations, we arrive at the overall complexity estimate

$$\mathcal{N}_{*\cdot} = O(dr^2 n \log n + r^{2d}).$$

In our particular case of equidistant grids we obtain (by setting $a = u_{k_\ell}^{(\ell)}, b = v_{m_\ell}^{(\ell)} \in \mathbb{R}^n$)

$$(u_{k_\ell}^{(\ell)} * v_{m_\ell}^{(\ell)})_j = \sum_{i=1}^{n} a_i b_{j-i+1}, \quad j = 1, ..., 2n-1.$$

Hence, the 1D convolution can be performed by FFT in $O(n \log n)$ operations.

We notice that the convolution product appears to be one of the most computationally elaborate operations since in general one might have r^{2d} terms in (2.56). Significant complexity reduction is already observed if at least one of the convolving tensors can be represented in the rank-R canonical format, so that we have only $r^d R$ terms in the sum (2.56).

2.4.2 Summary on MLA operations in rank-R canonical format

In our numerical scheme we apply the following linear operations with dth order tensors:

1. summation of tensors;
2. scalar product of tensors;
3. Hadamard product of tensors;
4. convolution of tensors.

We consider tensors A_1, A_2, represented in the rank-R canonical format, (2.6),

$$A_1 = \sum_{k=1}^{R_1} c_k u_k^{(1)} \otimes \ldots \otimes u_k^{(d)}, \quad A_2 = \sum_{m=1}^{R_2} b_m v_m^{(1)} \otimes \ldots \otimes v_m^{(d)}, \tag{2.58}$$

with normalized vectors $u_k^{(\ell)}, v_m^{(\ell)} \in \mathbb{R}^{n_\ell}$. For simplicity of discussion, we assume $n_\ell = n$, $\ell = 1, ..., d$.

1. A sum of two canonical tensors given by (2.58) can be written as

$$A_1 + A_2 = \sum_{k=1}^{R_1} c_k u_k^{(1)} \otimes \ldots \otimes u_k^{(d)} + \sum_{m=1}^{R_2} b_m v_m^{(1)} \otimes \ldots \otimes v_m^{(d)}, \tag{2.59}$$

resulting in the canonical tensor with the rank at most $R_S = R_1 + R_2$. This operation has no cost since it is simply a concatenation of two tensors.

2. For given canonical tensors A_1, A_2, the *scalar product* (2.2) is computed by (see (2.53))

$$\langle A_1, A_2 \rangle := \sum_{k=1}^{R_1} \sum_{m=1}^{R_2} c_k b_m \prod_{\ell=1}^{d} \left\langle u_k^{(\ell)}, v_m^{(\ell)} \right\rangle . \tag{2.60}$$

Calculation of (2.60) includes $R_1 R_2$ scalar products of vectors in $\mathbb{R}^n$, leading to the overall complexity

$$\mathcal{N}_{\langle \cdot, \cdot \rangle} = O(dnR_1R_2).$$

3. For A_1, A_2 given by (2.58), we tensorize the Hadamard product by (see (2.55))

$$A_1 \odot A_2 := \sum_{k=1}^{R_1} \sum_{m=1}^{R_2} c_k b_m \left(u_k^{(1)} \odot v_m^{(1)} \right) \otimes \ldots \otimes \left(u_k^{(d)} \odot v_m^{(d)} \right). \tag{2.61}$$

This leads to the complexity $O(dnR_1R_2)$.

4. The convolution product of two tensors in the canonical format (2.58), is given by (see (2.57))

$$A_1 * A_2 := \sum_{k=1}^{R_1} \sum_{m=1}^{R_2} c_k b_m \left(u_k^{(1)} * v_m^{(1)} \right) \otimes \ldots \otimes \left(u_k^{(d)} * v_m^{(d)} \right), \tag{2.62}$$

leading to the asymptotic complexity $O(dn \log n R_1 R_2)$.

3 Multigrid Tucker approximation of function related tensors

3.1 Motivations

In the previous section we have discussed the general BTA algorithms, which provide complexity of the Tucker tensor approximation of the order

$$W_{F2T} = O(n^{d+1}) \tag{3.1}$$

for full format tensors and

$$W_{C2T} = O(Rn \min\{R, n\} + r^{d-1} n \min\{r^{d-1}, n\}), \tag{3.2}$$

for the canonical rank-R input tensors. These bounds restrict application of the general BTA scheme to small dimensions d and moderate grid size n.

Notice, that the general BTA algorithm is computationally not feasible in electronic structure calculations on large $n \times n \times n$ 3D Cartesian grids, since:

1. For the full format tensors, $O(n^4)$ complexity of HOSVD in the general BTA algorithm restricts the size of the input tensors (maximum size $n \approx 128$, for conventional computers). In this case, our goal is to reach linear in the volume complexity $O(n^3)$, allowing maximum size of the input tensors up to $\approx 512^3$, for conventional computers.

2. In the case of rank-R input data, in our applications, both the canonical rank R and the univariate grid size n might be at least of the order 10^4. (Fine grids are necessary to resolve strong cusps due to core electrons in the Hartree potential.) It means that one has to compute the SVD of side matrices of the sizes $\approx 10^4 \times 10^4$, with complexity of order 10^{12} which is computationally unfeasible.

To avoid the above limitations, we introduce the *multigrid accelerated (MGA) Tucker decomposition* [68], which is based on the successive reiteration of the ALS Tucker approximation on a sequence of refined grids, using the results of the coarse

grid approximation as the initial guess for the dominating subspaces on finer grid levels. The idea of the multilevel acceleration originates from investigation of the numerical examples of BTA for the function related tensors, described in Section 2. These include Remarks 2.21 and 2.20 on the decay of the Tucker core entries and the weak dependence of the shape of the orthogonal vectors on the discretization parameter n, respectively.

We show that in the case of rank-R canonical target tensors in $\mathbb{R}^{n\times n\times n}$, the MGA method provides linear complexity (up to low order terms) of the canonical-to-Tucker decomposition with respect to all input parameters: the maximal univariate grid size n, the canonical rank R and the Tucker rank r,

$$W_{C2T} = O(rRn).$$

The resulting complexity of the decomposition for full format tensors is

$$W_{F2T} = O(n^3),$$

which currently makes possible the application of multigrid accelerated F2T algorithm to the 3D function-related tensors with the maximal grid size $n \times n \times n = 512^3$. In fact, applications are only bounded by the storage size for the input tensor. These grids provide the accuracy level required for the consistent electronic structure calculations in pseudopotential cases.

3.2 Multigrid accelerated BTA of canonical tensors

3.2.1 Basic concept

The concept of the MGA Tucker approximation applies to the multi-dimensional data obtained as a discretization of physically relevant continuous multivariate functions on a sequence of refined spatial grids. The typical application areas include the tensor approximation of multi-dimensional operators and functionals, the solution of integral-differential equations in $\mathbb{R}^d$, data-structured representation of physically relevant quantities [14, 52].

For a fixed grid parameter n, let us introduce the equidistant tensor grid

$$\omega_{\mathbf{d},n} := \omega_1 \times \omega_2 \cdots \times \omega_d, \tag{3.3}$$

where $\omega_\ell := \{-b + (k-1)h : k = 1, ..., n+1\}$ $(\ell = 1, ..., d)$ with mesh-size $h = 2b/n$. Define a set of collocation points $\{x_{\mathbf{i}}\}$ in $\Omega := [-b, b]^d \in \mathbb{R}^d$, located at the midpoints of the grid-cells, and numbered by $\mathbf{i} \in \mathcal{I} := \{1, ..., n\}^d$ (see the explicit definition in (2.41)). For fixed n, the target tensor $A_n = [a_{n,\mathbf{i}}] \in \mathbb{R}^{\mathcal{I}}$ is

defined by sampling the given continuous multivariate function $f : \Omega \to \mathbb{R}$ on the set of collocation points $\{x_{\mathbf{i}}\}$ as follows

$$a_{n,\mathbf{i}} = f(x_{\mathbf{i}}), \quad \mathbf{i} \in \mathcal{I}.$$

The idea of the *multigrid accelerated* best orthogonal Tucker approximation is based on the following principles (topics 3-4 below apply to $\boldsymbol{\mathcal{C}}_{R,\mathbf{n}}$ initial data):

1. *General multigrid concept.* Solving a *sequence of nonlinear approximation problems* for $A = A_n$ as in (2.12) with $n = n_m := n_0 2^m$, $m = 0, 1, ..., M$, corresponding to a sequence of (d-adic) refined spatial grids $\omega_{\mathbf{d},n_m}$. The sequence of approximation problems is treated successively in one run from coarse-to-fine grid.

2. *Coarse initial approximation to the side-matrices $V^{(q)}$, $q = 1, ..., d$.* Specifically, the initial approximation of the q-mode orthogonal side-matrices $V^{(q)}$ on finer grid $\omega_{\mathbf{d},n_m}$ is obtained by the linear interpolation of the corresponding orthogonal vectors from the coarser grid $\omega_{\mathbf{d},n_{m-1}}$.

3. *Most important fibers.* (Applies to $\boldsymbol{\mathcal{C}}_{R,\mathbf{n}}$ initial data.) We employ the idea of "most important fibers" (MIFs) of the q-mode unfolding matrices $B_{(q)} \in \mathbb{R}^{n \times \overline{r}_q}$ (see (2.26) in Step 2 of basic Algorithm G_BTA, Section 2.2.2), whose positions are extracted from data on the coarser grids. To identify the location of MIFs we apply the so-called *maximal energy principle* as follows. On the coarse grid, we calculate a projection of the q-mode unfolding matrix $B_{(q)}$ onto the true q-mode subspace $span\{v_1^{(q)}, ..., v_{r_q}^{(q)}\}$ with $V^{(q)} = [v_1^{(q)} ... v_{r_q}^{(q)}]$, which is computed as the matrix product,

$$\boldsymbol{\beta}_{(q)} = {V^{(q)}}^T B_{(q)} \in \mathbb{R}^{r_q \times \overline{r}_q}. \tag{3.4}$$

   Now the maximal energy principle specifies the location of MIFs by finding pr columns in $\boldsymbol{\beta}_{(q)}$ with maximal Euclidean norms (supposing that $pr \ll \overline{r}_q$), see Figures 3.1 and 3.2. The positions of MIFs are numbered by the index set $J_{q,p}$ with $\#J_{q,p} = pr$, being the subset of the larger index set

$$J_{q,p} \subset J_{\overline{r}_q} := \{1, ..., \overline{r}_q\}, \quad \#J_{\overline{r}_q} = \overline{r}_q = O(r^{d-1}).$$

   This strategy allows to predict a fixed portion of q-mode fibers in the Tucker core on fine grids, which accumulate the maximum part of the Frobenius norm. The union of selected fibers from every mode q (specified by the index set $J_{q,p}$, $q = 1, ..., d$) accumulates the important information on the structure of the rank-R tensor in the space of Tucker coefficients $\mathbb{R}^{r_1 \times \cdots \times r_d}$. This information enormously reduces the amount of computational work on the fine grids.

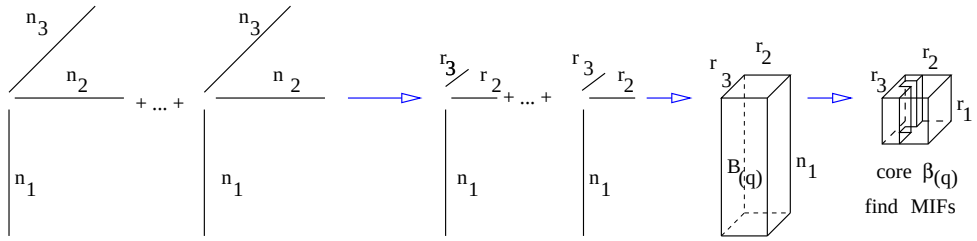

Figure 3.1: Illustration for $d = 3$. Finding MIFs in the "preliminary core" $\boldsymbol{\beta}_{(q)}$ for $q = 1$ for the rank-R initial data on the coarse grid $\mathbf{n} = \mathbf{n}_0 = (n_1, n_2, n_3)$. $B_{(q)}$ is presented in a tensor form for explanatory reasons.

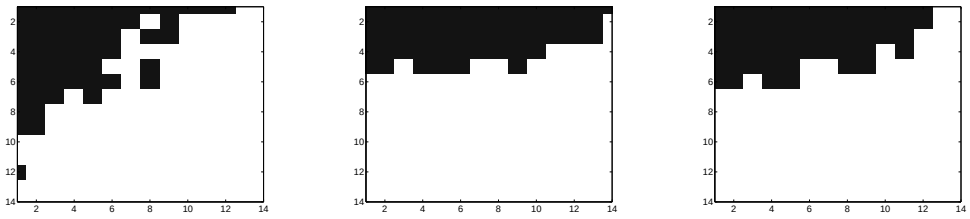

Figure 3.2: MIFs: selected positions of the fibers of the preliminary "cores" for computing $V^{(1)}$(left), $V^{(2)}$ (middle) and $V^{(3)}$ (right). The example is taken from the multigrid rank compression in the computation of the Hartree potential for H_2O, $r = 14$, $p = 4$.

4. *Performing restricted ALS iteration.* The proposed choice of MIFs allows to reduce the cost of ALS iteration to solving the problem of best rank-r approximation to the large unfolding matrix $B_{(q)} \in \mathbb{R}^{n \times \overline{r}_q}$ with dominating second dimension $\overline{r}_q = r^{d-1}$ (always the case for large d). In fact, we reduce one step of ALS iteration to computation of the r-dimensional dominating subspace of small $n \times pr$ submatrices $B_{(q,p)}$ of $B_{(q)}$ $(q = 1, ..., d)$, where $p = O(1)$ is some fixed parameter (SVD with matrix-size $n \times pr$ instead of $n \times \overline{r}_q$).

The invention of above principles leads to dramatic complexity reduction of the standard tensor algorithms G_BTA($\mathbb{V}_{\mathbf{n}} \to \boldsymbol{\mathcal{T}}_{\mathbb{B}_{\mathbf{r}}}$) and C_BTA($\boldsymbol{\mathcal{C}}_{R,\mathbf{n}} \to \boldsymbol{\mathcal{T}}_{\mathcal{C}_R,\mathbf{r}}$). In the latter case, this approach leads to the efficient tensor approximation method with linear scaling in n and R, up to the computational cost on the coarsest level. In the case of fully populated tensors we arrive, at least, at the linear cost $O(n^d)$, corresponding to the storage space for the initial tensor.

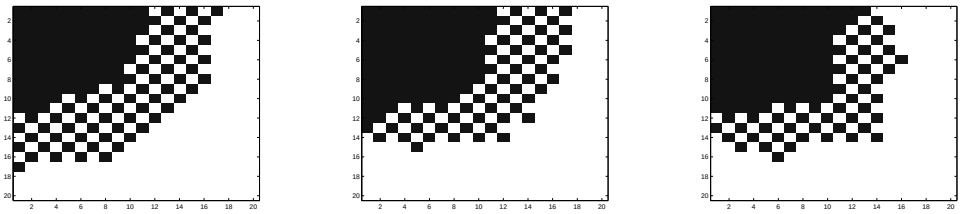

Figure 3.3: MIFs: selected projections of the fibers of the preliminary "cores" for computing $V^{(1)}$(left), $V^{(2)}$ (middle) and $V^{(3)}$ (right). The example from the MGA rank reduction in computation of V_H, in pseudopotential case of CH_4 with $r = 22$, and number of MIFs $p = 8$.

3.2.2 Description of the Algorithm and complexity bound

For further constructions, we use the 1D interpolation operator $\mathbf{I}^{(\ell)}_{(m-1,m)}$ from the coarse to fine grids acting in spatial direction $\ell = 1, ..., d$. This might be either the interpolation by piecewise linear or cubic splines (the latter is our choice in the current implementation). In the following we focus on the case of rank-R input. The proposed algorithm of the MGA best Tucker approximation for $A \in \boldsymbol{\mathcal{C}}_{R,\mathbf{n}}$ can be outlined as follows:

Algorithm MG_C_BTA ($\boldsymbol{\mathcal{C}}_{R,\mathbf{n}_M} \to \boldsymbol{\mathcal{T}}_{\mathcal{C}_R,\mathbf{r}}$). (Multigrid accelerated canonical-to-Tucker approximation).

1. Given $A_m \in \boldsymbol{\mathcal{C}}_{R,\mathbf{n}_m}$ in the form (2.6), corresponding to a sequence of grid parameters $n_m := n_0 2^m$, $m = 0, 1, ..., M$. Fix a structural constant $p = O(1)$ (i.e. $pr \ll r^{d-1}$), iteration parameter k_{max}, and the Tucker rank $\mathbf{r}$.

2. For $m = 0$, solve C_BTA($\mathcal{C}_{R,\mathbf{n}_0} \to \mathcal{T}_{\mathcal{C}_R,\mathbf{r}}$) and compute the index set $J_{q,p}(n_0) \subset J_{\overline{r}_q}$ via identification of MIFs in the matrix unfolding $B_{(q)}$, $q = 1, ..., d$, using *the maximum energy principle* applied to the q-mode unfolding of the Tucker core $\boldsymbol{\beta}_{(q)}$ as in (3.4).

3. For $m = 1, ..., M$ perform the *cascadic MGA nonlinear Tucker approximation* by the restricted ALS iteration:

   3a) Compute the initial guess for side matrices on level m by interpolation $\mathbf{I}_{(m-1,m)}$ of the side matrix from level $m - 1$ (by using piecewise linear or cubic splines)

   $$V^{(q)} = V^{(q)}_m = \mathbf{I}_{(m-1,m)}(V^{(q)}_{m-1}), \quad q = 1, ..., d.$$

   3b) For each $q = 1, ..., d$, fix $V^{(\ell)}$ ($\ell = 1, ..., d,\ \ell \neq q$) and perform:

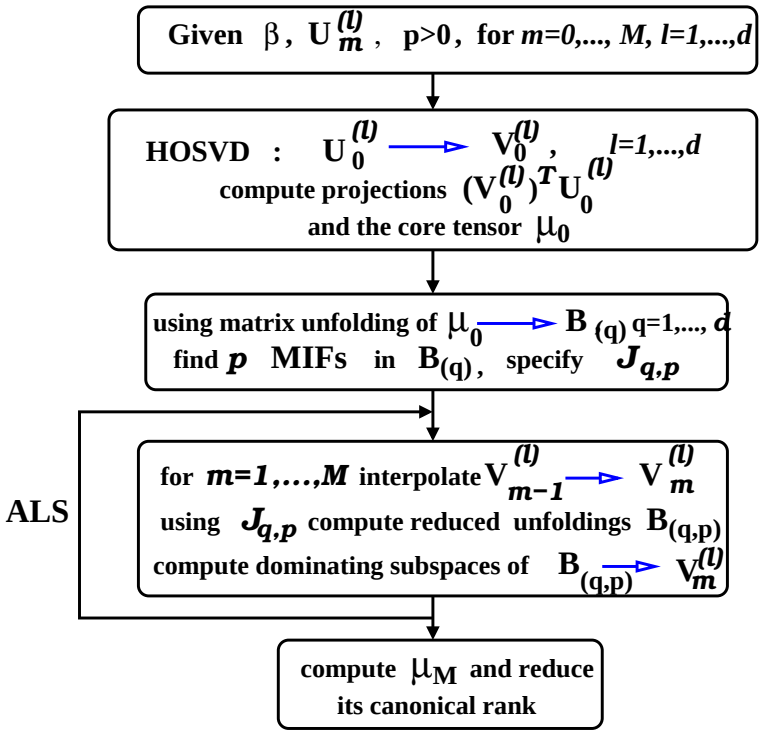

Figure 3.4: Flow chart of Algorithm MG_C_BTA applied to the rank-R target.

→ Compute matrix products $V^{(\ell)^T}U^{(\ell)}$, $\ell = 1, ..., d; \ell \neq q$, and construct the *"restricted"* q-mode matrix unfolding $B_{(q,p)}$

$$B_{(q,p)} = B_{(q)_{|J_{q,p}(n_0)}} \in \mathbb{R}^{n_m \times pr},$$

by calculating pr columns in the complete unfolding matrix $B_{(q)} \in \mathbb{R}^{n_m \times \overline{r}_q}$.

→ Update the orthogonal matrix $V^{(q)} = V_m^{(q)} \in \mathbb{R}^{n_m \times r}$ via computing the r-dimensional dominating subspace for the *"restricted"* matrix unfolding $B_{(q,p)}$ (truncated SVD of $n_m \times pr$ matrix).

4. Compute the rank-R core tensor $\boldsymbol{\beta} \in \boldsymbol{\mathcal{C}}_{R,\mathbf{r}}$, as in Step 3 of basic algorithm C_BTA ($\mathcal{C}_{R,\mathbf{n}} \to \mathcal{T}_{\mathcal{C}_{R,\mathbf{r}}}$).

Figure 3.4 shows the flow chart of Algorithm MG_C_BTA.
The next statement proves the linear complexity of Algorithm MG_C_BTA.

Theorem 3.1 *Algorithm MG_C_BTA($\boldsymbol{\mathcal{C}}_{R,\mathbf{n}_M} \to \boldsymbol{\mathcal{T}}_{\mathcal{C}_{R,\mathbf{r}}}$) amounts to*

$$O(dRrn_M + dp^2r^2n_M)$$

operations per ALS loop, plus extra cost of the coarse mesh solver C_BTA ($\boldsymbol{\mathcal{C}}_{R,\mathbf{n}_0} \to \boldsymbol{\mathcal{T}}_{\mathcal{C}_{R,\mathbf{r}}}$). It requires $O(drn_M + drR)$ storage to represent the result.

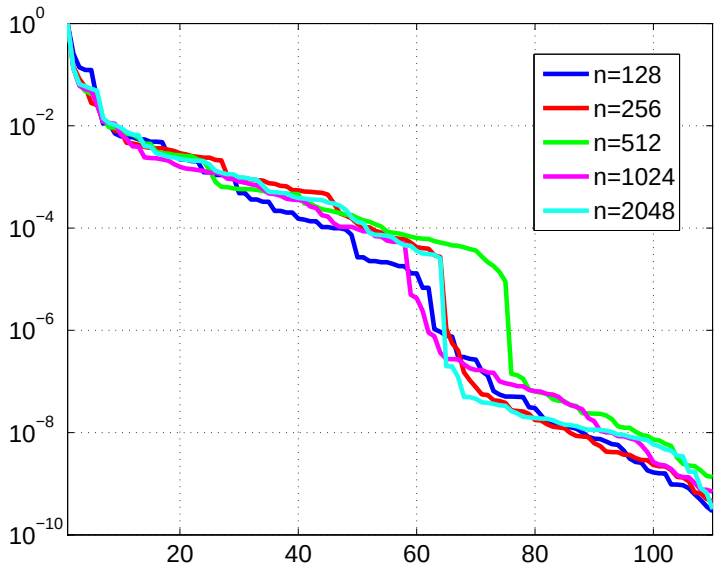

Figure 3.5: Singular values of the mode-1 matrix unfolding $B_{(1,p)}$, $p = 4$.

Proof: Step 3a) requires $O(drn_M)$ operations and memory. Assume without loss of generality that $pr \leq n_M$, hence the complexity of Step 3b) on the finest level is bounded by $O(dRrn_M + dprn_M + dp^2r^2n_M)$ per iteration loop. The rank-R representation of $\boldsymbol{\beta} \in \boldsymbol{\mathcal{C}}_{R,\mathbf{r}}$ requires $O(drRn_M)$ operations and $O(drR)$-storage. Summing up these costs over the levels $m = 1, ..., M$, proves the result since the relation $n_M(1 + 1/2 + ...1/2^{M-1}) < 2n_M$. ■

Figure 3.5 shows the singular values of the mode-1 matrix unfolding $B_{(1,p)}$ with the choice $p = 4$, which demonstrates the reliability of the maximal energy principle in the error control. Similar fast decay of respective singular values is typical in most of our numerical examples in electronic structure calculations considered so far. Remarkably, that the "representative subset" of fibers $J_{q,p}$ normally has the size pr of several r-s with $p \ll r$. The (controllable) decay of singular values of the small-size restricted unfolding matrix $B_{(q,p)}$ provides a criterion for the satisfactory choice of parameter p. If the decay is not fast enough the algorithm can be restarted with the larger parameter $p \to p + 1$.

Figure 3.6 demonstrates the linear scaling of the MGA Tucker approximation in the input rank R, and in the grid size n, applied to C2T rank reduction of the electron density of CH_4. Further numerical illustrations to the above algorithm will be presented in Section 3.2.3.

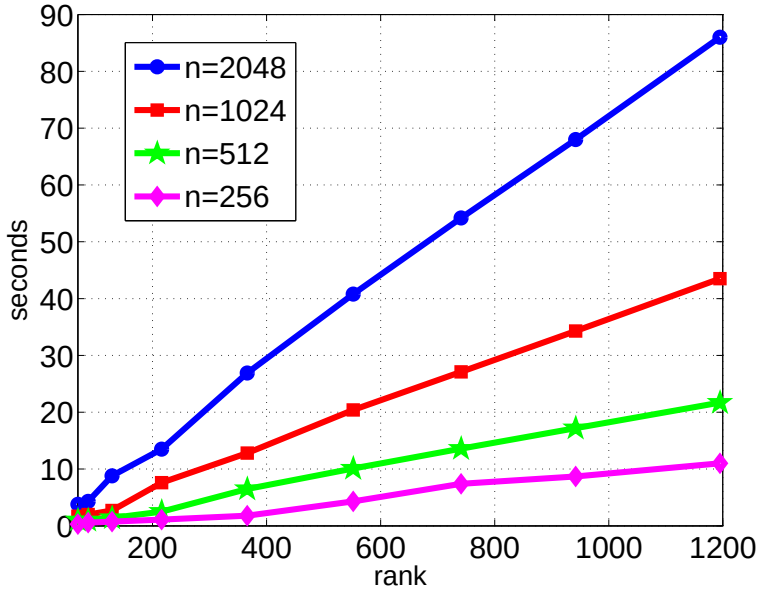

Figure 3.6: Linear scaling in R and n, of the C2T rank reduction algorithm.

Notice that the complexity and error of the MGA Tucker approximation can be effectively controlled by the adaptive choice of the governing parameters p, r and n_0. Figure 3.7 shows the dependence of computational accuracy of Algorithm MG_C_BTA on the choice of the number of important fiber pr and the Tucker rank r, in the case of Hartree potential of C_2H_6.

3.2.3 Numerics on rank reduction of the electron density ρ

The MG_C_BTA algorithm has been evoked by the problem of fast computation of the Hartree potential V_H and the respective Coulomb matrix in the Fock operator, using multilinear algebra in the tensor-structured formats, see Section 4.

In the evaluation of the Hartree potential for *pseudodensities* of some simple molecules good accuracy of order 10^{-6} hartree in the max-norm is achieved already by computation on moderate $n \times n \times n$ grids with $n = 400$ and $n = 800$. In this case the unigrid C2T algorithm described in Section 2.2.3 is sufficient.

However, when computing the *all electron densities* of molecules, which contain strong cusps due to core electrons contribution (see the example of all electron density for the water molecule presented in Figure 3.8), large grid parameters n of the order of several thousands are required to ensure the high resolution of local singularities.

In [19], where the wavelet basis set is used for approximation of the electronic

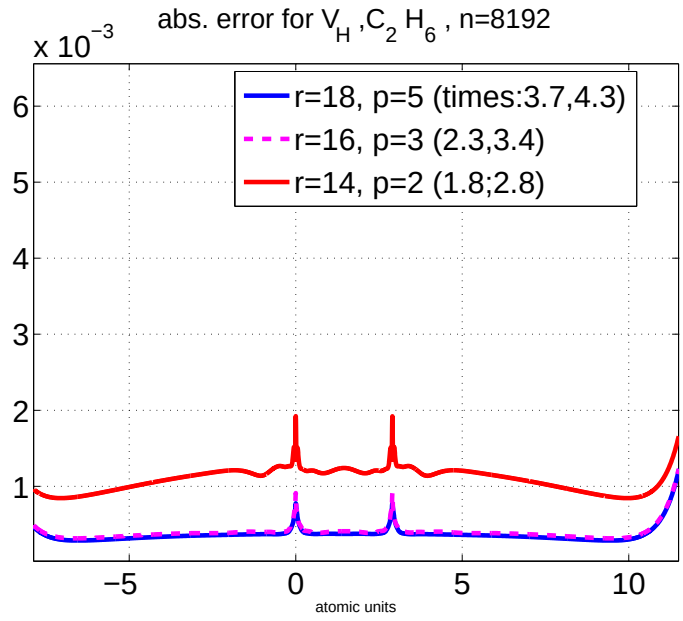

Figure 3.7: Absolute error in the Hartree potential of C_2H_6 vs. different multigrid parameters r and p, visualised in the grid interval centered at $(0, 0, 0)$.

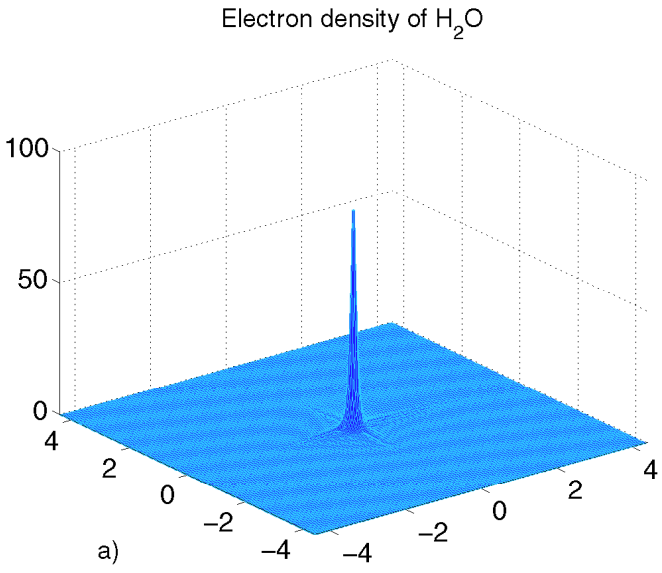

Figure 3.8: Electron density of H_2O in the cross-section $\Omega = [-4, 4] \times [-4, 4] \times \{0\}$.

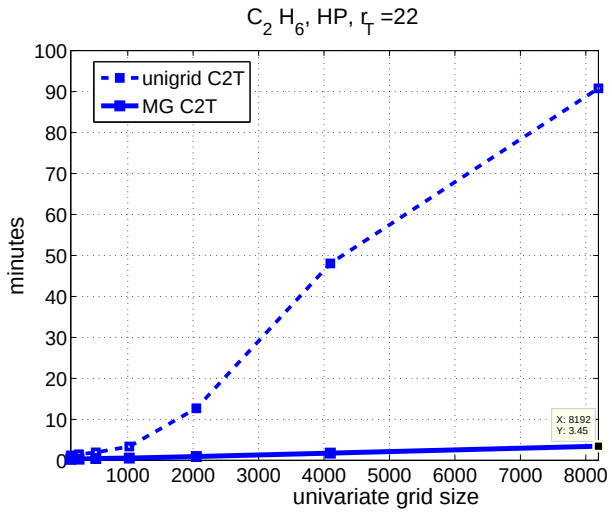

Figure 3.9: Multigrid vs. single grid MATLAB times for the canonical-to-Tucker transform in computations of the Hartree potential of C_2H_6 molecule, $r = 22$, $p = 4$.

structure quantities, it is shown that the Hartree potential of CH_4 and C_2H_6 molecules can be resolved in the cusp area with accuracies of the order of 10^{-3}, by computations with the univariate grid size $n = 5.1 \cdot 10^3$ in the volume of $[-b, b]^3$ with $b = 20$ au. Hence, the univariate mesh size of 3D Cartesian grids should be not larger than $h = 2b/n \leq 8 \cdot 10^{-3}$ au.

In our tensor-structured computations, we apply uniform grids with the mesh-size up to $h = 1.3 \cdot 10^{-3}$ au, corresponding to the univariate grid size $n = 16384$ with $b = 10.6$ au. Large grids are required for the representation of functions with multiple strong singularities discretized on large 3D uniform grids. The examples of cusps of electron densities of some molecules are presented in Figures 3.8 for the water molecule, and in Figure 2.19 for CH_4 and C_2H_6 molecules.

The algorithm for computation of the Hartree potential by the tensor-product convolution will be discussed in Section 4.2, where we demonstrate numerical results on the accuracy and computational cost. Here we present the comparison of the MATLAB times for the unigrid and multigrid rank reduction algorithms which are used in the accurate and fast computation of the Hartree potential on large 3D Cartesian grids. Figures 3.9 and 3.10 show the comparison of MATLAB times of the unigrid C2T versus MGA C2T algorithms applied to calculations for C_2H_6 and CH_4 molecules, respectively. Figures 3.9 and 3.10 show the comparison of MATLAB times of the unigrid C2T versus MGA C2T algorithms applied to C_2H_6 and CH_4 molecules, respectively.

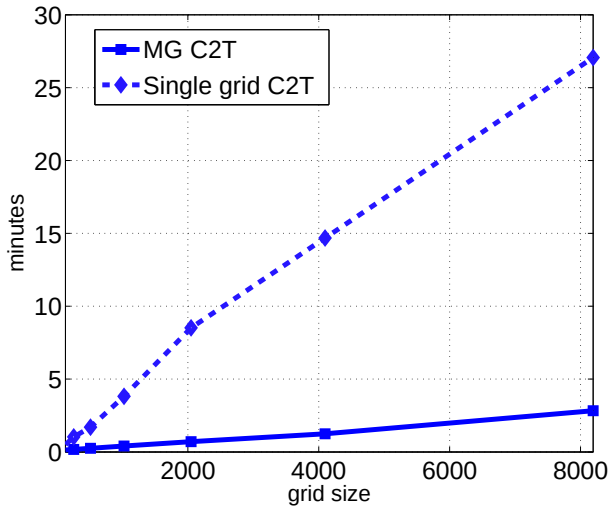

Figure 3.10: Multigrid vs. single grid CPU times for the canonical-to-Tucker transform in computations of the Hartree potential of CH_4 molecule.

	n^3	128^2	256^3	512^3	1024^3	2048^3	4096^3	8192^3
$p = 4$	C2T	10	12	19	41	52	95	188
$r = 20$	CONV	0.2	0.8	1.5	10.6	22	58	160
$p = 16$	C2T	34	44	67	118	200	388	770
$r = 28$	CONV	0.5	1.8	3.2	15.6	35	108.2	352

Table 3.1: Elapsed times (in sec) for the C2T rank reduction of ρ and the tensor-product convolution (CONV) in the computation of V_H for the C_2H_6 molecule.

Tables 3.1 and 3.2 give computation times for the C2T rank reduction and of the convolution with the Newton kernel for electron densities of H_2O and C_2H_6 molecules. The initial canonical ranks R_{ρ_0} of the tensors are 861 and 4656, for H_2O and C_2H_6, respectively. The C2T algorithm yields the ranks $R_\rho \approx r\,p$. Computation times depend on the level of the thresholds ε in the algorithms C2T and T2C. For example, we observe accuracies of the order 10^{-4} for parameters $p = 2$, $r = 16$, and of the order 10^{-5} for parameters $p = 8$, $r = 20$ in computations for H_2O molecule. For C_2H_6 molecule, $p = 4$, $r = 20$ yield accuracies of the order $10{-}3$, and $p = 16$, $r = 28$, the accuracies of the order $10{-}3$. We observe, that for moderate accuracies the times for the C2T and T2C rank reduction and the

	n^3	256^3	512^3	1024^3	2048^3	4096^3	8192^3	16384^3
$p=2$	C2T	4	4.5	5.5	5.7	12.2	23.7	66
$r=16$	CONV	0.6	1.1	5.5	12	38	127	255
$p=8$	C2T	6.1	8	12	18	39	75	129
$r=20$	CONV	1.8	3.2	15.6	34	140	378	784

Table 3.2: Elapsed times (in sec) for the C2T rank reduction of ρ and the tensor-product convolution (CONV) in the computation of V_H for H_2O molecule.

corresponding convolution times are reduced dramatically.

3.3 Multigrid accelerated BTA for the full format function related tensors

In the case of full format tensors the main principles of the multigrid concept are based on topics 1, 2 and 4 from §3.2.1. Here we describe the algorithm of the MGA Tucker approximation of the function related tensors discretized on a sequence of grids specified as in Section 3.2.

Algorithm MG_G_BTA ($\mathbb{V}_{\mathbf{n}} \to \boldsymbol{\mathcal{T}}_{\mathbf{r}}$). (MGA full-to-Tucker approximation).

1. Given $A_m \in \mathbb{V}_{\mathbf{n}}$ in the form (2.1), corresponding to a sequence of grid parameters $n_m := n_0 2^m$, $m = 0, 1, ..., M$. Fix the Tucker rank $\mathbf{r}$, and the iteration number k_{max}.

2. For $m = 0$, solve the approximation problem by Algorithm G_BTA($\mathbb{V}_{\mathbf{n}_0} \to \boldsymbol{\mathcal{T}}_{\mathbf{r}}$) via k_{max} steps of ALS iteration.

3. For $m = 1, ..., M$, perform the *cascadic MGA Tucker approximation*:

   3a) Compute the initial guess for the side matrices on level m by interpolation $\mathbf{I}_{(m-1,m)}$ from level $m-1$ (using piecewise linear or cubic splines)

   $$V^{(\ell)} = V_m^{(\ell)} = \mathbf{I}_{(m-1,m)}(V_{m-1}^{(\ell)}), \quad \ell = 1, ..., d.$$

   3b) Starting with the initial guess $V^{(\ell)}$ ($\ell = 1, ..., d$) perform k_{max} steps of the ALS iteration as in Step 2 of Algorithm G_BTA (see §2).

4. Compute the core $\boldsymbol{\beta}$ by the orthogonal projection of A onto $\mathbb{T}_{\mathbf{n}} = \otimes_{\ell=1}^{d} \mathbb{T}_\ell$ with $\mathbb{T}_\ell = \mathrm{span}\{v_\nu^{(\ell)}\}_{\nu=1}^{r_\ell}$ (see Remark 2.7),

   $$\boldsymbol{\beta} = A \times_1 {V^{(1)}}^T \times_2 ... \times_d {V^{(d)}}^T \in \mathbb{B}_{\mathbf{r}},$$

at the cost $O(r^d n)$.

The complexity of the MGA Tucker approximation by the ALS algorithm applied to full format tensors is given in the following Lemma.

Lemma 3.2 *Suppose that $r^2 \leq n_m$ for large m, then the numerical cost of Algorithm MG_G_BTA is estimated by*

$$W_{F\to T} = O(n_M^3 r + n_M^2 r^2 + n_M r^4 + n_0^4) = O(n_M^3 r + n_0^4).$$

Proof: In Step 2, the HOSVD on the coarsest grid level requires $O(n_0^4)$ operations (which for large $n = n_m$ is negligible compared to other costs in the algorithm). Next, for fixed $n = n_m$ the assumption $r^2 \leq n$ implies that at every step of the ALS iterations the costs of the consequent contractions to compute the $n \times r^2$ unfolding matrix $B_{(q)}$ is estimated by $O(n^3 r + n^2 r^2)$, while the SVD of $B_{(q)}$, requires $O(nr^4)$ operations. Summing up over the levels completes the proof, taking into account that the Tucker core is computed in $O(n_M^3 r)$ operations. ■

3.3.1 Numerics on the MGA Tucker approximation ($\rho^{1/3}$)

Figure 3.11 shows the numerical example of the MGA Tucker approximation to fully populated tensors given by the 3D Slater function $e^{-\|x\|}$, ($x \in [-b, b]^3$, $b = 5.0$), sampled over large $n \times n \times n$ uniform grids with $n = 64$, 128, 256 and 512. The MATLAB times (min) of the MGA Tucker decomposition corresponding to data in Figure 3.11 are shown in Figure 3.12. It is worth to note that the times for the grid size 256^3 outperform essentially the existing benchmark high performance algorithm based on the Newton-type method on the Grassman manifold presented in [92] (maximal grid size there is less than 256^3). Another efficient approach for the Tucker decomposition based on the cross-approximation algorithm was recently presented in [86].

The results on the Tucker approximation for the irrational function of electron density ρ, $\rho^{1/3}$, discretized over the tensor grids in $[-b, b]^3$, $b = 5.0$, with $n \leq 512$, are shown in Figure 3.13 (corresponding to CH_4 molecule). Notice that the low-rank tensor representation of the "exchange" potential $\rho^{1/3}$, is an important issue in the density functional theory computations. As it was mentioned before, the convergence upon the Tucker rank depends on physical "relevance" (regularity properties) of the function. Our multigrid accelerated scheme requires SVD of complexity $O(nr^2 \min\{n, r^2\})$, where $r \ll n$, instead of $O(n^4)$ in the unigrid approach. As a result, the admissible grid size for applicability of the MGA Tucker decomposition to full-format tensors is limited only by the amount of available computer memory for tensor representation, $O(n^3)$.

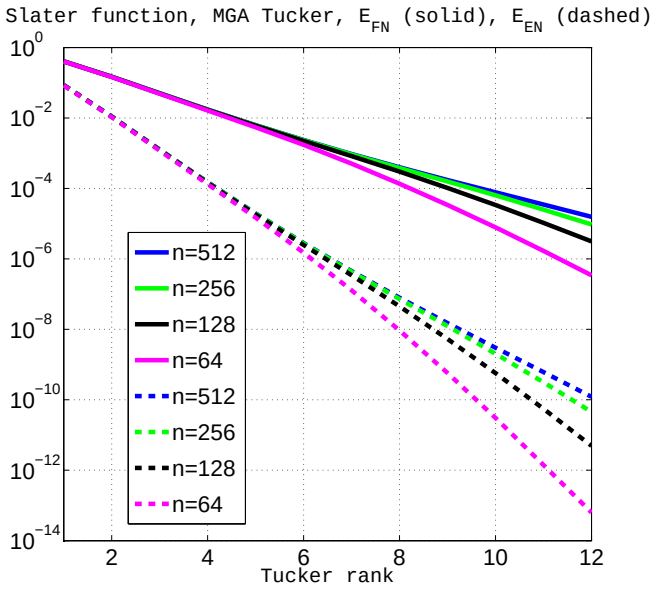

Figure 3.11: Convergence of the MGA Tucker approximation with respect to the Tucker rank r applied to the discretized Slater function (relative Frobenius norm).

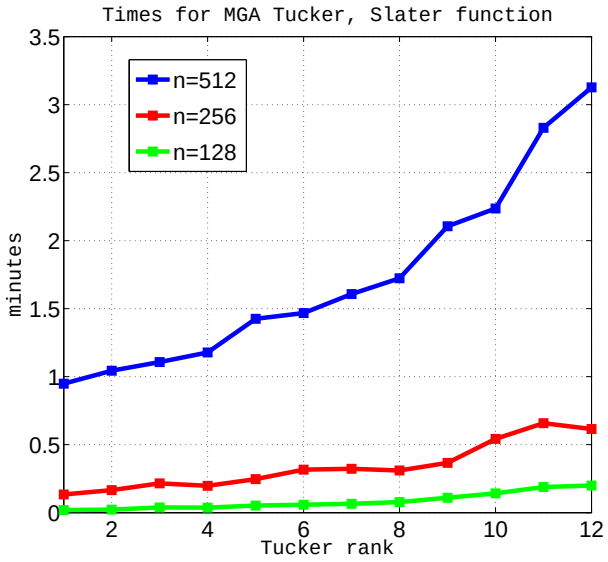

Figure 3.12: MATLAB times for the MGA Tucker approximation for the discretized Slater function.

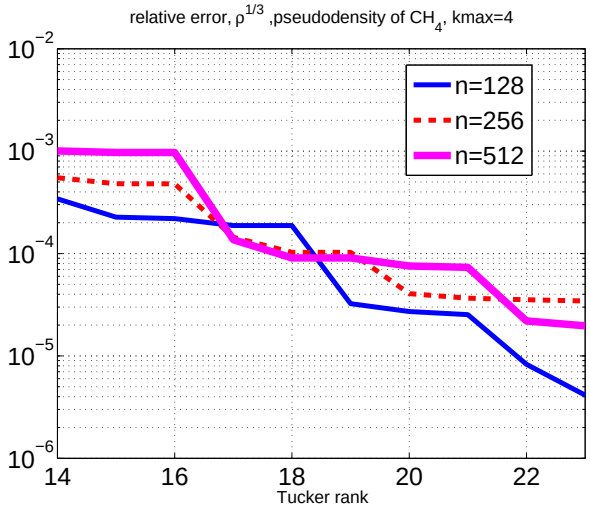

Figure 3.13: Relative approximation error (Frobenius norm) of the MGA Tucker approximation applied to the discretized "exchange" potential $\rho^{1/3}$.

3.3.2 BTA of the electron density of Aluminium clusters

In our next example, we consider the Tucker approximation of the electron density of the Aluminium molecular clusters originating from the large scale finite element (FE) calculations in the OFDFT method [32, 33]. By using the multigrid accelerated Tucker decomposition procedure, the appropriate mapping subspaces are computed for the data from the FE simulations interpolated to the uniform 3D Cartesian grid.

FE computations have been performed for two configuration of the Aluminium lattice, further called cluster_{14} and cluster_{172}, containing 14 and 172 atoms, respectively. Figure 3.14 visualises the middle-point plane cross-section of electron densities for these two configurations.

First, we interpolated (by cubic splines) the electron density from the initial FE unstructured grid onto an $n_m \times n_m \times n_m$ Cartesian grid for a sequence of mesh parameters n_m, thus obtaining 3D tensors A_{n_m}, $m = 0, 1, ..., M$. Since the accuracy level of the finite element discretization for the considered examples was resolved on a Cartesian grid of size $n_M^3 = 200^3$, there was no need for finer interpolation grids. Then the tensor A_M is approximated by the rank-(r, r, r) Tucker model applying Algorithm **MG_G_BTA** to full-format tensors. We check the Tucker approximation error versus the rank-parameter r, increasing from $r = 1, 2, \ldots$ to some predefined value.

Figure 3.15 shows the first 6 orthogonal vectors of the matrix $V^{(1)}$, for cluster_{14} (left) and cluster_{172} (right), respectively. We can observe that the shape of the

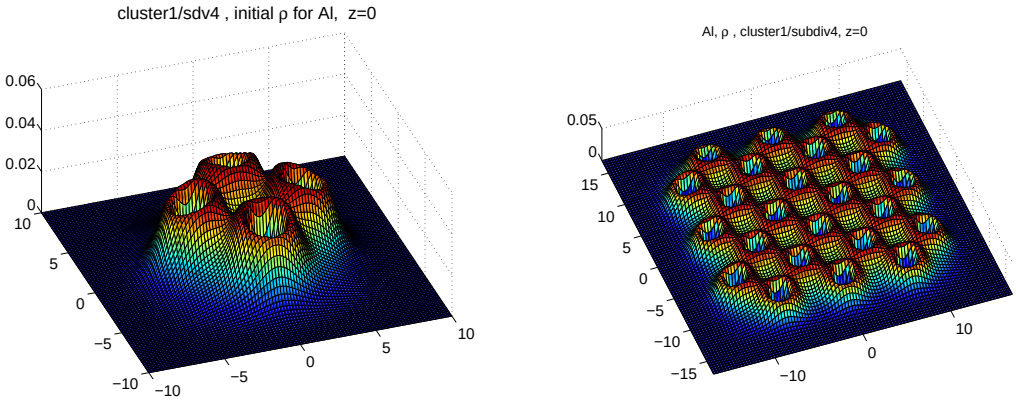

Figure 3.14: a) Pseudo-density of Aluminium cluster on the regular $n^{\otimes 3}$-grid for $n = 200$: cluster_{14} (left), cluster_{172} (right).

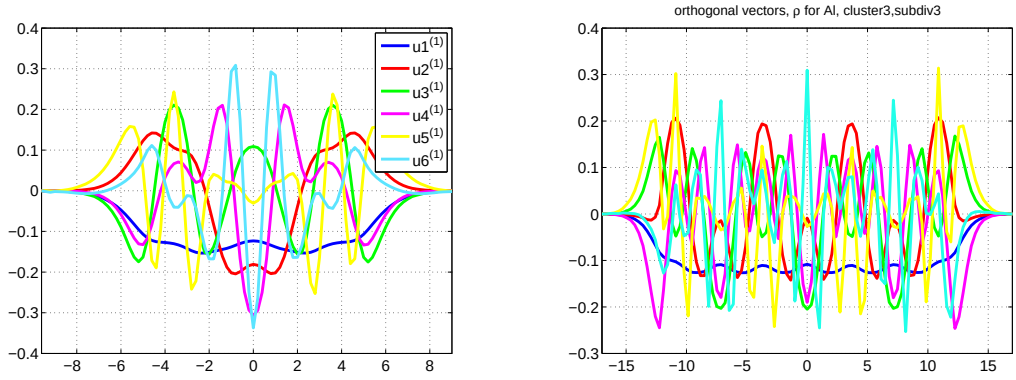

Figure 3.15: a) Orthogonal vectors of matrices $V^{(1)}$ for cluster_{14} (left) and cluster_{172} (right), $(r = 6)$.

Tucker orthogonal basis functions "resolves" the complicated shape of the considered lattice structure, providing good approximation properties already with moderate Tucker ranks, as seen in the next Figure 3.16. This feature can be useful for the construction of the small-size set of problem-adapted orthogonal basis functions.

Figure 3.16 presents the absolute error in the Tucker approximation with the rank $\mathbf{r} = 10$ for the cluster_{14} (left) and for the cluster_{172} (right). The maximum absolute approximation errors for both clusters are bounded as $\leq 10^{-4}$, which is in the range of the error of the employed FE approximation, see [14]. We observe convergence in the Frobenius norms E_{FN} with respect to the Tucker rank r over Cartesian grids of size 101^3, 201^3 for cluster_{14} (left), and 91^3, 181^3 for cluster_{172}

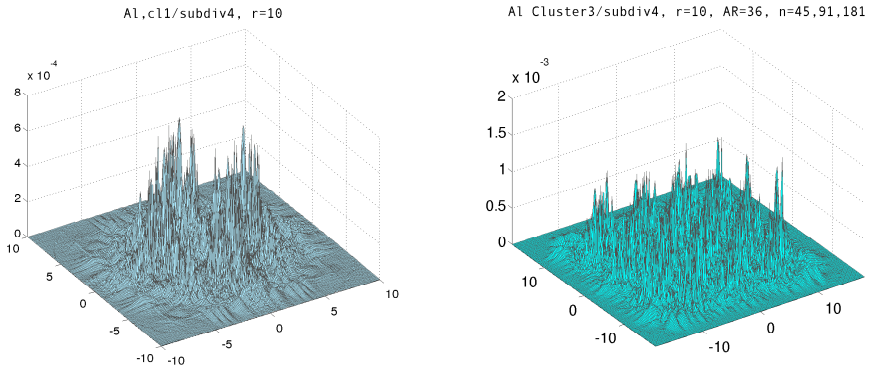

Figure 3.16: a) The absolute error of the rank -10 Tucker approximation to the Aluminium cluster$_{14}$ with $n = 201$ (left) in the cross-section $S = [-10, 10] \times [-10, 10] \times \{0\}$, and for cluster$_{172}$ with $n = 181$ in the cross-section $S = [-18, 18] \times [-18, 18] \times \{0\}$ (right).

(right), correspondingly.

Figures in 3.17 demonstrate that even the Tucker rank $r = 6$ is sufficient to represent the data from FE simulations with the absolute error up to $10^{-4} \div 10^{-5}$ (corresponding to relative accuracy $10^{-2} \div 10^{-3}$, see blue lines in Figure 3.17). For the Tucker rank $r = 8$ and $n = 200$, the storage requirements are $O(r^3 + 3rn) \cong 5300$, in contrast to approximately 20MB of the original data.

We observe that the original tensor can be represented in the Tucker or canonical tensor format using a relatively tiny number of coefficients. For example, the original 3D tensor corresponding to the electron density of the Aluminium cluster$_{172}$ can be approximated (up to relative accuracy 10^{-3}) either by $r_T^3 = 8^3$ basis functions constructed using the combinations of the orthogonal vectors in $\mathbb{R}^n$ from the respective Tucker mapping, or by $R \leq r_T^2$ basis functions using the canonical vectors in $\mathbb{R}^n$. Note, that the Tucker rank r to achieve the resolution of FE scheme remains almost independent of the increasing number of atoms in a cluster, as we already observed in the numerics on (almost) periodic structures in Section 2.3.2. It indicates that the numerical complexity for solving larger problems would increase only linearly in the univariate grid size n.

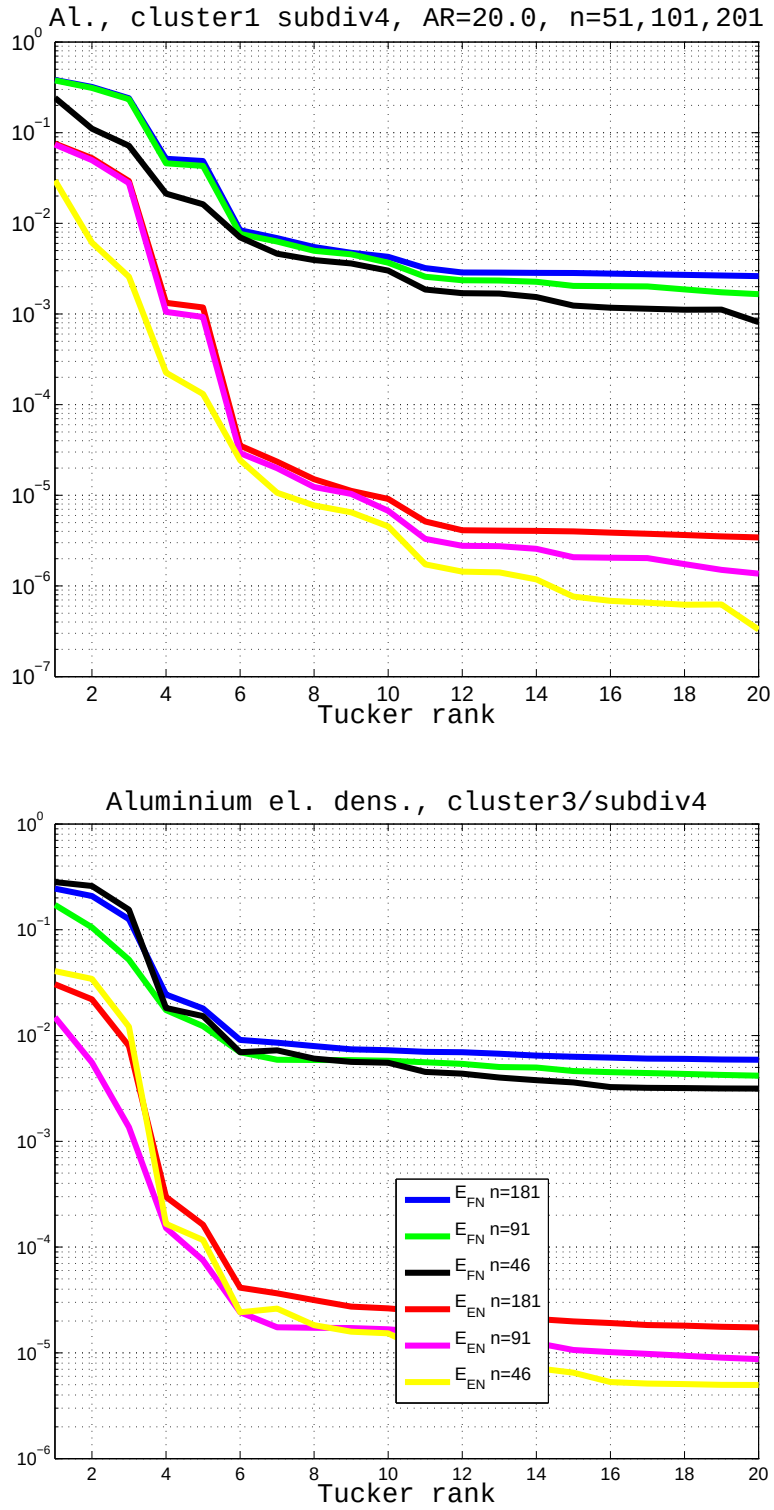

Figure 3.17: Convergence of the Tucker tensor approximation for cluster_{14} (top) and cluster_{172} (bottom).

4 TS computation of the Coulomb and exchange Galerkin matrices

4.1 General remarks

In this section, we consider a novel approach for the numerical evaluation of the Hartree and exchange integral operators in the Hartree-Fock equation. It is based on the tensor-structured representation of the involved functions and operators on $3D$ Cartesian grids and the *agglomerated* computations of the Hartree potential and the Coulomb and exchange matrices using the tensor-structured operations described in Section 2.4.2. This provides linear complexity scaling with respect to the univariate grid size n.

Reduction of the computational complexity in electronic structure calculations based on low-rank separable representations of functions is a usual practice in quantum chemistry. But, the low rank concept is applied in the choice of well-separable basis functions enabling the analytical evaluation of the one- and two-electron integrals corresponding to the Hartree and the exchange operators. Usually, *Gaussian-type orbital* (GTO) basis sets are used for the evaluation of the involved integrals [3, 53, 25, 20].

Our grid-based approach for the TS computations of functions and operators in the Hartree-Fock equation is essentially different. We discretize the basis functions on the $n \times n \times n$ Cartesian grid and perform integrations with the agglomerated densities/orbitals in tensor-product format using efficient multilinear algebra on low-rank tensors. Therefore, our main goal is to construct the numerical algorithms which enable computations on fine enough spatial grids to fulfill the accuracy requirements, and to introduce stable rank reduction schemes, also conserving the required high accuracy.

For reducing the initial or intermediate ranks of the canonical tensors, we use the combination of the MGA C2T with the consequent T2C transforms, also scaling linearly in all input parameters. As shown in Section 2.3.3 on the examples of the low-rank orthogonal Tucker tensor approximations to electron densities and Hartree potentials of some molecules, exponential convergence with respect to the Tucker rank is observed.

This enables an efficient tensor-product convolution for computation of the Hartree potential using a collocation-type approximation via piecewise constant basis functions on a uniform $n \times n \times n$ grid. In a similar way, the tensor-product convolution is applied to the Hartree-Fock exchange. As it was already mentioned, the complexity of the tensor product convolution introduced in [61] is of order

$$W_{C*C} = O(R_1 R_2 n \log n),$$

where R_1 and R_2 are the canonical ranks of 3D tensors representing the convolving kernel and density, respectively, and n is the one-dimension grid size. Note that the tensor-product convolution outperforms significantly the 3D FFT of complexity $O(n^3 \log n)$, that is linear-logarithmic with respect to the volume size of the 3D tensor (see Table 4.1).

It should be noted, that our algorithms for the computation of the Coulomb and the exchange matrices work as "black-box" schemes, since in the convolution integrals (1.8) and (1.10) only a pair of 3D tensors is involved - the grid-based electron density/molecular orbitals and the Newton kernel. Therefore, there are no restrictions on grid-based basis functions which can be used for the grid representation of the electron density and orbitals.

Notice, that due to the grid-based concept, our approach is very flexible concerning the character of the chosen Galerkin basis set, see properties (A)–(D) in Section 5.1.3. In the present computations, we use the GTO basis sets, mostly, due to possibility of easy evaluation of the computational accuracy for all important entities (comparison with MOLPRO), beginning from the calculation of the Hartree and exchange potentials, and up to energy estimates from the solution of the Hartree-Fock equation in the tensor-structured format.

4.2 Accurate evaluation of the Hartree potential by the tensor-product convolution in $\mathbb{R}^3$

We consider the computation of the Hartree potential

$$V_H(x) := \int_{\mathbb{R}^3} \frac{\rho(y)}{\|x-y\|}\, dy = \left(\rho * \frac{1}{\|\cdot\|}\right)(x), \quad x \in \mathbb{R}^3, \tag{4.1}$$

that is the convolution product of the Newton kernel with the electron density

$$\rho(y) = 2 \sum_{a=1}^{N_{orb}} (\varphi_a(y))^2. \tag{4.2}$$

We apply the discrete tensor-product convolution on tensor grids in $\mathbb{R}^3$, described in [61].

In general, our computational scheme for the convolution integral (4.1) involves the following steps (which will be considered further in details):

1. Compute the grid-based canonical representation of the electron density of the molecule using the expansion coefficients for GTOs for the electron orbitals, and by discretizing the corresponding GTO basis functions on $n \times n \times n$ tensor grid. In this way, the initial rank R_{ρ_0} of the canonical tensor representing ρ is of the order 10^3 or even 10^4, depending on the molecule.

2. Reduce the rank of the electron density by consequent MGA C2T and T2C transforms. Then the canonical rank of ρ is reduced by an order of magnitude, which is sufficient for the fast discrete tensor-product convolution. As shown in Section 3.2 the MGA C2T algorithm yields linear scaling in n and the initial rank R_{ρ_0}. As a result of this step, we obtain the computationally feasible rank $R_\rho \ll R_{\rho_0}$.

3. Compute the convolution (4.1) (representing the Hartree potential) in tensor-product format using rank-R_N canonical representation of the Newton potential with R_N about $20 \div 30$ and canonical representation of the electron density obtained in Step 2.

We use the total electron density $\rho(y)$, $y = (y^1, y^2, y^3) \in \mathbb{R}^3$, in a form including rank-R_0 separable representation of orbitals in GTO basis set,

$$\varphi_a(x) = \sum_{k=1}^{R_0} c_{ka} g_k(x), \quad a = 1, ..., N_{orb}, \tag{4.3}$$

so that $\rho(y)$ is given by the polynomial-exponential sum

$$\rho(y) := 2 \sum_{\nu=1}^{N_{orb}} \left(\sum_{k=1}^{R_0} c_{k\nu} \prod_{\ell=1}^{3} (y^\ell - A_k^\ell)^{\beta_k^\ell} e^{-\alpha_k \|y - A_k\|^2} \right)^2, \tag{4.4}$$

where $A_k = (A_k^1, A_k^2, A_k^3) \in \mathbb{R}^3$ $(k = 1, ..., R_0)$ correspond to the locations of atoms in a molecule, $\beta_k^\ell \in \mathbb{N}_0$, N_{orb} is the number of electron pairs, and R_0 is the number of GTO basis functions. For example, the number of GTO basis functions is given by $R_0 = 55$, 41 and 96 for CH_4, H_2O and C_2H_6 molecules, respectively.

We assume that a particular molecule is embedded in an appropriate computational box $[-b, b]^3$. We use $b = 10.6$ atomic units (au) for H_2O and $b = 14.6$ au for CH_4 and C_2H_6 molecules. In the following, we represent the convolving tensor corresponding to $\rho(y)$ in the canonical format. Since the products of two Gaussians in (4.4) can be written in the form of a single Gaussian by recomputing the coefficients as

$$e^{-\lambda(y-a)^2} \cdot e^{-\beta(y-b)^2} = e^\sigma \cdot e^{-\gamma(y-c)^2}, \quad \sigma = \frac{\lambda\beta(a-b)^2}{\lambda+\beta},\ \gamma = \lambda + \beta,\ c = \frac{a\lambda + b\beta}{\lambda+\beta},$$

and taking into account the symmetry of the representation, we arrive at the following bound on the initial rank of the input tensor

$$R \le R_{\rho_0} = \frac{R_0(R_0+1)}{2}. \tag{4.5}$$

Hence, for the considered particular molecules, we have the following ranks of the discrete canonical representation of the electron densities:

$$R_{\rho_0,CH_4} = 1540, \quad R_{\rho_0,C_2H_6} = 4656, \quad R_{\rho_0,H_2O} = 861.$$

In our computational scheme, we apply Algorithm MG_C_BTA for rank reduction of the electron density tensor (see the discussion below).

We apply the collocation scheme to discretise the convolution product in tensor formats (see [61]). To that end we introduce the equidistant tensor grid in the computational box $[-b,b]^3$,

$$\omega_{\mathbf{3},n} := \omega_1 \times \omega_2 \times \omega_3, \quad \omega_\ell := \{-b + (m-1)h : m = 1, ..., n+1\}, \tag{4.6}$$

with $\ell = 1, 2, 3$, and mesh-size $h = 2b/n$, and define a set of collocation points $\{x_{\mathbf{m}}\} \in \omega_{\mathbf{3},n}$, $\mathbf{m} \in \mathcal{M} := \{1, ..., n+1\}^3$, composing the tensor grid $\omega_{\mathbf{3},n}$. For technical reasons we further assume that $n = 2k$, $k \in \mathbb{N}$. Now we choose a set of piecewise constant basis functions $\{\phi_{\mathbf{i}}\}$, $\mathbf{i} \in \mathcal{I} := \{1, ..., n\}^3$, defined as the characteristic functions of elementary grid-cells in $\omega_{\mathbf{3},n}$. For a given continuous function f supported in the computational box $[-b,b]^3$ (i.e. $f(y) = 0$ for $y \in \mathbb{R}^3 \setminus [-b,b]^3$), let $f_{\mathbf{i}} = f(y_{\mathbf{i}})$, $\mathbf{i} \in \mathcal{I}$, be the (collocation) representation coefficients of f in the basis set $\{\phi_{\mathbf{i}}\}$,

$$f(y) \approx \sum_{\mathbf{i}\in\mathcal{I}} f_{\mathbf{i}}\phi_{\mathbf{i}}(y), \quad y \in [-b,b]^3, \tag{4.7}$$

where $y_{\mathbf{i}}$ is the midpoint of the grid-cell numbered by $\mathbf{i} \in \mathcal{I}$ (see (2.41) for explicit definition).

Now the discrete *collocation convolution scheme* recovers approximately the values of the exact convolution product

$$(f * p)(x) = \int_{\mathbb{R}^3} f(y)p(x-y)\,dy, \quad x \in [-b,b]^3,$$

in the set of collocation points $\{x_{\mathbf{m}}\}$,

$$f * p \approx [w_{\mathbf{m}}]_{\mathbf{m}\in\mathcal{M}}, \quad w_{\mathbf{m}} := \sum_{\mathbf{i}\in\mathcal{I}} f_{\mathbf{i}} \int_{\mathbb{R}^3} \phi_{\mathbf{i}}(y)p(x_{\mathbf{m}}-y)dy, \quad x_{\mathbf{m}} \in \omega_{\mathbf{3},n}.$$

We refer to [61] concerning particular assumptions on the convolving density f and convolving kernel function p.

In the following applications, our particular choice is specified by $f(y) = \rho(y)$, $y \in [-b,b]^3$, where ρ is the electron density, and $p(x-y) = 1/\|x-y\|$, being the classical Newton (Coulomb) potential. To compute the integral transforms, we apply the piecewise constant approximation to discretize the separable GTO basis functions of the type

$$g_k(y) = \prod_{\ell=1}^{3} (y^\ell - A_k^\ell)^{\beta_k^\ell} e^{-\alpha_k \|y-A_k\|^2} \equiv \prod_{\ell=1}^{3} g_k^{(\ell)}(y^\ell), \quad y \in \mathbb{R}^3, \quad k = 1, \ldots, R_0, \tag{4.8}$$

by rank-1 $n \times n \times n$ tensors. The respective canonical vectors are obtained by sampling the univariate functions $g_k^{(\ell)}(y^\ell)$ at the centers of intervals prescribed by the tensor grid $\omega_{\mathbf{3},n}$. Specifically, we define the sampling points $\{y_{\mathbf{i}} = (y_{i_1}^1, y_{i_2}^2, y_{i_3}^3)\}$, $i_\ell \in I = \{1, \ldots, n\}$ for $\ell = 1, 2, 3$, where, as above, $y_{\mathbf{i}}$ is the midpoint of the grid-cell numbered by $\mathbf{i} \in \mathcal{I}$.

The rank-1 tensor representing the single Gaussian g_k, $k = 1, ..., R_0$, is given by the canonical rank-1 tensor

$$G_k \equiv [g_{\mathbf{i}}]_{\mathbf{i}\in\mathcal{I}} = \gamma^{(1)} \otimes \gamma^{(2)} \otimes \gamma^{(3)} \in \mathbb{V}_{\mathbf{n}} \quad \text{with entries} \quad g_{\mathbf{i}} = g_{i_1}^{(1)} \cdot g_{i_2}^{(2)} \cdot g_{i_3}^{(3)}, \tag{4.9}$$

where

$$\gamma_k^{(\ell)} = \{\gamma_{k,i}^{(\ell)}\}_{i\in I_\ell} \in \mathbb{V}_\ell, \quad \gamma_{k,i}^{(\ell)} = (y_i^\ell - A_k^\ell)^{\beta_k^\ell} e^{-\alpha_k (y_i^\ell - A_k^\ell)^2}, \quad \ell = 1, 2, 3.$$

At the *first step*, the 3rd order coefficients tensor $F = [f_{\mathbf{i}}] \in \mathbb{R}^{\mathcal{I}}$ approximating the electron density ρ, is represented by a rank-R_{ρ_0} canonical tensor in the "discretized" GTO basis set[1] corresponding to (4.4).

At the *second step*, we precompute the coefficients tensor $P = [p_{\mathbf{i}}] \in \mathbb{R}^{\mathcal{I}}$,

$$p_{\mathbf{i}} = \int_{\mathbb{R}^3} \frac{\phi_{\mathbf{i}}(y)}{\|y\|} dy, \quad \mathbf{i} \in \mathcal{I}. \tag{4.10}$$

The coefficient tensor $P = [p_{\mathbf{i}}]$ corresponding to the Coulomb potential $\frac{1}{\|x-y\|}$ is approximated in the rank-R_N canonical tensor format using optimised *sinc*-quadratures [98, 10, 61], where the rank parameter $R_N = O(|\log \varepsilon| \log n)$ depends logarithmically on both the required accuracy $\varepsilon > 0$ and the grid-size n. In all computations presented below we choose the tensor rank in the range $R_N \in [20, 30]$ to ensure the desired accuracy of order $10^{-4} \div 10^{-6}$.

[1] To reduce the numerical complexity of the tensor-product convolution it is approximated either in the rank-(r,r,r) Tucker format or via the canonical model with the tensor rank $R < R_{\rho_0}$ using the MGA canonical-to-Tucker-to-canonical rank reduction scheme described in Section 3.

At the *third step*, following [61, 67], we compute the set of values $w_{\mathbf{m}}$, $\mathbf{m} \in \mathcal{M}$, by copying the corresponding portion of entries (centred at $\mathbf{j} = \mathbf{n}$) taken from the *discrete tensor convolution* of 3rd order tensors,

$$F * P := \{z_{\mathbf{j}}\}, \quad z_{\mathbf{j}} := \sum_{\mathbf{i} \in \mathcal{I}} f_{\mathbf{i}} p_{\mathbf{j}-\mathbf{i}+\mathbf{1}}, \quad \mathbf{j} \in \mathcal{J} := \{1, ..., 2n-1\}^3, \tag{4.11}$$

where the sum is over all $\mathbf{i}, \mathbf{j} \in \mathcal{I}$, which lead to legal subscripts for $p_{\mathbf{j}-\mathbf{i}+\mathbf{1}}$, i.e., $\mathbf{j} - \mathbf{i} + \mathbf{1} \in \mathcal{I}$. Specifically, we define $w_{\mathbf{m}} = z_{\mathbf{m}+\mathbf{n}/2-\mathbf{1}}$, $\mathbf{m} \in \mathcal{M}$.

Remark 4.1 *The tensor* $[w_{\mathbf{m}}]$ *can be identified with the piecewise trilinear interpolating function uniquely defined by its values at the grid (collocation) points* $\{x_{\mathbf{m}}\}$, $\mathbf{m} \in \mathcal{M}$. *Sampling this interpolant at cell-centered points* $\{y_{\mathbf{i}}\}$, $\mathbf{i} \in \mathcal{I}$, *defined above, we return the coefficient tensor* $V \in \mathbb{V}_{\mathbf{n}} = \mathbb{R}^{\mathcal{I}}$ *of the resultant approximate convolution, providing the representation in the same basis set* $\{\phi_{\mathbf{i}}\}$ *as for the initial electron density* $f = \rho$. *In the following, the resultant coefficients tensor* $V \in \mathbb{V}_{\mathbf{n}}$ *over the index set* $\mathcal{I}$ *will be denoted by* $V \equiv F *_T P \approx f * p$.

Representing F in the rank-R canonical format (see (2.6)) enables us to compute $F * P$ in the form (see Section 2.4.2)

$$F * P = \sum_{k=1}^{R_N} \sum_{m=1}^{R} c_k b_m \left(u_k^{(1)} * v_m^{(1)}\right) \otimes \left(u_k^{(2)} * v_m^{(2)}\right) \otimes \left(u_k^{(3)} * v_m^{(3)}\right), \tag{4.12}$$

which leads to the cost

$$\mathcal{N}_{C*C} = O(RR_N n \log n).$$

Thus, computation of the convolution product with the rank $R = R_{\rho_0}$ of the input tensors has practical limitations since the exact rank of the resulting tensor is the product of those for the convolving arrays. For reducing the tensor rank of the convolving density, we apply the fast algorithm MG_C_BTA($\boldsymbol{\mathcal{C}}_{R,\mathbf{n}_M} \to \boldsymbol{\mathcal{T}}_{\mathcal{C}_R,\mathbf{r}}$) for the canonical-to-Tucker multigrid transform defined on the sequence of refined grids, followed by the Tucker-to-canonical transform of the core tensor. In this way, the canonical rank R can be reduced by the order of magnitude, from several thousands to few hundreds or even tens, depending on the input data and the required accuracy.

Table 4.1 shows the advantage of the fast tensor-product convolution method with the rank recompression via the MG_C_BTA algorithm, compared with those based on 3D FFT (of the complexity $O(n^3 \log n)$). We present the MATLAB CPU time for a high accuracy computation of the Hartree potential for the H_2O

n^3	128^3	256^3	512^3	1024^3	2048^3	4096^3	8192^3	16384^3
$3D$ FFT (sec)	4.3	55.4	582.8	~ 6000	–	–	–	~ 2 years
$Conv_{CC}$ (sec)	1.0	3.1	5.3	21.9	43.7	127.1	368.6	700.2
$C_R \to T_r$ (sec)	1.5	3.8	8.2	16.4	32.0	64.0	136.0	

Table 4.1: Comparison of the 3D FFT and the tensor-product convolution. The bottom line shows the times for C2T rank reduction.

molecule on a Sun Fire X4600 computer with 2,6 GHz processor. The CPU time for the FFT-based scheme with $n \geq 1024$ is obtained by extrapolation, with factor 10 for each step of grid refinement.

As it was mentioned, in general, the complexity of the single grid canonical-to-Tucker transform depends polynomially on the parameters of the model, see Algorithm C_BTA ($\boldsymbol{\mathcal{C}}_{R,\mathbf{n}} \to \boldsymbol{\mathcal{T}}_{\mathcal{C}_R,\mathbf{r}}$). The *multigrid acceleration technique* employed by MG_C_BTA algorithm provides calculations of the 3D integral transform (4.1) using benchmark grid sizes up to $\mathcal{N}_{volume} = 16384^3$ in small computational times, of the multigrid preprocessing and discrete 3D convolution. Figure 4.2 b) demonstrates the linear scaling of the rank reduction algorithm in the grid-size n.

The approximation error of the discrete tensor-product convolution $V_H^{(n)} = V$ approximating the Hartree potential $V_H(\mathbf{x})$ (see Remark 4.1) and applied to the particular class of electron density functions appears to be of order $O(h^2)$ (in the Frobenius norm), see the error analysis in Theorems 2.2 and 2.3, [61]. Following [61], we apply the Richardson extrapolation technique to obtain higher accuracy approximations of order $O(h^3)$ without extra computational cost. The corresponding Richardson extrapolant $V_{H,Rich}^{(n)}$ approximating $V_H(\mathbf{x})$ over a pair of nested grids $\omega_{\mathbf{3},n}$ and $\omega_{\mathbf{3},2n}$ and defined on the coarser $n \times n \times n$ grid is given by

$$V_{H,Rich}^{(n)} = (4 \cdot V_H^{(2n)} - V_H^{(n)})/3 \quad \text{over the grid-points in } \omega_{\mathbf{3},n}. \tag{4.13}$$

Figure 4.1 illustrates the effect of the Richardson extrapolation in the computation of V_H for the pseudodensity case of CH_4 on small $n \times n \times n$ grids with $n = 112, 224, 448$. Due to a distinct asymptotic convergence ratio of 4 in the computations on dyadically refined grids, the Richardson method gives an improvement of accuracy from 10^{-3} to $10^{-5} \div 10^{-6}$.

For the all electron case of moderate size molecules large grids are required to enable high accuracy of the computations in the presence of cusps in the electron density due to core electrons contribution. Figures 4.2 a), 4.3 a) and 4.4 a) show the accuracy of the computation of the Hartree potential of the H_2O, CH_4 and C_2H_6 molecules on logarithmic scale. We present the absolute error for V_H in the subinterval along the x-axis compared with the corresponding values of V_H

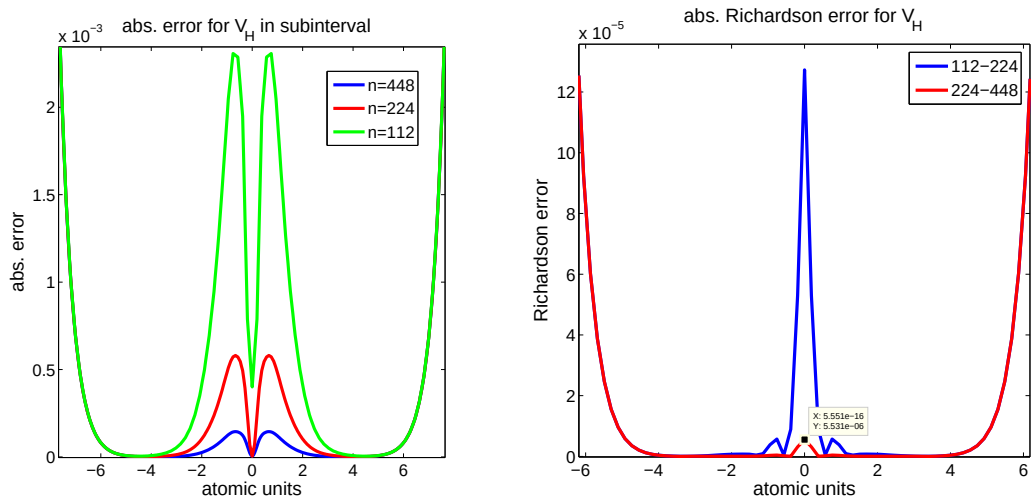

Figure 4.1: Absolute approximation error in the Hartree potential V_H for the pseudo-density of CH_4 in the subinterval $\Omega = [-7, 7] \times \{0\} \times \{0\}$ (left) and the reduced error by Richardson extrapolation involving two pairs of grids (right).

computed by the MOLPRO package. We compare the computational error for the grid sizes $n = 4096, 8192$ and for the corresponding Richardson extrapolation of order $O(h^3)$.

We observe the accuracy $8 \cdot 10^{-5}$ hartree at the cusp region corresponding to Carbon atom in CH_4, $5 \cdot 10^{-5}$ hartree at the cusp region corresponding to the Oxygen atom in H_2O, and $5 \cdot 10^{-6}$ hartree at the cusps corresponding to the Carbon atoms in C_2H_6. Note that maximum values of the Hartree potential at the cusp points are $V_H(0, 0, 0) = 8.35$, 11.73 and 9.49 hartree for the CH_4, H_2O and C_2H_6 molecules, respectively. This yields relative accuracy of the order 10^{-6} in the cusp region for the considered molecules.

Figures 4.2 b), 4.3 b) and 4.4 b) show the CPU times for the CH_4, H_2O and C_2H_6 molecules, respectively, for C2T preprocessing and 3D convolution. The total time for V_H at a fixed grid size $n = n_f$ consists of a sum of preprocessing times from all previous levels, starting from the initial grid with, say $n_0 = 64$, up to n_f, plus the convolution time for the level with $n = n_f$.

The computational time depends strongly on the chosen accuracy of approximation, which is prescribed by the multigrid parameters p and r, see Theorem 3.1. It should be noted that the CPU times can be crucially reduced if the accuracy of the result is not so demanding, say up to 10^{-3}. In the applications discussed above the accuracy requirements are challenging, which leads to the in-

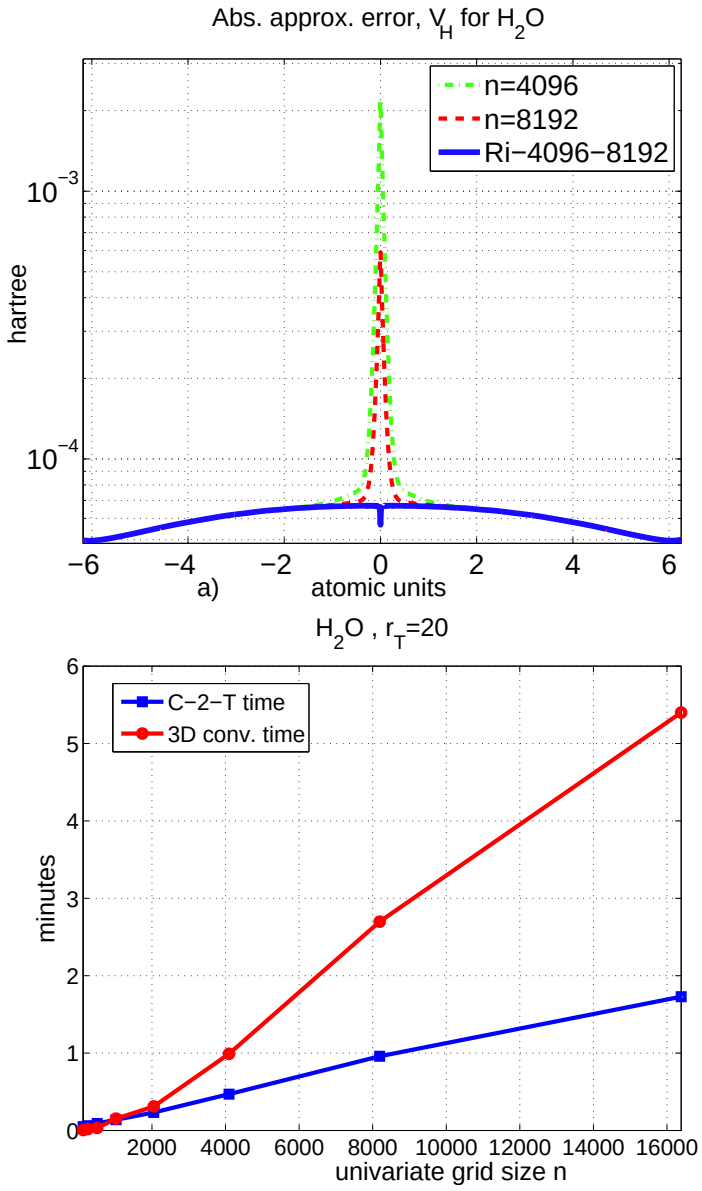

Figure 4.2: a) Absolute approximation error of the tensor-product computation of the Hartree potential of the water molecule in the subinterval $\Omega = [-6, 6] \times \{0\} \times \{0\}$, and the corresponding CPU times (bottom).

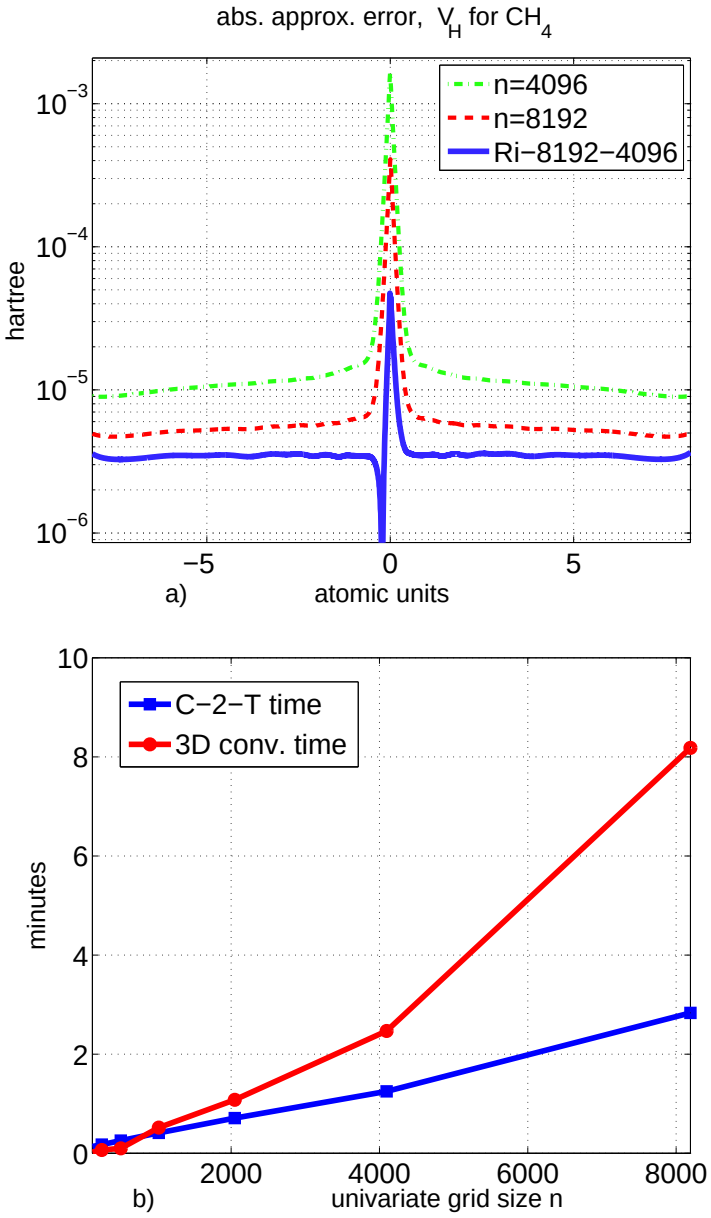

Figure 4.3: a) Absolute approximation error in the Hartree potential of CH_4 molecule measured in the subinterval $\Omega = [-8, 8] \times \{0\} \times \{0\}$, and b) the corresponding CPU times.

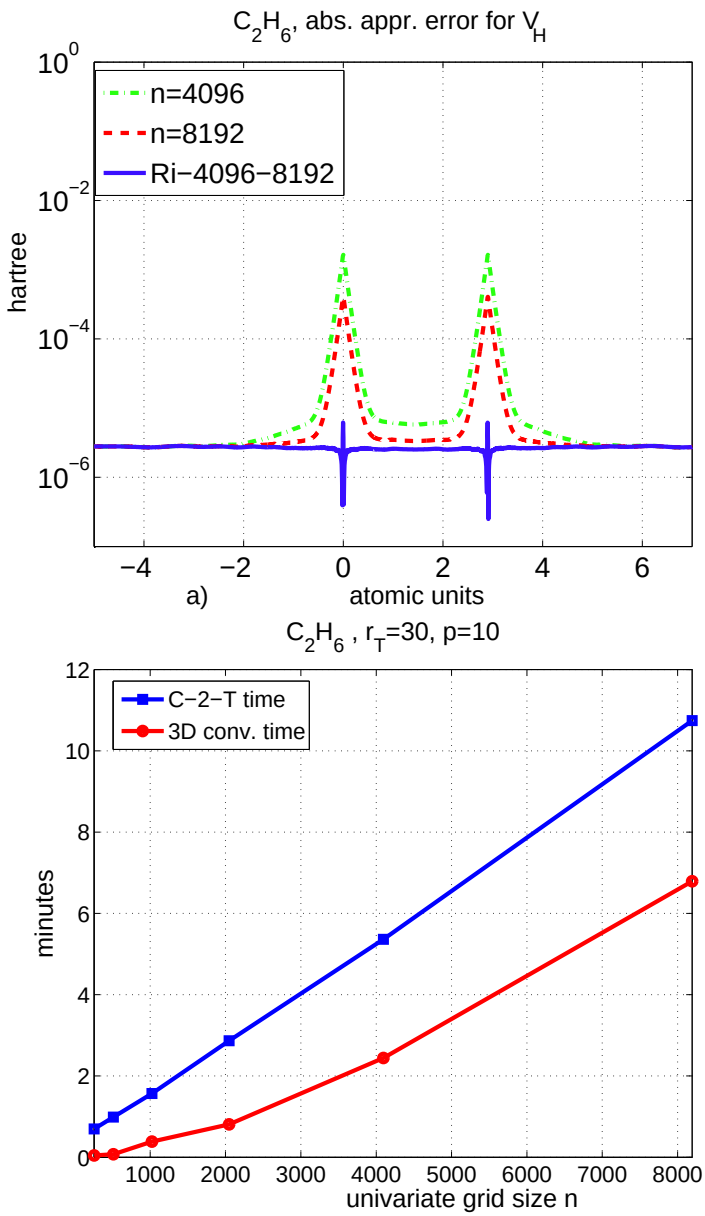

Figure 4.4: a) Absolute approximation error in the Hartree potential of C_2H_6 in the subinterval $\Omega = [-5, 7] \times \{0\} \times \{0\}$, the corresponding CPU times (bottom).

crease of parameters r and p in the MGA scheme, and consequently, the demands on computational resources.

4.3 Tensor computation of the Coulomb matrix

The Coulomb (Galerkin) matrix $J = \{J_{km}\}_{k,m=1}^{R_0}$ for the Hartree potential $V_H(x)$ with respect to the set of normalized Gaussians $\{\widetilde{g}_k\}$ is given elementwise by

$$J_{km} := \int_{\mathbb{R}^3} \widetilde{g}_k(x)\widetilde{g}_m(x)V_H(x)dx, \quad k,m = 1,\dots R_0. \tag{4.14}$$

For given rank-1 tensors G_k representing Gaussians $\{\widetilde{g}_k\}$ on $n \times n \times n$-grid, and the Hartree potential tensor $V = V_H^{(n)}$ computed for the considered molecule as above, we calculate the Galerkin Coulomb matrix $\{J_{km}\}$ using the tensor scalar product and Hadamard product operations as discussed in Section 2.4,

$$J_{km} := \langle G_k, G_m \odot V_H^{(n)} \rangle, \quad k,m = 1,\dots R_0. \tag{4.15}$$

Since the molecular orbitals are specified by the Galerkin coefficients matrix $C = \{c_{ka}\} \in \mathbb{R}^{R_0 \times N_{orb}}$ as in (4.3), in the following, we denote the nonlinear dependence in J by $J = J(C)$.

4.4 Numerics: the Coulomb matrices of CH_4, C_2H_6 and H_2O molecules

In this section we present numerical results on the tensor-structured computation of the Coulomb matrix for some particular molecules. Next figures show the difference between the reference matrices obtained by MOLPRO and our TS calculations of the Coulomb matrix for H_2O and small organic molecules in all electron case. Figure 4.7 visualises $[J_{km}]$ for H_2O and the absolute error of the TS computations.

Figures 4.6 shows absolute values of $[J_{km}]$ for C_2H_6 and the absolute approximation error of our TS calculations using the MGA parameters $r = 26$ and $p = 18$. Figures 4.5 show the Coulomb matrix errors for computations over the grids with the univariate sizes $n = 4096$ and $n = 8192$. Note, that for matrix elements the decay of the error has a factor of 4. This relation is a prerequisite for efficiency of the Richardson extrapolation (4.13). Then we obtain the resulting Coulomb matrix errors shown in Figure 4.6. Note, that the entries of the Coulomb matrix corresponding to cusp areas are approximated by the Richardson technique with

even better accuracy than other diagonal matrix entries, due to the almost exact convergence factor of 4 observed.

Results for the Coulomb matrix of CH_4 molecule are shown in Figure 4.8. The upper Figure shows the absolute values of the matrix entries. We perform the multigrid tensor-structured calculations, using rank reduction with the MGA parameters Tucker rank $r = 24$ and the number $p = 16$ of most important fibers. Lower figure in 4.8 shows the ultimate approximation error in computations using the Richardson extrapolation over the grids with $n = 4096$ and $n = 8192$.

Notice, that the errors for the diagonal matrix elements corresponding to cusp areas, are below $4{\cdot}10^{-6}$, $8{\cdot}10^{-6}$ and $8{\cdot}10^{-5}$ for the CH_4, C_2H_6 and H_2O molecules, respectively. The accuracy of the order of $10^{-5} \div 10^{-6}$ is defined by the chosen error control parameter $\varepsilon > 0$ in the tensor-structured computations of the Coulomb matrix. By using smaller values of ε at all steps of computations it is possible to get better accuracies at the expense of the computation time.

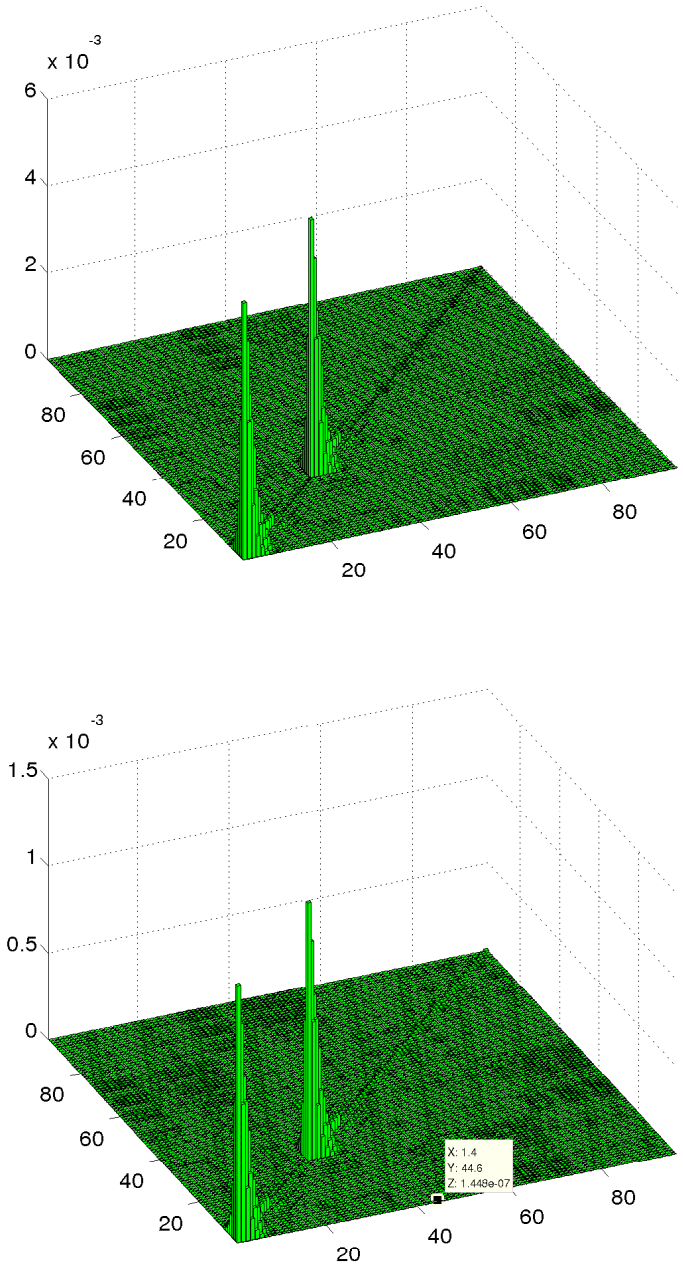

Figure 4.5: Absolute approximation error in the Coulomb matrix entries of C_2H_6 computed with the grid sizes 4096^3 (top) and 8192^3 (bottom).

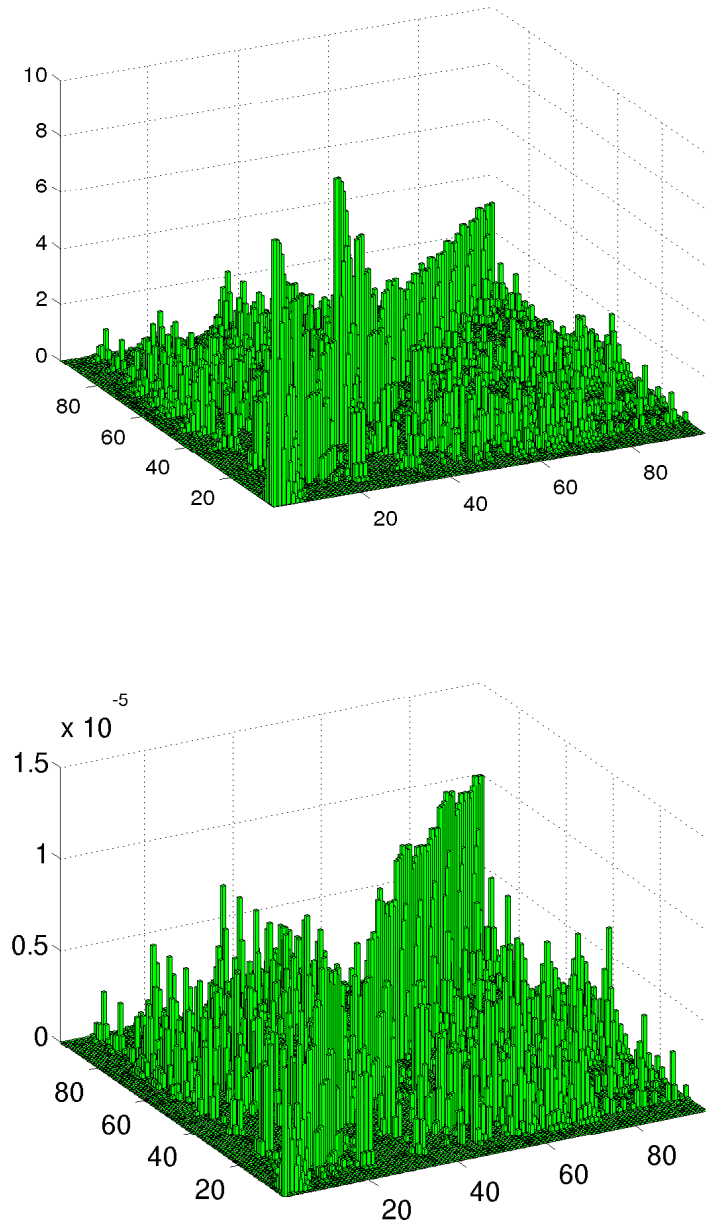

Figure 4.6: Absolute values of the Coulomb matrix entries of the C_2H_6 molecule (top) and absolute approximation error of calculations using MGA rank reduction (bottom).

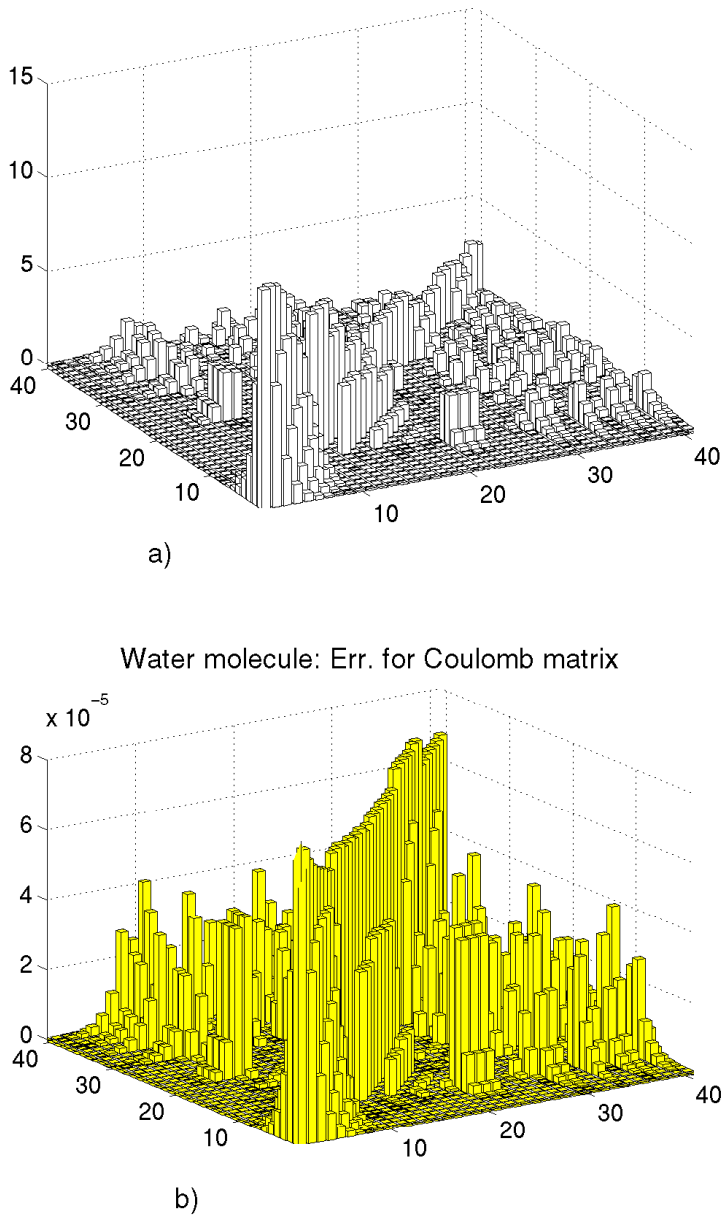

Figure 4.7: a) Coulomb matrix (absolute values) for H_2O, b) the absolute approximation error of the multigrid tensor product computation of the Coulomb matrix for H_2O.

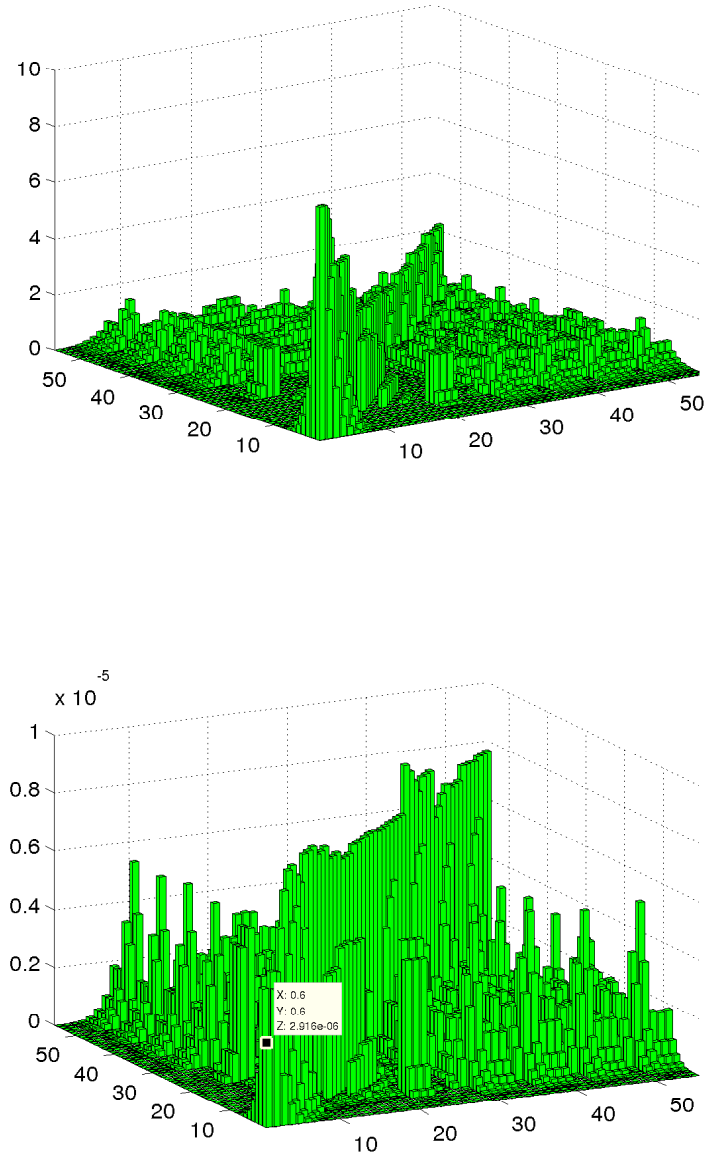

Figure 4.8: CH_4 molecule. Top: absolute values of the Coulomb matrix entries. Bottom: absolute approximation error in the Coulomb matrix obtained by the MGA tensor-structured method ($r = 24$, $p = 16$), with the Richardson extrapolation over the grids with $n = 4096$ and $n = 8192$.

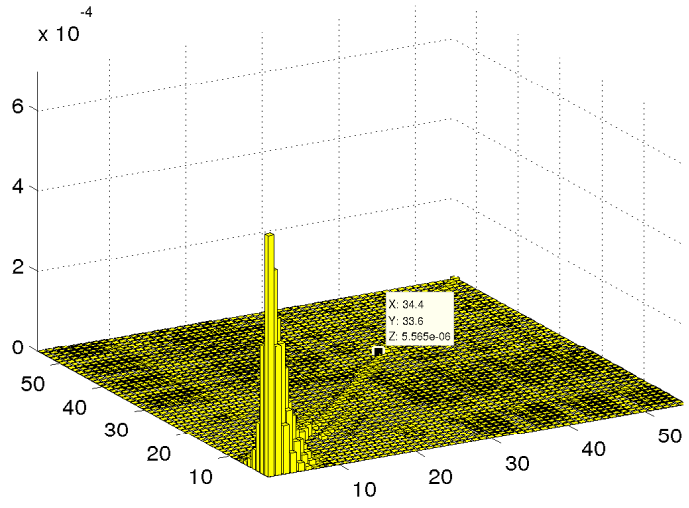

Figure 4.9: Absolute approximation error in the Coulomb matrix entries of CH_4 molecule computed with the grid size 16384^3.

4.5 Agglomerated computation of the Hartree-Fock exchange

In this section, we consider the tensor product approximation of the nonlocal (integral) exchange operator $\mathcal{K}$ in the Hartree-Fock equation by the agglomerated tensor-product operations used in Section 4.2 for the computation of the Hartree operator. Note that the calculation of the exchange Galerkin matrix in the Hartree-Fock equation is a challenging problem due to the nonlocal character of the exchange operator

$$(\mathcal{K}\psi)(x) := \sum_{a=1}^{N_{orb}} \int_{\mathbb{R}^3} \frac{\varphi_a(x)\varphi_a(y)}{\|x-y\|}\psi(y)\,dy \quad x \in \mathbb{R}^3, \tag{4.16}$$

which leads to the integration in six dimensions (see (4.17)). This problem is usually solved analytically by evaluating the so-called two-electron integrals using naturally separable basis sets like Gaussians, see [109, 78] and references therein.

Here, we propose and implement the grid-based evaluation of the Hartree-Fock exchange (4.16) by using the tensor product approximation of the included operators and functions on the 3D Cartesian grid. We apply the fast tensor product

convolution for the multivariate functions in $\mathbb{R}^d$ (see Section 4.2), providing complexity $O(dn \log n)$.

To cover the general case of molecular geometries, in the numerical examples, we use equal grid sizes n for three spatial dimensions (a cubic computational box) and do not employ information on a symmetry of the molecules. Therefore, our scheme works as a "grey-box" algebraic algorithm, where as the input data only the discrete representation of the Galerkin basis functions is used. However, the algorithm works as well with arbitrary $n_1 \times n_2 \times n_3$ grids.

Our initial algorithm for the evaluation of (4.16) has the complexity $O(R_0^2\, n \log n + n_{ef}\, R_0^4\, N_{orb})$, where $n_{ef} \ll n$ is the "effective" univariate grid size, and R_0 is the number of Galerkin basis functions. Here we reduce the constant in the linear complexity scaling in n by truncating the effective size of the computation intervals, where the values of rapidly decaying basis functions (in particular, Gaussians) are less than a threshold controlling the accuracy of computations. Thus, we have for the number of grid points in effective support of the interacting vectors, $n_{ef} = \alpha n$, with α much less than 1.

To reduce the R_0-asymptotics to $O(R_0^3)$, we further apply the canonical-to-Tucker algorithm for decreasing the ranks of intermediate results after every convolution step. The corresponding rank reduction algorithms are considered in Section 3.

The accuracy of the computation of matrix entries on a particular grid is estimated in numerical experiments by $O(h^2)$, where $h = O(n^{-1})$ is the step-size of the grid. We achieve $O(h^3)$ accuracy in our evaluation of the exchange matrix by using the Richardson extrapolation on a couple of consequent grids. Usually, the size of the computational box for small organic molecules is in the range of $14 \div 20$ $\mathring{A}$. Since the TS methods enable computations on huge 3D Cartesian grids, the univariate grid step-sizes of applied discretizations range from $h \approx 0.02$ $\mathring{A}$ for $n = 1024$, up to $h \approx 0.0008$ $\mathring{A}$ for the benchmark grids with the number of entries $n^3 = 16384^3$.

4.5.1 Galerkin exchange operator in the Gaussian basis

The exchange Galerkin matrix $K = K_{ex}$ with respect to the set of normalized "Cartesian Gaussians" $\{g_k\}_{k=1,\dots R_0}$ is given by

$$K_{ex} = \{K_{ij}\}_{i,j=1}^{R_0}, \quad K_{ij} := \frac{1}{2}\int_{\mathbb{R}^3}\int_{\mathbb{R}^3} g_i(x)\frac{\tau(x,y)}{\|x-y\|}g_j(y)dxdy, \quad i,j = 1,\dots R_0, \tag{4.17}$$

where the density matrix $\tau(x, y)$ is defined in terms of electron orbitals as

$$\tau(x, y) = 2 \sum_{a=1}^{N_{orb}} \varphi_a(x)\varphi_a(y),$$

over all occupied orbitals a.

The low cost of the three-dimensional convolution using the canonical representation of the convolving tensors makes possible the agglomerated numerical evaluation of the exchange matrix in the Fock operator. For this purpose, we split the integration in (4.17) into the following steps. First, we compute the convolutions of the pointwise products of molecular orbitals with the vectors from the normalized Gaussian basis set

$$W_{aj}(x) = \int_{\mathbb{R}^3} \frac{\varphi_a(y)g_j(y)}{\|x - y\|} dy \quad a = 1, \ldots, N_{orb},\ j = 1, \ldots, R_0. \tag{4.18}$$

These quantities are further used for the calculation of contributions to the Galerkin matrix entries from every orbital a,

$$V_{ij,a} = \int_{\mathbb{R}^3} \varphi_a(x)g_i(x)W_{aj}(x)dx, \quad i, j = 1, \ldots R_0. \tag{4.19}$$

The entries of the exchange matrix are then the sums of the corresponding values over all orbitals

$$K_{ij} = \sum_{a=1}^{N_{orb}} V_{ij,a}, \quad i, j = 1, \ldots N_{orb}. \tag{4.20}$$

We compute the exchange matrix (4.17) by the numerical scheme (4.18) - (4.20) using the discrete tensor product representation of arising functions and operators.

The occupied orbital of the molecule is considered as an expansion over the basis set of separable continuous functions $g_k(x)$,

$$\varphi_a(x) = \sum_{k=1}^{R_0} c_{ka} g_k(x), \quad x = (x_1, x_2, x_3) \in \mathbb{R}^3, \tag{4.21}$$

where the basis functions g_k, $k = 1, \ldots, R_0$, are represented as the rank-1 canonical tensor products,

$$g_k(x) = g_k^{(1)}(x_1)\, g_k^{(2)}(x_2)\, g_k^{(3)}(x_3), \tag{4.22}$$

with 1, 2, 3 designating spatial dimensions. Hence, with a fixed set of Galerkin basis functions $\{g_k\}$, the exchange matrix K depends (nonlinearly) on the representation coefficients matrix $C = \{c_{ka}\} \in \mathbb{R}^{R_0 \times N_{orb}}$, that will be specified as $K = K(C)$.

4.5.2 Discrete computational scheme

GTOs are used as conventional basis sets in electronic structure calculations due to their separability in spatial variables which is useful in the analytical evaluation of the two-electron integrals in the calculation of the Hartree and exchange potentials.

In the following, for numerical illustrations, we choose the discretized Gaussians as vectors in the rank-1 canonical representations of the basis functions, mainly for the sake of convenient verification of the computational results (the corresponding Galerkin matrix) with the standart MOLPRO output [108].

The rank-1 GTO basis functions $g_k(x)$, $k = 1, \dots R_0$, are given by (4.22) with $R = 1$, where $g_k^{(\ell)}(y^{(\ell)})$ denotes the generalized univariate Gaussians. The univariate Gaussians $g_k^{(\ell)}(y^{(\ell)})$, $\ell = 1, 2, 3$, are functions with infinite support given as

$$g_k^{(\ell)}(y^{(\ell)}) = (y^{(\ell)} - A_k^{(\ell)})^{\beta_k^{(\ell)}} \exp(-\alpha_k (y^{(\ell)} - A_k^{(\ell)})^2), \quad y^{(\ell)} \in \mathbb{R},\ \alpha_k > 0,$$

where $\beta_k^{(\ell)} = 0, 1, \dots$ is the polynomial degree, and the points $(A_k^1, A_k^2, A_k^3) \in \mathbb{R}^3$ specify the positions of nuclei in a molecule. In our scheme we use the *discrete* basis functions (given by vectors of the canonical tensor representation (2.6)) which are constructed by discretizing the Gaussians on the given tensor grid by using the associated piecewise constant basis functions, as in Section 4.2.

Assume that the molecule is embedded in a certain fixed computational box $[-b, b]^3$ with a suitable $b > 0$. For simplicity of notation, we take $n_\ell = n$ equal for all dimensions. We use the equidistant tensor grid $\omega_{\mathbf{3},n}$, see (4.6), with grid points $\{x_{\mathbf{m}}\}$, $\mathbf{m} \in \mathcal{M} := \{1, ..., n+1\}^3$. We use a representation like (4.7) with $f(y) = g_k(y)$, where the rank-1 coefficients tensor $G_k = \gamma_k^{(1)} \otimes \gamma_k^{(2)} \otimes \gamma_k^{(3)}$ is given by the values of ℓ-mode functions $g_k^{(\ell)}$ at the centers $y_{i_\ell}^{(\ell)}$ of the intervals of the univariate grid $[x_{i_\ell}^{(\ell)}, x_{i_\ell+1}^{(\ell)}]$, $i_\ell = 1, \dots, n$. This results in canonical vectors of length n with the entries $\{g_k^{(\ell)}(y_{i_\ell}^{(\ell)})\}_{i_\ell=1}^n$,

$$\gamma_k^{(\ell)} = \{g_k^{(\ell)}(y_{i_\ell}^{(\ell)})\}_{i_\ell=1}^n \in \mathbb{R}^n, \quad \text{for } \ell = 1, 2, 3,\ k = 1, \dots R_0. \tag{4.23}$$

such that we have $G_k = \gamma_k^{(1)} \otimes \gamma_k^{(2)} \otimes \gamma_k^{(3)}$. Given the coefficients matrix $C = \{c_{ka}\}$ $(k, a = 1, ..., R_0)$ corresponding to expansion (4.21), then by summing tensor products of the canonical vectors with the corresponding weights c_{ka}, we obtain the discrete representation of the orbital φ_a, $a = 1, \dots N_{orb}$, in the rank-R_0 canonical format,

$$U_a = \sum_{k=1}^{R_0} c_{ka} \gamma_k^{(1)} \otimes \gamma_k^{(2)} \otimes \gamma_k^{(3)}, \quad c_{ka} \in \mathbb{R}, \tag{4.24}$$

where R_0 is the number of basis functions. This discretization can be considered as a representation in the Galerkin set of basis functions $\{G_k\}$ obtained by representing the initial continuous basis set $\{g_k\}$ via piecewise constant basis functions $\{\phi_{\mathbf{i}}\}$ on the uniform grid (see (4.23)).

We use the rank-R_N canonical tensor product representation of the coefficient tensor $P = [p_{\mathbf{i}}] \in \mathbb{R}^{\mathcal{I}}$ for the Newton potential $\frac{1}{\|x-y\|}$, given in (4.10). As in Section 4.2 this tensor is precomputed by using the optimized sinc-quadratures [10, 61], where the rank parameter $R_N = O(|\log \varepsilon| \log n)$ depends logarithmically on both the required accuracy $\varepsilon > 0$ and the univariate grid size n. Recall that for our computations tensor P, representing the Newton potential has the canonical rank in the range $20 \le R_N \le 30$, depending on the one-dimension grid size n and accuracy requirements $\varepsilon > 0$.

Below, we present Algorithm 1 describing the computational scheme for evaluation of (5.11) - (5.13) in tensor product format[2].

Lemma 4.2 *The complexity of Algorithm 1 for the computation of the exchange Galerkin matrix K_{ex} in the Hartree-Fock equation using the discretized GTO basis is estimated by*

$$W_{K_{ex}} = O(N_{orb} R_N (R_0^2 n \log n + R_0^4 n_{ef})).$$

Proof: This estimate includes the cost of the evaluation of convolutions in (5.11) for every orbital, $O(N_{orb} R_N R_0^2 n \log n)$, and the scalar product (5.12) of the rank-$/R_0 R_N$) tensor $\Theta_{a,k}$ with the products of the orbitals and Gaussians, $O(N_{orb} R_N R_0^4 n_{ef})$. ∎

Since the canonical rank R_N of tensor P corresponding to the Coulomb potential depends only logarithmically on n, it can be treated as a constant in the following complexity estimate.

Remark 4.3 *Notice that the rank reduction of the canonical tensor $\Theta_{a,k}$ after step (5.11) reduces the complexity to*

$$W_{K_{ex}} = O(N_{orb} R_0^3 n_{ef}). \tag{4.25}$$

In the case of large molecules further optimization up to $O(N_{orb} R_0^2 n_{ef})$-complexity is possible due to the rank reduction applied to the rank-R_0 orbitals (tensors U_a).

[2]The Hadamard product $\theta_{a,j} = U_a \odot G_j$ in the Algorithm 1 can be either (1) stored for all vectors γ_k at step **(A)** or (2) recomputed before evaluation of the scalar products at step **(C)** . Due to very low cost of this operation, and large storage requirements for the case of large grids, $O(R_0^2 n)$, we prefer the case (2).

Algorithm 1 Computation of the Exchange Matrix in Tensor Arithmetic

Input data: rank-R_0 canonical tensors $U_a \in \mathbb{V}_{\mathbf{n}}$, $a = 1, \ldots, N_{orb}$, specified by the coefficients matrix $C = \{c_{ka}\} \in \mathbb{R}^{R_0 \times R_0}$, rank-$R_N$ tensor $P \in \mathbb{V}_{\mathbf{n}}$, *rank-1 canonical tensors* $G_k = \gamma_k^{(1)} \otimes \gamma_k^{(2)} \otimes \gamma_k^{(3)}$, $k = 1, \ldots R_0$, and the filtering threshold $\varepsilon_F > 0$.

(A0) Find effective supports $\sigma_j \subset [-b, b]^3$ for γ_j, $j = 1, \ldots, R_0$, by ε_F-thresholding,

$$\sigma_j = \sigma_j^{(1)} \times \sigma_j^{(2)} \times \sigma_j^{(3)}, \text{ where } \sigma_j^{(\ell)} = \{i : |\gamma_j^{(\ell)}(y_i^{(\ell)})| \geq \varepsilon_F\} \subset \{1, \ldots, n\}, \quad \ell = 1, 2, 3.$$

for $a = 1, \ldots, N_{orb}$
for $k = 1, \ldots, R_0$
(A) Compute the Hadamard product $\theta_{a,k} = U_a \odot G_k$ of tensors U_a and G_k by using (2.61).
(B) Compute the tensor convolution $\Theta_{a,k} = \theta_{a,k} * P$ by using (4.12).
for $j = 1, \ldots, R_0$
(C) Compute the restricted scalar products in the window σ_j,

$$K_{a,k,j} = \langle \theta_{a,j}, \Theta_{a,k} \rangle_{|\sigma_j},$$

end for j
end for k
end for a.
(D) Sum the matrix elements over all orbital indices, $K_{kj} = \sum_{a=1}^{N_{orb}} K_{a,k,j}$, for $k, j = 1, \ldots, R_0$.
Output data: the exchange matrix $K_{ex}(C) = \{K_{kj}\}_{k,j=1}^{R_0}$.

Remark 4.4 *The rank-R_0 tensors U_a, $a = 1, \ldots, N_{orb}$, representing the orbitals, can be chosen as the Galerkin basis set $\{G_a\}$, $a = 1, \ldots, N_{orb}$, where N_{orb} is usually much smaller than R_0. This may relax the critical dependence, $O(R_0^4)$ and $O(R_0^3)$ as in Lemma 4.2 and Remark 4.3 above (see also Lemma 3.1 in [70]).*

1. Reducing complexity by reduction of the initial rank $R_\Theta = R_N R_0$.
The maximal initial rank of tensor $\Theta_{a,k}$ at the step (B) in Algorithm 1 is given by $R_\Theta = R_N R_0$. We perform the rank reduction for this tensor by the C2T and T2C algorithms introduced and discussed in details in Sections 2 and 3. In particular, it is shown that the multigrid version of the C2T algorithm applied to the 3-rd order rank-R canonical tensors has linear complexity with respect to all input parameters: the canonical rank R, the Tucker rank r, and the univariate grid size n. Thus, we can reduce the complexity of Algorithm 1 to (4.25) by

	CH_4	CH_3OH	C_2H_5OH
R_Θ	1250	1875	2775
$r_T = 12$, $\epsilon_T \le 10^{-7}$, R_{RED}	80	90	110
$coef_R$	15	20	23
$r_T = 10$, $\epsilon_T \le 10^{-6}$, R_{RED}	50	70	100
$coef_R$	25	26	27

Table 4.2: Rank reduction for $\Theta_{a,k}$ in computation of the exchange matrix for the pseudopotential case of some molecules.

solely multilinear algebraic methods, which do not take into account any previous knowledge on the molecular structure.

Table 4.2 shows the average rank reduction by the C2T and T2C algorithms applied to tensor $\Theta_{a,k}$ in calculations for the molecules CH_4, CH_3OH and C_2H_5OH. We present the reduced canonical ranks R_{RED} (and respective Tucker ranks r_T) of the tensors corresponding to the *largest value*, over the parameters $a = 1, \ldots, N_{orb}$, $k = 1, \ldots R_0$, to achieve the prescribed approximation error ϵ_T,

$$R_{RED} = \max_{1 \le a \le N_{orb},\, 1 \le k \le R_0} R_{RED}(a,k),$$

where $R_{RED}(a,k)$ denotes the reduced canonical rank of $\Theta_{a,k}$, for a given φ_a and g_k. Table 4.2 gives also the corresponding reduction coefficient, $coef_R = \frac{R_\Theta}{R_{RED}}$.

2. Windowing procedure for fast computation of the scalar products.

We compute the algebraic tensor representation of the discrete electron orbitals U_a given by (4.24) using the coefficients of their representation in the discrete Gaussian basis set $\gamma_k^{(\ell)}$. It turns out by the construction that most of $\gamma_k^{(\ell)}$ have local character (fast exponential decay) with respect to the size of the whole computation domain $[-b,b]^3$. Therefore we precompute effective supports of the canonical vectors $\gamma_k^{(\ell)}$ by truncating their parts, which are below some predefined threshold $\varepsilon > 0$. We call it the "windowing" procedure for finding the active interval for each Gaussian. In our case, the resulting effective vector size of the canonical vectors is at average 3 times smaller than the corresponding grid size n even for small molecules. The resulting "effective" univariate grid size is $n_{ef} = \alpha n$, with $\alpha = \alpha(\varepsilon) < 1$. For example, for small molecules $\alpha \sim 0.2 \div 0.3$ for $\varepsilon = 10^{-5}$. This leads to reduced cost of the scalar products with respect to the univariate grid size n.

We expect much stronger windowing effect in the case of large molecules, while in this case, it can be directly applied to the Hadamard products $U_a \odot G_k$.

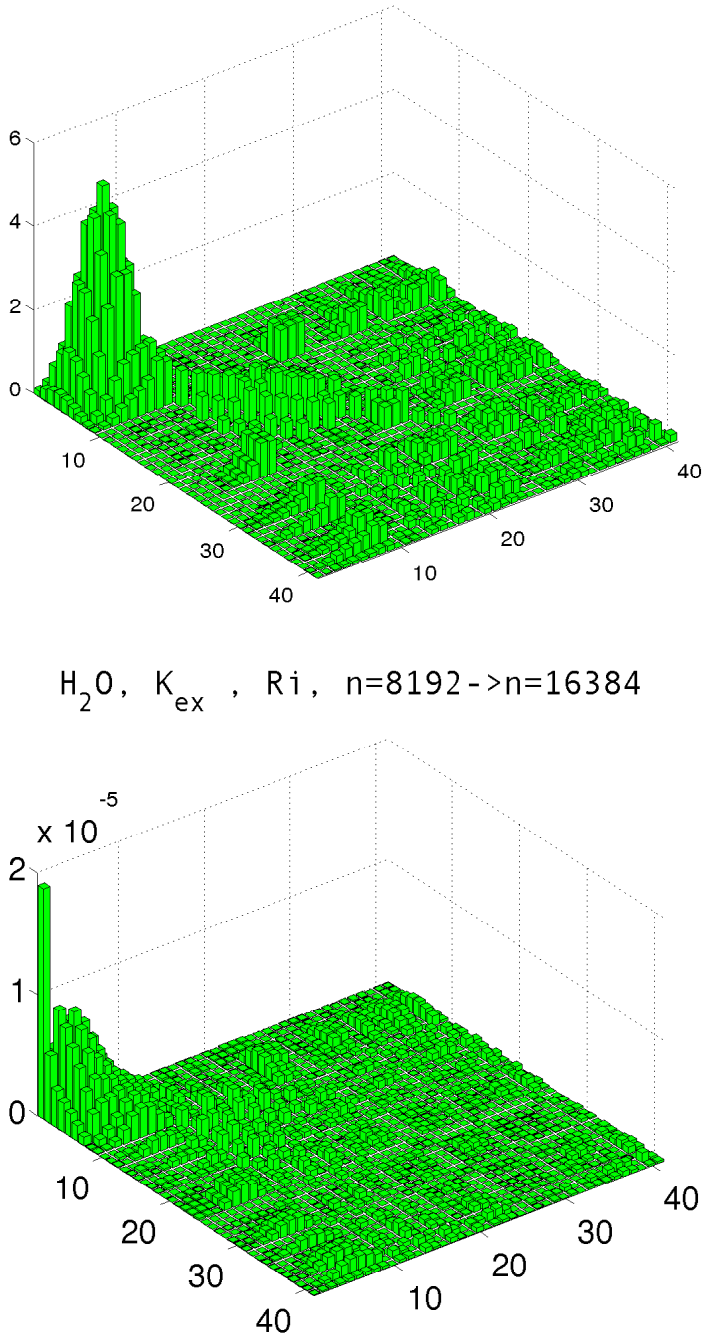

Figure 4.10: Top: entries of the exchange matrix for the all electron case of H_2O. Bottom: absolute error in $K_{ex} \in \mathbb{R}^{41\times 41}$ extrapolated over $n \times n \times n$ 3D Cartesian grids with $n = 8192$ and $n = 16384$.

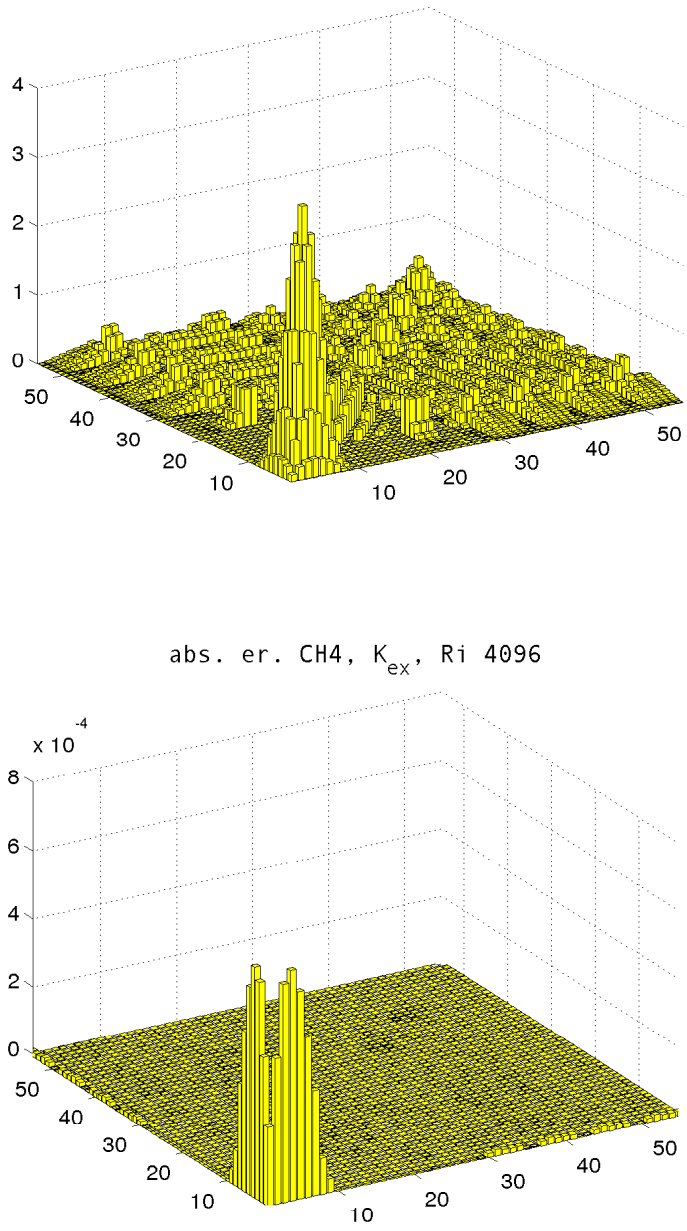

Figure 4.11: Top: the entries of exchange matrix for CH_4. Bottom: absolute approximation error in K_{ex} computed on 3D grids with one-dimension sizes $n = 2048$ and $n = 4096$.

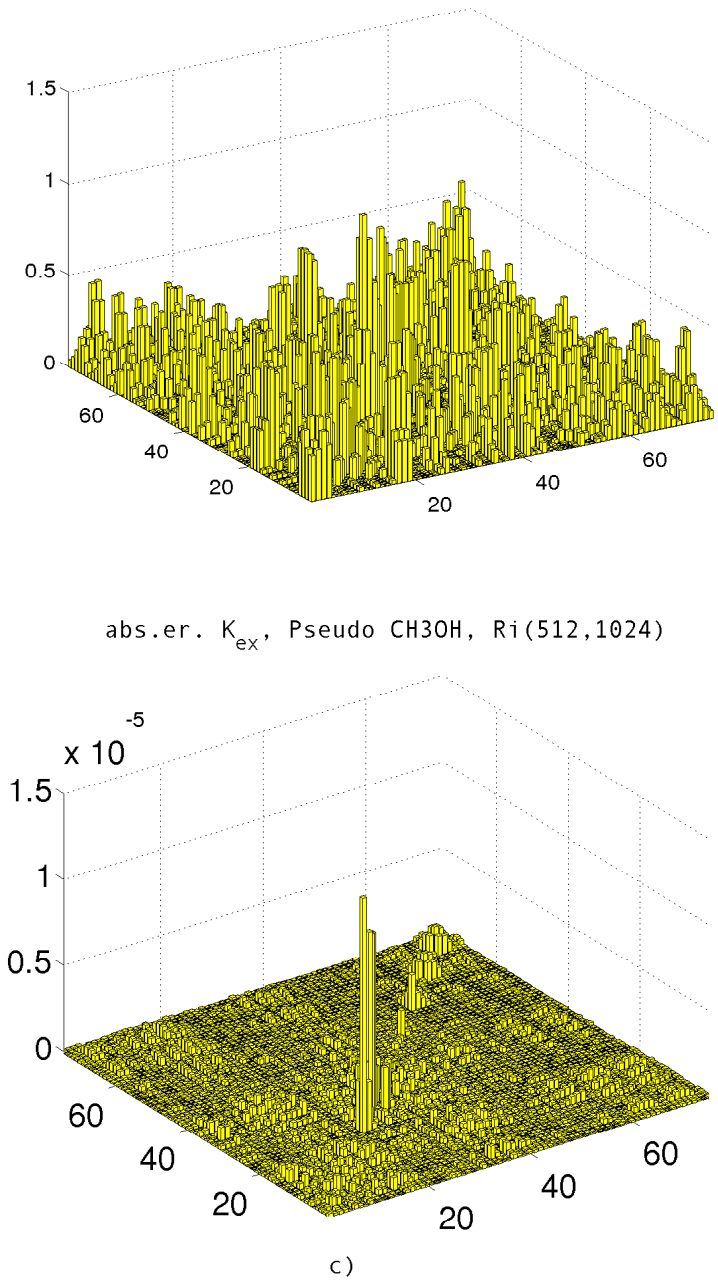

Figure 4.12: Top: the exchange matrix for the *pseudopotential* case of CH_3OH. Bottom: absolute approximation error of computations on the $n \times n \times n$ grids with $n = 512$ and $n = 1024$.

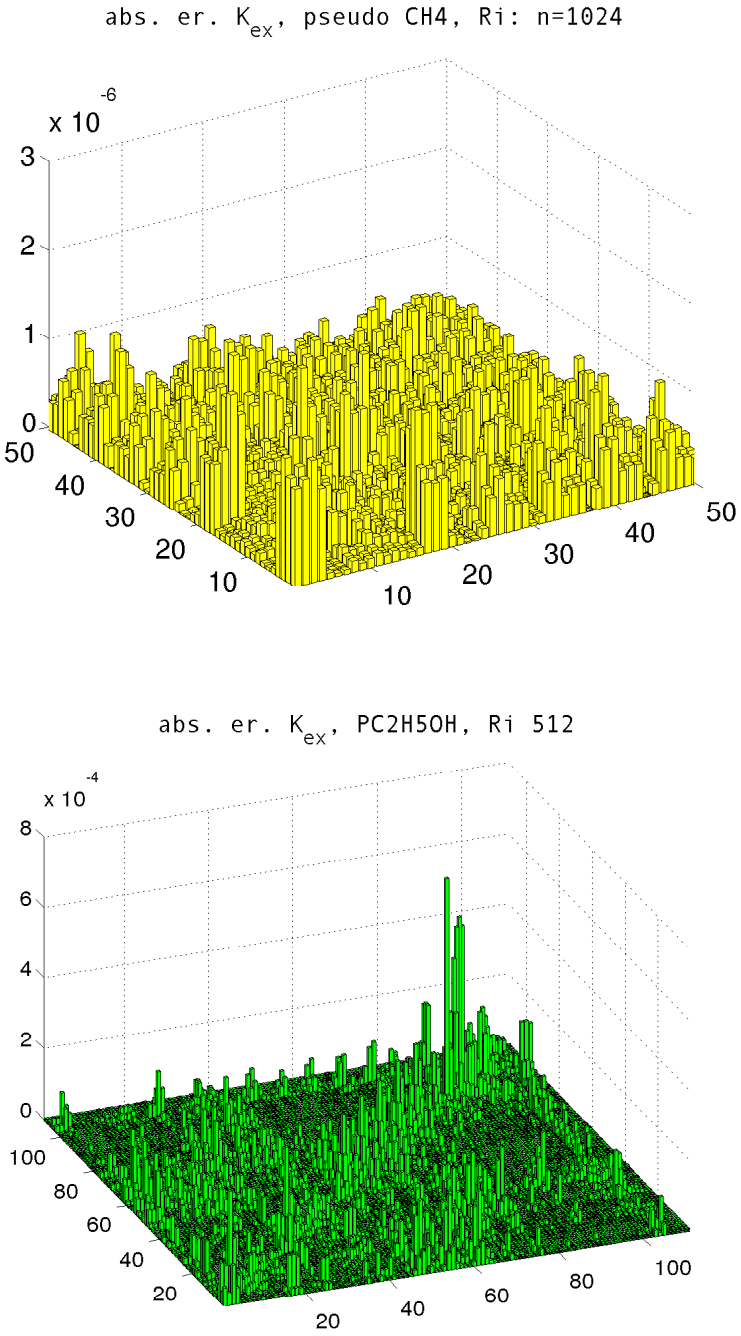

Figure 4.13: Absolute error in the tensor-product computation of K_{ex} the pseudopotential case of molecules CH_4 (top) and C_2H_5OH (bottom).

4.6 Numericals experiments

We tested the presented tensor-structured method in computation of the exchange Galerkin matrix for the following molecules:

- all electron case : H_2O ($N_{orb} = 5,\ R_0 = 41$), CH_4 ($N_{orb} = 5, R_0 = 55$);
- pseudopotential case: CH_4 ($N_{orb} = 4, R_0 = 50$), CH_3OH ($N_{orb} = 7,\ R_0 = 75$) and C_2H_5OH ($N_{orb} = 11,\ R_0 = 111$).

The calculations are performed on a standard SUN station using Matlab 7.6. In presented figures we give the absolute difference of the results of our computations with the corresponding exchange matrix calculated by the MOLPRO program [108].

The computational box $[-b, b]^3$ for small molecules is in the range of $2b = 14$ $\mathring{A}$ for H_2O, and $2b = 20$ $\mathring{A}$ for CH_4, C_2H_5OH, and CH_3OH. The developed tensor-structured algorithm enables computation of the Hartree-Fock exchange on huge $n \times n \times n$ 3D Cartesian grids, with the number of entries up to $n^3 = 16384^3$. This corresponds to the usage of univariate mesh-sizes from $h \approx 2 \cdot 10^{-2}$ for the grids with $n = 1024$, to $h \approx 8 \cdot 10^{-4}$ $\mathring{A}$ for the grids with $n = 16384$.

4.6.1 All electron case

For molecules with moderate size R_0 of basis sets, like CH_4 or H_2O the grid-sizes up to $n = 16384$ are computationally feasible for MATLAB, that is equivalent to computations with $\sim 4.4 \cdot 10^{12}$ nodes in the volume. These grids provide the resolution of the strong cusps in electron orbitals corresponding to the core electrons in a molecule, thus enabling accurate computations of the exchange matrix for all electron case.

Computation of the exchange Galerkin matrix for the all electron case of H_2O molecule is a challenging problem due to "sharp" Gaussians corresponding to core electrons of the Oxygen atom. Figure 4.10 (top) shows the absolute values of the exchange matrix entries for H_2O, Figure 4.10 (bottom) presents the absolute error of the tensor-structured computations of this matrix using the Richardson extrapolation on $n \times n \times n$ 3D Cartesian grids with $n = 8192$ and $n = 16384$. We achieve high accuracy $1.89 \cdot 10^{-5}$ in the "cusp area", the remaining entries are computed with the absolute error in the range of $10^{-6} \div 10^{-8}$.

Figure 4.11 (top) displays the absolute values of the exchange matrix of CH_4 and Figure 4.11 (bottom) shows the absolute error in K_{ex} reaching the accuracy 10^{-4} by using the Richardson extrapolation on the grids with $n = 2048$ and

n^3	64^3	128^3	256^3	512^3	1024^3
H_2O	1	1.3	2.0	3.2	8.0
CH_4 (ps)	1	1.3	2.0	3.6	8.9
CH_3OH (ps)	1	1.3	1.9	3.3	5.1

Table 4.3: Comparison of relative times.

$n = 4096$. Again, the matrix entries apart from the "cusp area" are computed with much higher accuracy.

4.6.2 Pseudopotential case

We consider the pseudopotential case for larger molecules, achieving an accuracy up to 10^{-6}, using smaller 3D grids with one-dimension size $n = 1024$.

Figure 4.12 (top) shows entries of the exchange matrix of CH_3OH molecule and Figure 4.12 (right) displays that tensor-structured computations for this molecule using the Richardson extrapolation on grids with $n = 512, 1024$ yield an accuracy $\sim 10^{-5}$. Figure 4.13 shows the absolute error in K_{ex}in the pseudopotential case of the CH_3OH molecule (top) and C_2H_5OH (bottom), correspondingly. For CH_3OH the Richardson extrapolation on two consequent grids with $n = 512, 1024$ yields the accuracy $\sim 10^{-5}$, while for C_2H_5OH we obtain $7 \cdot 10^{-4}$, already on small 3D grids with the one-dimension size $n = 256,\ 512$.

Table 4.6.2 illustrates linear scaling of the relative one orbital computation time, with respect to the one-dimension grid size n, in respective units of the coarsest grid calculations ($n = 64$).

5 Solution of the Hartree-Fock equation by multilevel TS methods

The traditional numerical approaches in *ab initio* electronic structure calculations are based on the Galerkin approximation in the naturally separable GTO basis and analytical evaluation of one- and two-electron integrals inherent to this approach. Many years of development of rigorous schemes for the analytical evaluation of the operators in the Hartree-Fock equation, yielded state-of-the-art packages like GAUSSIAN, Abinit and MOLPRO [5, 108]. In analytical-based programs, elaborated by large scientific groups, precomputed parameters and "non-zero" initial approximations are used for accelerating the iterative solution of the nonlinear EVP (1.6).

The Hartree-Fock model presupposes at least cubic (or fourfold) scaling in the number of the basis functions. When using the conventional Gaussian bases, the number of basis functions rapidly increases for larger molecules, thus making this model computationally unfeasible.

As a first remedy, there are simplified models based on the appropriately adjusted pseudopotentials and the grid-oriented methods over $n \times n \times n$ spatial grids. These include the traditional plane waves, wavelet or finite element discretizations, at the expense that scales linearly in the volume size, $\mathcal{N}_{vol} = n^3$, [4, 5]. Accuracy of these approaches is limited due to the constraints on practically tractable grid size $n \approx 500$.

Here, we introduce the *novel multilevel scheme* for the numerical solution of the Hartree-Fock equation using the *grid-based tensor-structured methods* described in previous sections, and providing $O(n \log n)$-complexity, i.e., sublinear in the volume, $O(\mathcal{N}_{vol}^{1/3})$. The new concept for the numerical solution of the Hartree-Fock equation is a "grey box" scheme based on a moderate number of problem-adapted discrete Galerkin basis functions represented on 3D Cartesian grid, which are used as the "global elements" with a low separation rank.

The core of our method is the tensor-structured computation of the electron density and the Galerkin matrices of the nonlinear Hartree and (nonlocal) Hartree-

Fock exchange operators (see Section 5.1.3) at all steps of iterations in the solution of the nonlinear EVP problem . Within the solution process, the multilinear algebra operations such as the scalar and Hadamard products, the 3D convolution transform, and the rank truncation are implemented with almost $O(n)$-complexity. In view of linear scaling in n of the 3D tensor-structured arithmetic, high accuracy is achieved due to computations over large $n \times n \times n$ tensor grids of size up to 16384^3 entries. In electronic structure calculations, this implies fine resolution with the mesh size $h \approx 10^{-4}$ $\mathring{A}$, providing possibility for arbitrary space orientation of a molecule in the computational box (like in the analytical approaches).

The piecewise constant representation of the Galerkin basis functions, and the electron density, leads to approximation error of order $O(h^2)$, in the Hartree and exchange potentials, where $h = O(n^{-1})$ is the respective mesh size. In turn, the two-grid version of the computational scheme improves the convergence rate up to $O(h^3)$, by using the Richardson extrapolation. These approximation properties are verified by the numerical experiments.

For solving the discrete Hartree-Fock equation on a fixed grid, we apply the self-consistent field (SCF) iteration based on the traditional *direct inversion in the iterative subspace* (DIIS) scheme commonly used in the physical literature [89]. In this iteration scheme, the current update to the Fock matrix is obtained by relaxation over its values at the previous steps. The discrete orbitals, represented by the Galerkin coefficients vectors, are updated by direct diagonalization of the arising system matrix at each iteration on nonlinearity.

To enhance the classical DIIS iteration in our tensor-structured grid-based approach, we propose the *multilevel strategy*, that provides fast and robust iterative solution method for the Hartree-Fock equation discretized on a sequence of refined grids. Iterations begin on the coarsest grid with the zero initial guess for the Hartree and exchange Galerkin matrices, $J(C) = 0$, $K(C) = 0$. We switch iteration from the coarser to finer grid using a grid-dependent termination criterion, such that the initial guess for the Coulomb and exchange matrices, obtained from previous coarse levels, ensures robust convergence on finer grids. Low cost of the iterations on the coarse grid levels reduces essentially the overall numerical complexity of the global solution process.

In general, the convergence proof for the nonlinear DIIS iteration is still an open question [78, 20]. We observe in numerical experiments for several small organic molecules, that our multigrid accelerated DIIS iteration exhibits fast and uniform in n convergence (linear convergence rate), so that the overall computational time scales almost linearly in n.

It is worth to note that the current version of the method still scales cubically

in the size of approximating basis. Hence, any *algebraic optimisation of this basis set* within the solution process gives the new opportunity to high accuracy *ab initio* computations for large molecules. The quadratic scaling in the size of approximating basis might be possible in the framework of direct minimization algorithms (see [95] for detailed discussion on the direct minimization).

5.1 Galerkin scheme for the Hartree-Fock equation

5.1.1 Problem setting

As it was already mentioned in the Introduction, the Hartree-Fock equation for pairwise L^2-orthogonal electronic orbitals $\varphi_i : \mathbb{R}^3 \to \mathbb{R}$, $\varphi_i \in H^1(\mathbb{R}^3)$, is a nonlinear EVP,

$$\mathcal{F}\varphi_i(x) = \lambda_i \varphi_i(x), \quad \int_{\mathbb{R}^3} \varphi_i \varphi_j dx = \delta_{ij},\ i,j = 1, ..., N_{orb} \tag{5.1}$$

with the nonlinear Fock operator $\mathcal{F}$,

$$\mathcal{F} := -\frac{1}{2}\Delta + V_c + V_H - \mathcal{K},$$

where δ_{ij} denotes the Kronecker delta, and N_{orb} is the number of electron pairs in a molecule.

Here, an external nuclear potential V_c is defined by

$$V_c(x) = -\sum_{\nu=1}^{M} \frac{Z_\nu}{\|x - A_\nu\|}, \tag{5.2}$$

where M is the number of nuclei in a molecule, and $Z_\nu > 0$, $A_\nu \in \mathbb{R}^3$ denote the charge and spatial coordinates of the nuclei, respectively. The Hartree potential V_H determines the Coulomb interaction of every single electron with the field generated by all electrons of the system,

$$V_H(x) := \int_{\mathbb{R}^3} \frac{\rho(y)}{\|x - y\|}\, dy, \quad x \in \mathbb{R}^3, \tag{5.3}$$

that corresponds to the convolution of the Coulomb potential with the electron density

$$\rho(y) = 2\sum_{i=1}^{N_{orb}} (\varphi_i(y))^2. \tag{5.4}$$

The exchange part $\mathcal{K}$ of the Fock operator is given by the convolution integral,

$$(\mathcal{K}\varphi)(x) := \frac{1}{2}\int_{\mathbb{R}^3} \frac{\tau(x,y)}{\|x-y\|}\varphi(y)dy, \tag{5.5}$$

with the density matrix

$$\tau(x,y) = 2\sum_{i=1}^{N_{orb}} \varphi_i(x)\varphi_i(y).$$

5.1.2 Traditional discretization

Usually, the Hartree-Fock equation is solved by the standard Galerkin approximation of the initial problem (5.1) posed in $H^1(\mathbb{R}^3)$ (see [78] for more details). For a given finite basis set $\{g_\mu\}_{1\le\mu\le R_0}$, $g_\mu \in H^1(\mathbb{R}^3)$, the molecular orbitals φ_i are expanded as

$$\varphi_i = \sum_{\mu=1}^{R_0} c_{\mu i} g_\mu, \quad i = 1, ..., N_{orb}. \tag{5.6}$$

To derive the equation for the unknown coefficients matrix $C = \{c_{\mu i}\} \in \mathbb{R}^{R_0 \times N_{orb}}$, one first introduces the mass (overlap) matrix $S = \{s_{\mu\nu}\}_{1\le\mu,\nu\le R_0}$, given by

$$s_{\mu\nu} = \int_{\mathbb{R}^3} g_\mu g_\nu dx,$$

and the stiffness matrix $H = \{h_{\mu\nu}\}$ of the core Hamiltonian part of the Fock operator, $\mathcal{H} = -\frac{1}{2}\Delta + V_c$, that includes the kinetic energy of electrons and the nuclear potential energy,

$$h_{\mu\nu} = \frac{1}{2}\int_{\mathbb{R}^3} \nabla g_\mu \cdot \nabla g_\nu dx + \int_{\mathbb{R}^3} V_c(x) g_\mu(x) g_\nu(x) dx, \quad 1 \le \mu, \nu \le R_0.$$

The nonlinear terms representing the Galerkin approximation of the Hartree and exchange operators are usually constructed by using the so-called two-electron convolution integrals (cf. for example [78]), defined as

$$b_{\mu\nu,\kappa\lambda} = \int_{\mathbb{R}^3}\int_{\mathbb{R}^3} \frac{g_\mu(x) g_\nu(x) g_\kappa(y) g_\lambda(y)}{\|x-y\|} dxdy, \quad 1 \le \mu, \nu, \kappa, \lambda \le R_0.$$

Traditionally, the Hartree and exchange parts in the Fock operator are computed by the analytical evaluation of one- and two-electron integrals, using the naturally separable Cartesian Gaussians g_k, $k = 1, \ldots, R_0$, represented in the rank-1 canonical tensor product form,

$$g_k(x) = g_k^{(1)}(x_1)\, g_k^{(2)}(x_2)\, g_k^{(3)}(x_3), \quad x \in \mathbb{R}^3,$$

with 1, 2, 3 designating the space dimensions.

Denoting by $D = 2CC^T \in \mathbb{R}^{R_0 \times R_0}$ the so-called density matrix, the $R_0 \times R_0$ Galerkin matrices $J(C)$ for the Hartree, and $K(C)$ for the exchange potentials, can be defined as (cf. [78])

$$J(C)_{\mu\nu} = \sum_{\kappa,\lambda=1}^{R_0} b_{\mu\nu,\kappa\lambda} D_{\kappa\lambda}, \quad K(C)_{\mu\nu} = \frac{1}{2} \sum_{\kappa,\lambda=1}^{R_0} b_{\mu\lambda,\nu\kappa} D_{\kappa\lambda}.$$

The complete Fock matrix $F = F(C)$ is then given by,

$$F(C) = H + G(C), \quad G(C) = J(C) + K(C). \tag{5.7}$$

The respective Galerkin system of nonlinear equations for the coefficients matrix $C \in \mathbb{R}^{R_0 \times N_{orb}}$ takes the form

$$\begin{aligned} &F(C)C = SC\Lambda, \quad \Lambda = diag(\lambda_1, \ldots, \lambda_{N_{orb}}), \\ &C^T SC = I_{N_{orb}}, \end{aligned} \tag{5.8}$$

where the second equation represents the orthogonality constraints $\int_{\mathbb{R}^3} \varphi_i \varphi_j = \delta_{ij}$, with $I_{N_{orb}}$ being the $N_{orb} \times N_{orb}$ identity matrix.

Since the traditional implementation of the SCF iteration for the Hartree-Fock equation is based on the precomputed two-electron integrals, the complexity to build up the matrix G normally scales as $O(R_0^4)$, that is dominated by computational cost for the exchange matrix $K(C)$. In turn, the core Hamiltonian H can be precomputed in $O(R_0^2)$ operations, hence, in the following, we focus on the efficient Galerkin approximation of the nonlinear Hartree and exchange operators to be updated at each step of SCF iteration.

The nonlinear system (5.8) can be solved by a certain SCF iteration, where at each iterative step the respective linear eigenvalue problem has to be solved with the updated matrix $G(C)$. Given $F(C)$, using the direct diagonalization for solving the system (5.8) leads to the cost $O(R_0^3)$ at each iterative step.

An alternative approach can be based on the direct minimization of the Hartree-Fock energy functional

$$I^{HF} = \inf \left\{ \frac{1}{2} \sum_{i=1}^{N_{orb}} \int_{\mathbb{R}^3} |\nabla \varphi_i|^2 + \int_{\mathbb{R}^3} \rho V_c + \int_{\mathbb{R}^3} \int_{\mathbb{R}^3} \frac{\rho(x)\rho(y) - |\tau(x,y)|^2}{\|x-y\|} dxdy \right\},$$

over $\varphi_i \in H^1(\mathbb{R}^3)$, under the orthogonality constraints in (5.1), see [95] for more details.

5.1.3 Novel scheme via agglomerated tensor-structured calculation of Galerkin matrices

We introduce the *novel tensor-structured method* for the numerical solution of the nonlinear Hartree-Fock equation, which does not require the analytical evaluation of the two-electron integrals described in Section 5.1.2. In our approach, we use the grid-based agglomerated calculation of the three- and six-dimensional integrals in evaluation of the Hartree and exchange operators and the corresponding Galerkin matrices $J(C)$ and $K(C)$.

The idea is based on a certain reorganisation of the standard computational scheme described in Section 5.1.2. Specifically, instead of precomputing the full set of two-electron integrals $b_{\mu\nu,\kappa\lambda}$ and the elements of the density matrix D, we use agglomerated representations for $J(C)$ and $K(C)$.

Now, let us recall some constructions from Section 4.2. We suppose that the initial problem is posed in the finite volume box $\Omega = [-b, b]^3 \in \mathbb{R}^3$ subject to the homogeneous Dirichlet boundary conditions on $\partial\Omega$. For given discretization parameter $n \in \mathbb{N}$, introduce the equidistant tensor grid $\omega_{\mathbf{3},n}$ with the mesh-size $h = 2b/n$, as in (4.6). Then define the set of piecewise constant basis functions $\{\phi_{\mathbf{i}}\}$, $\mathbf{i} \in \mathcal{I} := \{1, ..., n\}^3$, associated with the respective grid-cells in $\omega_{\mathbf{3},n}$ (indicator functions), and introduce the set of collocation discretisations of GTO basis functions, $\{\overline{g}_k\}$, represented in this basis by the rank-1 coefficients tensor $\{G_k\} \in \mathbb{R}^{\mathcal{I}}$ $(k = 1, ..., R_0)$. The projected Newton potential is represented in the basis set $\{\phi_{\mathbf{i}}\}$ by the low-rank coefficients tensor $P_N \in \mathbb{R}^{\mathcal{I}}$.

Now the computational scheme for the Coulomb matrix can be written by the following tensor operations:

$$\rho \approx \Theta := \sum_{a=1}^{N_{orb}} \left(\sum_{\kappa,\lambda=1}^{R_0} c_{\kappa a} c_{\lambda a} G_\kappa \odot G_\lambda \right),$$

and then by the tensor-product convolution (see Section 4.2),

$$V_H = \rho * \frac{1}{\|\cdot\|} \approx \Theta * P_N, \tag{5.9}$$

with $P_N \in \mathbb{V}_n$ being the projection tensor for the Coulomb potential. This implies the tensor representation of the Coulomb matrix,

$$\begin{aligned} J(C)_{\mu\nu} &= \langle \overline{g}_\mu(x)\overline{g}_\nu(x), V_H(x)\rangle \\ &\approx \langle G_\mu \odot G_\nu, \Theta * P_N\rangle, \quad 1 \le \mu, \nu \le R_0. \end{aligned} \tag{5.10}$$

We have $rank(G_\mu) = 1$, while 3rd order tensors Θ and P_N are approximated by low-rank tensors (see Section 4). Hence, the corresponding tensor operations

are carried out using fast multilinear algebra supplemented by the corresponding rank optimization (tensor truncation).

In turn, as proposed in Section 4.5, we represent the matrix $K(C)$ using tensor operations by the following three loops. For $a = 1, ..., N_{orb}$, and $\nu = 1, ..., R_0$, compute the convolution integrals,

$$W_{a\nu}(x) = \int_{\mathbb{R}^3} \frac{\overline{g}_\nu(y) \sum_{m=1}^{R_0} c_{ma} \overline{g}_m(y)}{\|x-y\|} dy$$
$$\approx \Upsilon_{a\nu} := \left[G_\nu \odot \sum_{m=1}^{R_0} c_{ma} G_m \right] * P_N, \tag{5.11}$$

and then the scalar products ($\mu, \nu = 1, ..., R_0$),

$$K_{\mu\nu,a} = \int_{\mathbb{R}^3} \left[\sum_{m=1}^{R_0} c_{ma} \overline{g}_m(x) \right] \overline{g}_\mu(x) W_{a\nu}(x) dx$$
$$\approx \chi_{\mu\nu,a} := \langle \left[\sum_{m=1}^{R_0} c_{ma} G_m \right] \odot G_\mu, \Upsilon_{a\nu} \rangle. \tag{5.12}$$

Finally, the entries of the exchange matrix are given by sums over all orbitals,

$$K(C)_{\mu\nu} = \sum_{a=1}^{N_{orb}} K_{\mu\nu,a}, \quad \mu, \nu = 1, ..., R_0. \tag{5.13}$$

This scheme gains from the efficient low-rank separable approximation of the Newton kernel, the discretised electron density $\rho(x)$, and of auxiliary potentials $W_{a\nu}(x)$ at step (5.11), that ensures low complexity of the three-dimensional tensor-structured operations including rank reduction algorithms.

Notice that the effective realization of such a concept is possible with more general basis sets $\{\overline{g}_\mu\}$, than those generated by analytically separable rank-1 GTO basis chosen above. The key features of the Galerkin basis functions $\overline{g}_\mu$ should include: (A) *approximability*, i.e., the Galerkin approximation error over the quantities in (5.8) is satisfactory, and (B) *separability*, i.e., the collocation coefficients tensor G_μ for the basis function $\overline{g}_\mu(x)$, can be represented by the rank-R_G expansion with small R_G,

$$G_\mu = \sum_{k=1}^{R_G} g^{(1)}_{\mu,k} \otimes g^{(2)}_{\mu,k} \otimes g^{(3)}_{\mu,k}, \quad \mu = 1, ..., R_0, \tag{5.14}$$

(see [70] for more detailed discussion on this topic). In this case, the tensor-product schemes as above remain essentially the same except that the rank of the collocation coefficients tensor G_μ ($\mu = 1, ..., R_0$) increases to R_G.

5.2 Multilevel tensor-truncated iteration via DIIS

5.2.1 General SCF iteration

The standard SCF algorithm can be formulated as the following "fixed-point" iteration ([78]): Starting from initial guess C_0, perform iterations of the form

$$\begin{aligned} \overline{F}_k C_{k+1} &= S C_{k+1} \Lambda_{k+1}, \quad \Lambda_{k+1} = \mathrm{diag}(\lambda_1^{k+1}, ..., \lambda_{N_{orb}}^{k+1}) \\ C_{k+1}^T S C_{k+1} &= I_{N_{orb}}, \end{aligned} \tag{5.15}$$

where the current Fock matrix $\overline{F}_k = \Phi(C_k, C_{k-1}, \ldots, C_0)$, $k = 0, 1, ...$, is specified by the particular relaxation scheme. For example, for the simplest approach, called the *Roothaan algorithm*, one has $\overline{F}_k = F(C_k)$. In practically interesting situations this algorithm usually leads to "flip-flop" stagnation [78].

Recall that here, $\lambda_1^{k+1} \le \lambda_2^{k+1} \le ... \le \lambda_{N_{orb}}^{k+1}$ are N_{orb} negative eigenvalues of the linear generalized eigenvalue problem

$$\overline{F}_k U = \lambda S U, \tag{5.16}$$

and the $R_0 \times N_{orb}$ matrices C_{k+1} contain the respective N_{orb} orthonormal eigenvectors $U_1, ..., U_{N_{orb}}$. We denote by $\overline{C}_{k+1} \in \mathbb{R}^{R_0 \times R_0}$ the matrix representing the full set of orthogonal eigenvectors in (5.16).

We use the particular choice of $\overline{F}_k$, $k = 0, 1, ...$, via the DIIS-algorithm, (cf. [89]), with the starting value $\overline{F}_0 = F(C_0) = H$.

We propose the modification to the standard DIIS iteration, by carrying out the iteration on a sequence of successively refined grids with the grid-dependent stopping criteria. The multilevel implementation provides robust convergence from the zero initial guess for the Hartree and exchange operators. The coarse-to-fine grids iteration, in turn, accelerates the solution process dramatically due to low cost of the coarse grid calculations.

The principal feature of our tensor-truncated iteration is revealed on the fast update of the Fock matrix $F(C)$ by using tensor-product multilinear algebra of 3-tensors accomplished with the rank truncation described above. Another important point is that the multilevel implementation provides simple and robust scheme for construction good initial guess on the fine grid-levels.

5.2.2 SCF iteration by using DIIS scheme

For each fixed discretization, we use the original version of DIIS scheme (cf. [53]), defined by the following choice of the *residual error vectors* (matrices),

$$E_i := [\overline{C}_{i+1}^T F(C_i) \overline{C}_{i+1}]_{|\{1 \le \mu \le N_{orb}; N_{orb}+1 \le \nu \le R_0\}} \in \mathbb{R}^{N_{orb} \times (R_0 - N_{orb})}, \tag{5.17}$$

for iteration number $i = 0, 1, ..., k$, that should vanish on the exact solutions of the Hartree-Fock Galerkin equation due to the orthogonality property. Hence, some stopping criterion applies to residual error vector E_i for $i = 0, 1, 2, ...$

The minimizing coefficient vector $\overline{c} := (c_0, ..., c_k)^T \in \mathbb{R}^{k+1}$ is computed by solving the constrained quadratic minimisation problem for the respective cost functional (the averaged residual error vector over previous iterands),

$$f(\overline{c}) := \frac{1}{2} \left\| \sum_{i=0}^{k} c_i E_i \right\|_F^2 \equiv \frac{1}{2} \langle B\overline{c}, \overline{c} \rangle \to \min, \quad \text{provided that} \quad \sum_{i=0}^{k} c_i = 1,$$

where

$$B = \{B_{ij}\}_{i,j=0}^{k} \quad \text{with} \quad B_{ij} = \langle E_i, E_j \rangle,$$

and with E_i defined by (5.17). Introducing the Lagrange multiplier $\xi \in \mathbb{R}$, the problem is reduced to minimization of the Lagrangian functional

$$L(\overline{c}, \xi) = f(\overline{c}) - \xi(\langle \mathbf{1}, \overline{c} \rangle - 1),$$

where $\mathbf{1} = (1, ..., 1)^T \in \mathbb{R}^{k+1}$, that leads to the linear augmented system of equations

$$\begin{aligned} B\overline{c} - \xi \mathbf{1} &= 0, \\ \langle \mathbf{1}, \overline{c} \rangle &= 1. \end{aligned} \tag{5.18}$$

Finally, the updated Fock operator $\overline{F}_k$ is built up by

$$\overline{F}_k = \sum_{i=0}^{k-1} c_i^{opt} \overline{F}_i + c_k^{opt} F(C_k), \quad k = 0, 1, 2, ..., \tag{5.19}$$

where the minimizing coefficients $c_i^{opt} = \overline{c}_i$ $(i = 0, 1, ..., k)$ solve the linear system (5.18). For $k = 0$ the first sum in (5.19) is assumed to be zero, hence providing $c_0^{opt} = 1$, and $\overline{F}_0 = F(C_0)$.

Recall that if the stopping criterion on C_k, $k = 1, ...,$ is not satisfied, one updates $\overline{F}_k$ by (5.19) and solves the eigenvalue problem (5.15) for C_{k+1}.

Note that in practice one can use the averaged residual vector only on a reduced subsequence of iterands, $E_k, E_{k-1}, ..., E_{k-k_0}$, $k - k_0 > 0$. In our numerical examples below, we usually set $k_0 = 4$.

5.2.3 Unigrid and multilevel tensor-truncated DIIS iteration

In this section, we describe the resultant numerical algorithm. Recall that the discrete nonlinear Fock operator is specified by a matrix

$$F(C) = H + J(C) + K(C), \tag{5.20}$$

where H corresponds to the core Hamiltonian (fixed in our scheme) and the discrete Hartree and exchange operators are given by tensor representations (5.10) and (5.12), respectively.

First, we describe the unigrid tensor-truncated DIIS scheme.

Algorithm TT_DIIS *(Unigrid tensor-truncated DIIS iteration).*

1. *Given the core Hamiltonian matrix H, the grid parameter n, and the termination parameter $\varepsilon > 0$.*

2. *Set $C_0 = 0$ (i.e. $J(C_0) = 0$, $K(C_0) = 0$), and $\overline{F}_0 = H$.*

3. *For $k = 0, 1, ...,$ perform*

a) Solve the full linear eigenvalue problem of size $R_0 \times R_0$, given by (5.16), and define C_{k+1} as the matrix containing the N_{orb} eigenvectors corresponding to N_{orb} minimal eigenvalues.

b) Terminate the iteration by checking the stopping criterion

$$\|C_{k+1} - C_k\|_F \leq \varepsilon.$$

c) If $\|C_{k+1} - C_k\|_F > \varepsilon$, compute the Fock matrix

$$F(C_{k+1}) = H + J(C_{k+1}) + K(C_{k+1})$$

by the tensor-structured calculations of $J(C_{k+1})$ and $K(C_{k+1})$, using grid-based basis functions with expansion coefficients C_{k+1}, (see Section 4), update the Fock matrix $\overline{F}_{k+1}$ by (5.19), and switch to Step a).

4. *Returns: Eigenvalues $\lambda_1, ..., \lambda_{N_{orb}}$ and eigenvectors $C \in \mathbb{R}^{R_0 \times N_{orb}}$.*

Figure 5.1 shows the convergence of Algorithm TT_DIIS for the solution of the Hartree-Fock equation in the pseudopotential case of CH_4. It demonstrates that the convergence history is almost independent on the grid size on the examples with $n = 64$ and $n = 256$, correspondingly.

To enhance the unigrid DIIS iteration, we propose the multilevel version of Algorithm TT_DIIS defined on a sequence of discrete Hartree-Fock equations specified by a sequence of grid parameters $n_p = n_0, 2n_0, \ldots, 2^M n_0$, with $p = 0, ..., M$, corresponding to the succession of dyadically refined spacial grids. To that end, for ease of exposition, we also introduce the incomplete version of Algorithm TT_DIIS, further called Algorithm **TT_DIIS**($\overline{k}$), which represents only its part starting from iteration number $k = \overline{k} \geq 1$. The input data for Algorithm TT_DIIS($\overline{k}$) include the current approximation $C_{\overline{k}}$ and a sequence of all already precomputed Fock matrices, $\overline{F}_0, \overline{F}_1, ..., \overline{F}_{\overline{k}-1}$.

We sketch this algorithm as follows.

Algorithm TT_DIIS($\overline{k}$) *(Incomplete unigrid tensor-truncated DIIS iteration).*
1. *Given the core Hamiltonian matrix H, the grid parameter n, the termination parameter $\varepsilon > 0$, $C_{\overline{k}}$, and a sequence of Fock matrices $\overline{F}_0, \overline{F}_1, ..., \overline{F}_{\overline{k}-1}$.*
2. *Compute $J(C_{\overline{k}})$, $K(C_{\overline{k}})$, $F(C_{\overline{k}}) = H + J(C_{\overline{k}}) + K(C_{\overline{k}})$, and $\overline{F}_{\overline{k}}$ by (5.19).*
3. *For $k = \overline{k}, \overline{k}+1, ...,$ perform steps a) - c) in Algorithm MTT_DIIS.*

We further assume that the core Hamiltonian H is precomputed beforehand.

Algorithm MTT_DIIS *(Multilevel tensor-truncated DIIS scheme).*
1. *Given the core Hamiltonian matrix H, the coarsest grid parameter n_0, the termination parameter $\varepsilon_0 > 0$, and the number of grid refinements M.*
2. *For $p = 0$, apply the unigrid Algorithm* **TT_DIIS** *with $n = n_0$, $\varepsilon_p = \varepsilon_0$, and return the number of iterations k_0, matrix C_{k_0+1}, and a sequence of Fock matrices $\overline{F}_0, \overline{F}_1, ..., \overline{F}_{k_0}$.*
3. *For $p = 1, ..., M$, apply successively Algorithm TT_DIIS($k_{p-1}+1$), with the input parameters $n_p := 2^p n_0$, $\varepsilon_p := \varepsilon_0 2^{-2p}$, $C_{k_{p-1}+1}$. Keep continuous numbering of the DIIS iterations through all levels, such that the maximal iteration number at level p is given by*

$$k_p = \sum_{p=0}^{p} m_p,$$

with m_p being the number of iterative steps at level p.
4. *Returns: k_M, C_{k_M+1}, and a sequence of Fock matrices $\overline{F}_0, \overline{F}_1, ..., \overline{F}_{k_M}$.*

Usually, we start calculations on an $n \times n \times n$ 3D Cartesian grid, with $n_0 = 64$, and end up with maximum $n_M = 8192$, for all electron case computations, or $n_M = 1024$, for the pseudopotential case. Further, in Section 5.3, we show by numerical examples that in large scale computations the multilevel Algorithm MTT_DIIS allows us to perform most of the iterative steps on coarse grids thus reducing dramatically the computational cost and, at the same time providing a good initial guess for the DIIS iteration on nonlinearity at each consequent approximation level.

The flow-chart in Figure 5.2 shows the general steps of the unigrid/multigrid tensor-structured SCF algorithms.

5.2.4 Complexity estimates in terms of R_0, N_{orb} and n

The rest of this section addresses the complexity estimate of the multilevel tensor-truncated iteration in terms of R_N, R_0, n and other governing parameters of the algorithm. For the ease of discussion we suppose that $rank(G_\mu) = 1$, $\mu = 1, ..., R_0$, (see [70] concerning the more detailed discussion on general case of $rank(G_\mu) \geq 1$).

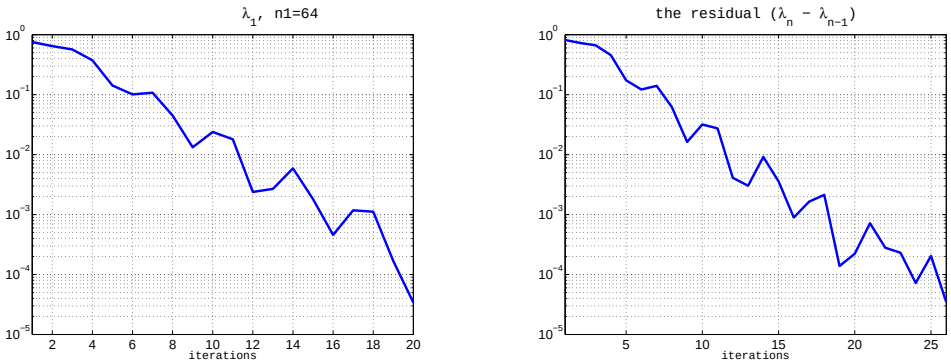

Figure 5.1: Convergence in the eigenvalues for the unigrid **TT_DIIS** algorithm, in the pseudopotential case of the CH_4 molecule: the univariate grid size $n = 64$ (left) and $n = 256$ (right).

Lemma 5.1 *Let* $rank(G_\mu) = 1$, $\mu = 1, \dots R_0$ *and* $rank(P_N) \le R_N \le CN_{orb}$. *Suppose that the rank reduction procedure applied to the convolution products* $\Upsilon_{a\nu}$ *in (5.11) provides the rank estimate* $rank(\Upsilon_{a\nu}) \le r_0$. *Then the numerical cost of one iterative step in Algorithm* **MTT_DIIS** *at level* p, *can be bounded by*

$$W_p = O(R_0 R_N n_p \log n_p + R_0^3 r_0 N_{orb} n_p).$$

Assume that the number of multigrid DIIS iterations at each level is bounded by the constant I_0, *then the total cost of Algorithm* **MTT_DIIS** *does not exceed the double cost at the finest level* $n = n_M$, $2W_M = O(I_0 R_0^3 r_0 N_{orb} n)$.

Proof: The rank bound $rank(G_k) = 1$ implies $rank(\sum_{m=1}^{R_0} c_{ma}\, G_m) \le R_0$. Hence, the numerical cost to compute the tensor-product convolution $\Upsilon_{a\nu}$ in (5.11) amounts to

$$W(\Upsilon_{a\nu}) = O(R_0 R_N n_p \log n_p).$$

Since the initial canonical rank of $\Upsilon_{a\nu}$ is estimated by $rank(\Upsilon_{a\nu}) \le R_0 R_N$, the multigrid rank reduction algorithm, having linear scaling in $rank(\Upsilon_{a\nu})$, see Section 3, provides the complexity bound $O(r_0 R_0 R_N n_p)$. Hence the total cost to compute scalar products in $\chi_{\mu\nu,a}$ (see (5.12)) can be estimated by

$$W(\chi_{\mu\nu,a}) = O(R_0^3 r_0 N_{orb} n_p),$$

which completes the first part of our proof. The second assertion is due to linear scaling of the unigrid algorithm in n_p, that implies the following bound

$$n_0 + 2n_0 + \dots + 2^p n_0 \le 2^{p+1} n_0 = 2n_M,$$

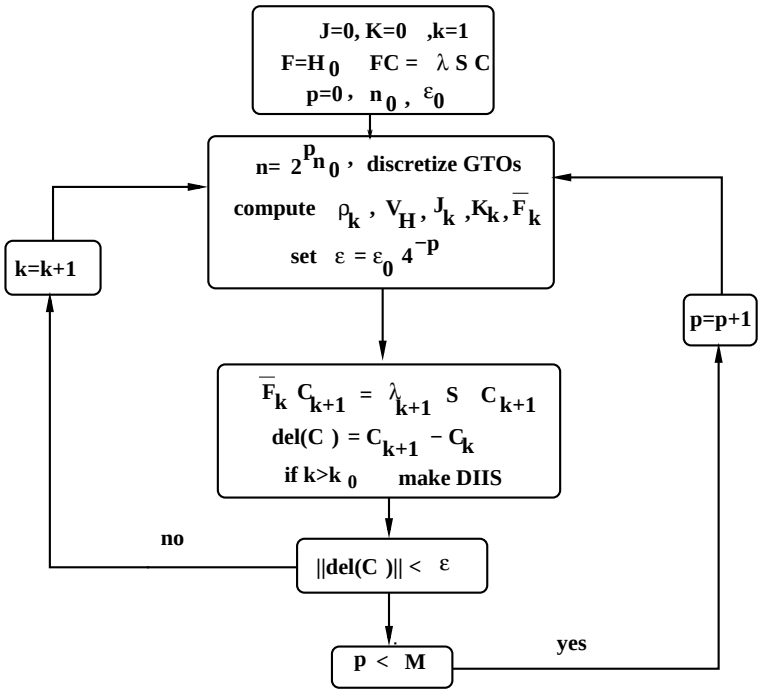

Figure 5.2: The flow-chart of the tensor-structured SCF algorithm.

hence, completing the proof. ■

Remark 5.2 *In the case of large molecules and $R_G = rank(G_\mu) \geq 1$, further optimisation of the algorithm up to $O(R_N R_0^2 n_p)$-complexity may be possible on the base of rank reduction applied to the rank-$R_G R_0$ orbitals and by using an iterative eigenvalue solver instead of currently employed direct solver via matrix diagonalization, or by using direct minimization schemes [95].*

5.3 Numerical illustrations

5.3.1 General discussion

Our algorithm for *ab initio* solution of the Hartree-Fock equation in *tensor-structured format* is examined numerically on some moderate size molecules. In particular, we consider the all electron case of H_2O, and the case of pseudopotential of CH_4 and CH_3OH molecules. In the present numerical examples, we use the discretised GTO basis functions for reasons of convenient comparison of the results with the output from the standard MOLPRO package based on the analytical evaluation of the integral operators in the GTO basis.

The size of the computational box $[-b,b]^3$ introduced in Section 5.1.3 varies from $2b = 11.2$ $\mathring{A}$ for H_2O up to $2b = 16$ $\mathring{A}$ for small organic molecules. The smallest step-size of the grid $h = 0.0013$ $\mathring{A}$ is reached in the SCF iterations for the H_2O molecule, using the finest level grid with $n = 8192$, while the average step size for the computations using the pseudopotentials for small organic molecules is about $h = 0.015$ $\mathring{A}$, corresponding to the grid size $n = 1024$.

5.3.2 Multilevel tensor-truncated SCF iteration applied to some moderate size molecules

We solve numerically the *ab initio* Hartree-Fock equation, by using Algorithms **TT_DIIS** and **MTT_DIIS** presented in Section 5.2.3. Starting with the zero initial guess for matrices $J(C) = 0$ and $K(C) = 0$ in the Galerkin Fock matrix (5.7), the eigenvalue problem at the first iterative step ($p = 0$) is solved by using only the H part of the Fock matrix in (5.7), that does not depend on the solution, and hence, can be precomputed beforehand.

Thus, the SCF iteration starts with the expansion coefficients $c_{\mu i}$ for orbitals in the GTO basis, computed using only the core Hamiltonian $\mathcal{H}$. At every iteration step, the Hartree and exchange potentials and the corresponding Galerkin matrices, are computed using the updated coefficients $c_{\mu i}$. The renewed Coulomb and exchange matrices generate the updated Fock matrix to be used for the solution of the eigenvalue problem. The minimization of the Frobenius norm of the virtual block of the Fock operator evaluated on eigenvectors of the consequent iterations, $\overline{C}_k, \overline{C}_{k-1}, ...$, is utilized for the DIIS scheme.

The multilevel solution of the nonlinear eigenvalue problem (5.8) is realised via the SCF iteration on a sequence of uniformly refined grids, beginning from the initial coarse grid, say, with $n_0 = 64$, and proceeding on the dyadically refined grids, $n_p = n_0 2^p$, $p = 1, ..., M$. We use the grid dependent termination criterion $\varepsilon_{n_p} := \varepsilon_0 2^{-2p}$, keeping a continuous numbering of the iterations.

Figure 5.6 (left) shows the convergence of the iterative scheme in the case of pseudopotential of CH_4. Convergence in the total Hartree-Fock energy reaching the absolute error $9 \cdot 10^{-6}$ on the grid size $n = 1024$ is shown in Figure 5.6 (right). The total energy is calculated by

$$E_{HF} = 2 \sum_{a=1}^{N_{orb}} \lambda_a - \sum_{a=1}^{N_{orb}} \left(\widetilde{J}_a - \widetilde{K}_a \right)$$

with $\widetilde{J}_a = \langle \psi_a, V_H \psi_a \rangle_{L^2}$, and $\widetilde{K}_a = \langle \psi_a, \mathcal{V}_{ex} \psi_a \rangle_{L^2}$, being the so-called Coulomb and exchange integrals, respectively, computed in the orbital basis ψ_a ($a = 1, ..., N_{orb}$).

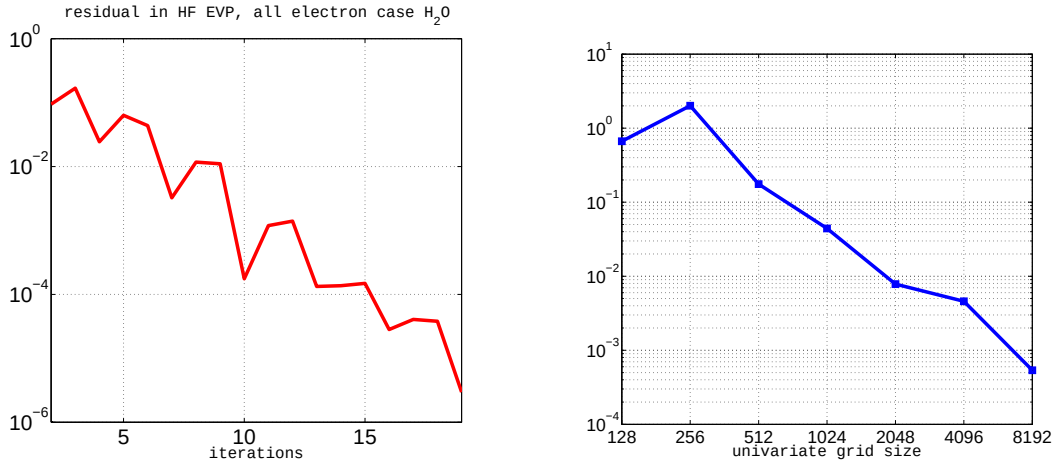

Figure 5.3: Multilevel convergence of the DIIS iteration applied to the all electron case of H_2O (left), and convergence in the energy in n (right).

Figure 5.4 (left) shows the linear scaling in n, corresponding to the CPU time of one iteration. Figure 5.4 (right) shows the number of "effective" iterations counted by rescaling the total computational time to the iteration time-unit observed at each iterative step at the finest grid-level: one iteration at level p is counted with the factor 2^{p-M}. Figure 5.3 (left) shows convergence of the SCF iteration for the

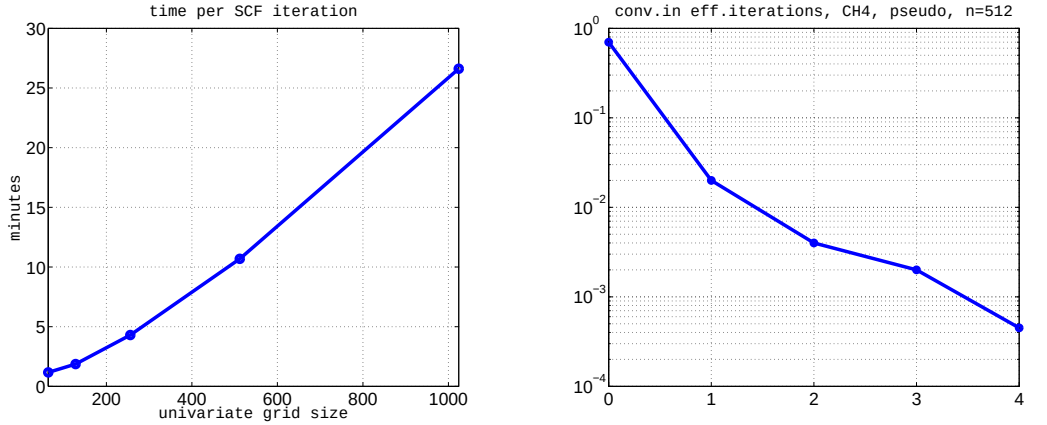

Figure 5.4: Linear scaling in n (left) and convergence in the effective iterations (right).

all electron case of H_2O. This challenging problem is solved efficiently due to the usage of large 3D Cartesian grids up to the volume size $\mathcal{N}_{vol} = 8192^3$. Figure 5.3 (right) shows convergence of the HF energy for the corresponding grid levels.

Figure 5.7 presents the convergence history of the nonlinear SCF iteration for CH_3OH (top) and C_2H_5OH (bottom) molecules. Red and blue lines show the convergence in the residual error, and in the largest eigenvalue, respectively.

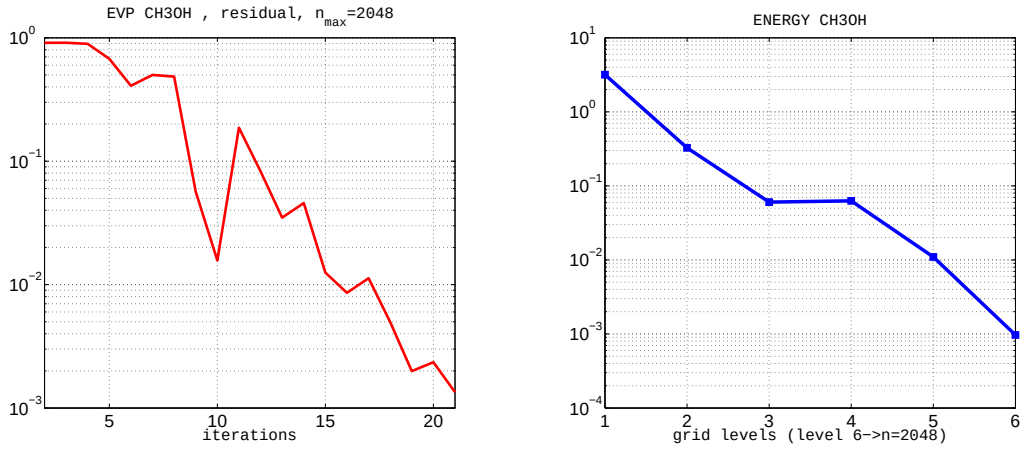

Figure 5.5: Iteration history for CH_3OH molecule: Residual (left) and the energy (right).

5.3.3 Conclusions to Section 5

We present the grid-based tensor-truncated numerical method for the robust and accurate iterative solution of the nonlinear Hartree-Fock equation at the cost $O(\mathcal{N}_{vol}^{1/3})$ in the volume size $\mathcal{N}_{vol} = n^3$. The computational scheme is based on the discrete tensor representation of the Fock operator over the 3D Cartesian grid at each step of the multilevel SCF iteration applied to the nonlinear 3D eigenvalue problem. The storage request is roughly estimated by $O(\mathcal{N}_{vol}^{1/3})$.

This scheme is neither restricted to the analytically separable basis functions like GTO orbitals nor to the traditional plane waves approximations. The Galerkin basis can be modified by adapting to the particular problem in the framework of the tensor-structured solution process.

Further improvement of the algorithm toward the $O(\log n)$-complexity on the base of quantics-TT approximation [87, 83, 88, 64, 84, 71], may open new perspectives for efficient *ab initio* numerical simulation of complex molecules and for the FEM-DFT computations of large molecular clusters.

The main computational blocks of the numerical scheme allow the natural parallelization on the level of matrix elements computation, rank decompositions, and the multilinear tensor operations.

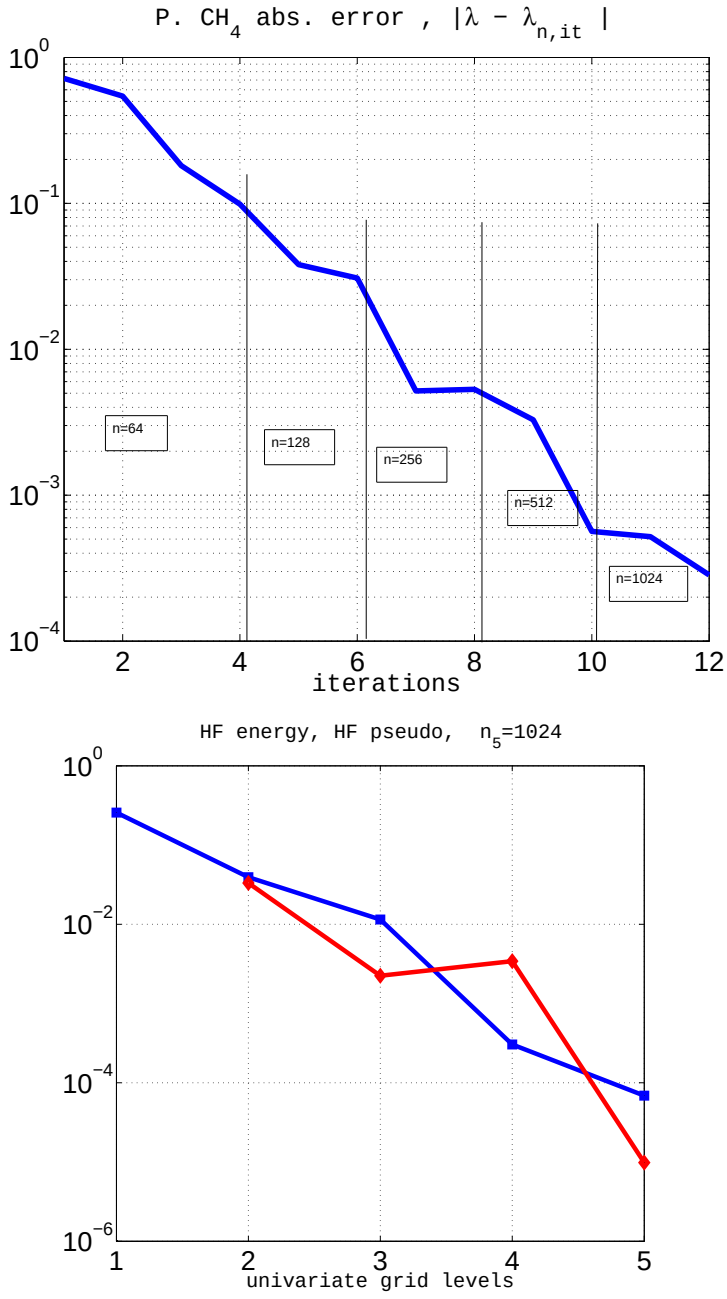

Figure 5.6: Multilevel convergence for the pseudopotential of CH_4 molecule (top), and convergence of the HF energy in the grid levels (bottom). Level 1 corresponds to $n = 64$, while on the finest level 5 we have $n = 1024$.

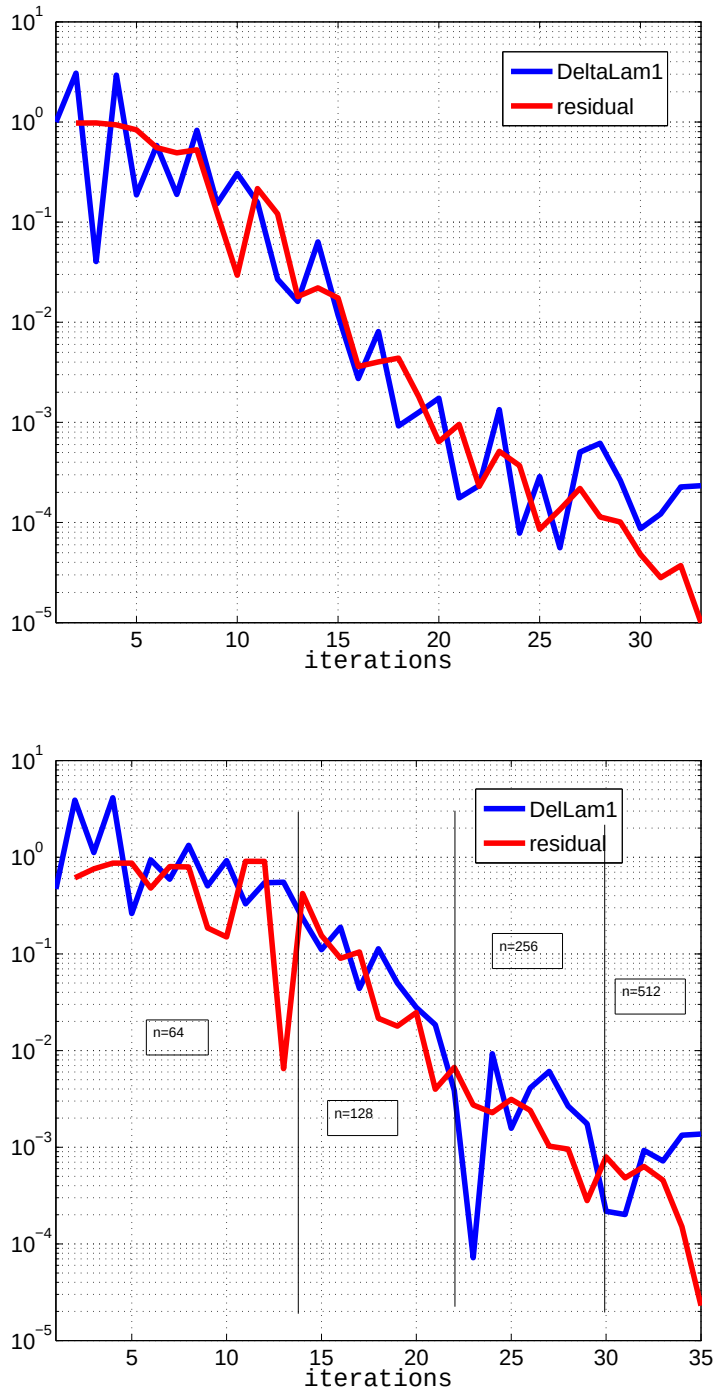

Figure 5.7: SCF iterations for the pseudopotentials of CH_3OH, with the maximum grid level $n = 2048$ (top) and C_2H_5OH with the maximum grid level $n = 512$ (bottom).

6 Summary of main results

6.1 Brief summary

In the present dissertation we developed and analysed tensor numerical methods and algorithms for efficient grid-based evaluation of multivariate functions and integral operators. These methods are successfully applied to the solution of the nonlinear Hartree-Fock equation in quantum chemistry. Here we present the summary of main results.

1. The developed tensor methods and algorithms.

- Mixed (two-level) best Tucker approximation (BTA) algorithm applied to the rank-R canonical input, combined with the rank reduction algorithm applied to the small-size rank-R Tucker core.
- Reduced HOSVD algorithm (RHOSVD) of complexity $O(dR^2n)$, for fast computation of the initial orthogonal vectors in the ALS iteration implementing the mixed BTA.
- The multigrid accelerated (MGA) mixed best Tucker approximation method based on the enhanced ALS iteration[1] applied to large rank-R canonical $n \times n \times n$-tensors represented on a sequence of refined grids ($O(Rrn)$ complexity, where r is the maximal Tucker rank). In the case of a full format target tensor the complexity of MGA BTA algorithm is linear in the volume size, $O(n^3)$, instead of $O(n^4)$ for HOSVD;
- Accurate and fast rank-structured tensor computation of the Hartree potential, with $O(Rn \log n)$ complexity, where R is the rank of the electron density. Main ingredients are the MGA BTA of the agglomerated electron density, and the tensor-product convolution with the low-rank approximand to the Newton potential. The computational complexity of the respective

[1] The MGA-ALS iteration has a three-fold gain: avoids the problem to compute HOSVD on large-size tensors, provides good initial guess for ALS corrections, resulting in the only few ALS iterations at each approximation level, and allows to optimize the ℓ-mode orthogonal subspaces only on the reduced set of "most important fibers".

Coulomb matrix is proportional to $R_0^2 n$, where R_0 is the number of Galerkin basis functions.

- Accurate tensor-structured computation of the Hartree-Fock exchange using agglomerated orbitals and applying enhanced MLA via the windowing and rank reduction techniques, providing the asymptotical complexity $O(R_0^3 n \log n)$;

- The multilevel tensor-truncated DIIS-based iterative method for the numerical solution of the nonlinear Hartree-Fock equation disretised on $n \times n \times n$-grid, that provides almost linear scaling in n, $O(n \log n)$ (a "grey-box" algorithm). The multilevel scheme has a four-fold effect: fast convergence with zero starting values for the Coulomb/exchange matrices, good initial guess at each grid level, improved approximation by the Richardson extrapolation, considerable reduction of the number of recomputed entries in the exchange matrix by using filtering strategy on fine grid levels. Notice that the existing benchmark grid-oriented solvers for the Hartree-Fock equation, based on the full-grid representation, scale at least linear in the volume size, $O(n^3)$;

- A 3D nonlinear EVP solver is implemented in MATLAB and verified (compared with MOLPRO output) in *ab initio* solution of the Hartree-Fock equation for particular molecules, H_2O (all electron case), and CH_4, CH_3OH, C_2H_5OH (pseudopotential case).

2. Analysis of algorithms.
Error and complexity analysis of presented methods include the following results.

- Theorem 2.14 on the error bound of RHOSVD in Algorithm C2T applied to a canonical tensor;

- Theorem 3.1 on the complexity of the MGA Algorithm C2T for a canonical input tensor;

- Lemma 3.2 on the complexity of the MGA Algorithm F2T for full format tensors.

- Lemma 4.2 on the complexity of the tensor-structured computational scheme for the Hartree-Fock exchange matrix.

- Lemma 5.1 on the complexity of the multilevel tensor-truncated iterative solver for the Hartree-Fock equation.

3. Numerical results.
All algorithms are implemented in MATLAB and verified by extensive numerical experiments in electronic structure calculations that confirm the theoretical performance of the algorithms, e.g., the almost linear scaling in all important rank and grid-discretization parameters. These algorithms enable using large 3D Cartesian grids with the benchmark sizes up to $\mathcal{N}_{vol} = 16384^3$, which ensures high approximation accuracy (resolution) for an arbitrary orientation of a molecule in the computational box.

4. Interesting observations based on numerical experiments.
In the numerical experiments, we found out that for the Tucker-type approximation of function related tensors (corresponding to the classical potentials, electron densities, and Hartree potentials):
(a) the error of the Tucker approximation decays exponentially with respect to the Tucker rank (known theoretical result for the Newton, Yukawa and Helmholtz potentials);
(b) the orthogonal vectors of the decomposition are of special shape, that is almost independent of the discretization step and resolves the peculiarities of the considered function;
(c) the core coefficients tensor of the orthogonal Tucker transform is of sparse character (up to certain threshold);
(d) the Tucker rank of the almost periodic 3D structures weakly depends on the number of cells;
(e) the ALS Tucker iteration usually demonstrates fast and robust local convergence (likely due to exponential decay of the Tucker approximation error, see item (a)).

This research project addresses many new and challenging mathematical and algorithmic problems to be considered in the future. These problems are related to the developing efficient solution methods that are free of the "curse of dimensionality", to be applied to high-dimensional equations arising in modern scientific computing.

6.2 Presentations

The author presented the following talks (and posters) on the topics of dissertation.

1. *Numerical Solution of the Hartree-Fock Equation in the Multilevel Tensor-Structured Format.*
   The 16-th Conference of the International Linear Algebra Society (ILAS). Pisa, Italy, June 21-25, 2010.

2. *Numerical Solution of the Hartree-Fock Equation by the Tensor-Structured Methods.* (Poster).
   First Principles in Quantum Chemistry: From Elementary Reactions to Enzyms. Bad Herrenalb, Germany, April 14-17, 2010.

3. *Tensor-Structured Methods in Electronic Structure Calculations.*
   GAMM 2010. 81-st Annual Meeting of the International Association of Applied Mathematics and Mechanics. Contributed Session S16. Karlsruhe Germany, March 22-26, 2010.

4. *Numerical Solution of the Hartree-Fock Equation by the Multilevel Tensor-Structured Methods.*
   26-th GAMM-Seminar Leipzig on Tensor Approximations and High-Dimensional Problems. Max-Planck-Institute for Mathematics in the Sciences, Leipzig, 22-24.02.2010.

5. *Numerical Solution of the Hartree-Fock Equation by the Tensor-Structured Techniques.*
   Invited talk at the Seminar of the Numerical Analysis Group. Mathematics Institute, University of Tübingen, 22.10.2009.

6. *Tensor Product Approximation of the Hartree and Exchange Operators in the Hartree-Fock Equation.*
   The eighth European Conference on Numerical Mathematics and Advanced Applications, ENUMATH 2009, Uppsala, Sweden, 29.06-3.07.2009.

7. *Towards Solution of the Hartree-Fock Equation by the Tensor-structured Methods.*
   Berlin-Leipzig Seminar, TU Berlin, May 18, 2009.

8. *Accurate Solution of the Hartree-Fock Equation by the Tensor-structured Methods.*

Evaluation Poster, Max-Planck-Institute for Mathematics in the Sciences, Leipzig, April 28-30, 2009.

9. *Efficient Tensor-product Approximation of the Hartree and Exchange Potentials in the Hartree-Fock Equation.*
   Saxonian Theoretical Seminar, Theoretical Methods for Complex molecular systems, Wilhelm-Ostwald Institute of Physical and Theoretical Chemistry, University of Leipzig, February 26-27, 2009.

10. *Multigrid Accelerated Tensor Approximation in Electronic Structure Calculations.*
    Workshop: Numerical Methods in Density Functional Theory, DFG Research Center MATHEON, TU Berlin, 23-25 July 2008.

11. *Multigrid Accelerated Tensor Approximation in 3D Electronic Structure Calculations.*
    Max-Planck-Institute for Mathematics in the Sciences, Leipzig, July 15, 2008.

12. (with H.-J. Flad, B. Khoromskij and S.R. Chinnamsetty) *Tensor Decomposition in Electronic Structure Calculations on 3D Cartesian Grids.*(Poster).
    CompPhys07, 8th NTZ-Workshop on Computational Physics, University of Leipzig, 29 November-01 December 2007.

7 Appendix

7.1 Singular value decomposition and the best rank-k approximation of a matrix

Here we recall the standard theorem of the numerical analysis on the singular value decomposition (SVD) [100].

Theorem 7.1 *Let $A \in \mathbb{R}^{m\times n}$, with $m \geq n$, for definiteness. Then there exist $U \in \mathbb{R}^{m\times n}$, $\Sigma \in \mathbb{R}^{n\times n}$ and $V \in \mathbb{R}^{n\times n}$ such that*

$$A = U\Sigma V^T, \tag{7.1}$$

where Σ is a diagonal matrix whose diagonal entries, σ_i, $i = 1, 2, \ldots, n$, are the ordered singular values of A, $\sigma_1 \geq \sigma_2 \geq \ldots \geq \sigma_n \geq 0$ and $U^TU = I_m$ and $V^TV = I_n$, with I_n denoting the $n \times n$ identity matrix.

The algebraic complexity of the SVD transform scales as $O(mn^2)$.

The best approximation of an arbitrary matrix $A \in \mathbb{R}^{m\times n}$ by a rank-k matrix A_k (say, in Frobenius norm, that is $\|A\|_F^2 = \sum\limits_{(i,j)\in m\times n} a_{ij}^2$) can be calculated by the truncated SVD as follows. Let us consider the SVD of a matrix $A = U\Sigma V^T$, and set $\Sigma_k = \mathrm{diag}\{\sigma_1, \ldots \sigma_k, 0, \ldots, 0\}$, then the best rank-$k$ approximation is given by

$$A_k := U\Sigma_k V^T = \sum_{i=1}^{k} \sigma_i u_i v_i^T,$$

where u_i, v_i are the respective left and right singular vectors of A. The approximation error in the Frobenius norm is bounded by

$$\|A_k - A\|_F \leq \sqrt{\sum_{i=k+1}^{n} \sigma_i^2}. \tag{7.2}$$

7.2 Reduced SVD of a rank-R matrix

Let us consider a rank-R matrix $M = AB^T \in \mathbb{R}^{n\times n}$, with the factor matrices $A \in \mathbb{R}^{n\times R}$ and $B \in \mathbb{R}^{n\times R}$, where $R \leq n$. We are interested in the best rank

r approximation of M, with $r < R$. It can be implemented using the following algorithm, that avoids the singular value decomposition of the target matrix M with possibly large n.

This algorithm includes the following steps.

1. Perform the QR-decomposition of the side matrices,

$$A = Q_A R_A, \quad B = Q_B R_B,$$

with the unitary matrices $Q_A, Q_B \in \mathbb{R}^{n\times R}$, and the upper triangular matrices $R_A, R_B \in \mathbb{R}^{R\times R}$.

2. Compute the SVD of the core matrix, $R_A R_B^T \in \mathbb{R}^{R\times R}$

$$R_A R_B^T = U\Sigma V^T,$$

with the diagonal matrix $\Sigma = diag\{\sigma_1, \ldots, \sigma_R\}$, and unitary matrices $U, V \in \mathbb{R}^{R\times R}$.

3. Compute the best rank-r approximation of the core matrix, $U_r\Sigma_r V_r^T$, by extracting the submatrix $\Sigma_r = diag\{\sigma_1, \ldots, \sigma_r\}$ in Σ, and the first r columns U_r, $V_r \in \mathbb{R}^{R\times r}$ in the unitary matrices U and V, respectively.

4. Finally, set the rank-r approximation $M_r = Q_A U_r \Sigma_r V_r^T Q_B^T$, where $Q_A U_r$ and $Q_B V_r$ are $n \times r$ unitary matrices.

The approximation error is bounded by $\sqrt{\sum_{i=r+1}^{R} \sigma_i^2}$. The complexity of above algorithm scales linearly in n, $O(nR^2) + O(R^3)$. In the case $R \ll n$, this reduces dramatically the cost $O(n^3)$ of the truncated SVD applied to the full-format $n \times n$ matrix M.

7.3 List of abbreviations

ALS	alternating least squares (algorithm)
BTA	best Tucker approximation
C2T (C→T)	canonical to Tucker transform
C_BTA	BTA algorithm for the canonical target tensor
DIIS	direct inversion of iterative subspaces
F2T (F→T)	full format to Tucker transform
G_BTA	BTA algorithm for the full format tensor
HOSVD	higher order singular value decomposition
MLA	multilinear algebra
MGA	multigrid accelerated BTA
MG_C_BTA	multigrid accelerated BTA algorithm for the canonical target tensor
MG_G_BTA	multigrid accelerated BTA algorithm for the full format tensor
MIFs	most important fibers in MG_C_BTA
RHOSVD	reduced higher order singular value decomposition for the canonical target tensor
SCF	self consistent field (iteration)
SVD	singular value decomposition
T2C (T→C)	Tucker to canonical transform

Bibliography

[1] P.-A. Absil, R. Mahoni and R. Sepulchre. *Optimization Algorithms on Matrix manifolds.* Princeton University Press, 2008.

[2] E. Acar, T. G. Kolda and D. M. Dunlavy. *An Optimization Approach for Fitting Canonical Tensor Decompositions.* Technical Report Number SAND2009-0857, Sandia National Laboratories, Albuquerque, NM and Livermore, CA, February 2009.

[3] J. Almlöf, *Direct methods in electronic structure theory.* In D. R. Yarkony, Ed., *Modern Electronic Structure Theory, Vol. II*, (World Scientific, Singapore, 1995) pp. 110–151.

[4] L. Genovese, A. Neelov, S. Goedecker, T. Deutsch, S. A. Ghasemi, A. Willand, D. Caliste, O. Zilberberg, M. Rayson, A. Bergman, R. Schneider. *Daubechies wavelets as a basis set for density functional pseudopotential calculations.* J. Chem. Phys. **129** (2008) 014109.

[5] X. Gonze, J.-M. Beuken, R. Caracas, F. Detraux, M. Fuchs, G.-M. Rignanese, L. Sindic, M. Verstraete, G. Zerah, F. Jollet, M. Torrent, A. Roy, M. Mikami, Ph. Ghosez, J.-Y. Raty, D. C. Allan. *First-principles computation of material properties: the ABINIT software project.* Comput. Mater. Sci. **25** (2002) 478.

[6] B.W. Bader and T.G. Kolda. *MATLAB Tensor Classes for Fast Algorithm Prototyping.* SANDIA Report, SAND2004-5187, Sandia National Laboratories, 2004.

[7] J. Ballani and L. Grasedyck. *A Projection Method to Solve Linear Systems in Tensor Format.* Preprint MIS MPI 22/2010, Leipzig.

[8] M. Bebendorf. *Hierarchical matrices. A means to efficiently solve elliptic boundary value problems.* Lecture Notes in Computational Science and Engineering, 63. Springer-Verlag, Berlin, 2008.

[9] M. Bebendorf. *Adaptive Cross Approximation of Multivariate functions.* Constructive Approximation. 2010, to appear.

[10] C. Bertoglio, B. N. Khoromskij. *Low rank tensor-product approximation of projected Green kernels via sinc-quadratures.* Preprint 79/2008, MPI MIS Leipzig, 2008.

[11] G. Beylkin and M.J. Mohlenkamp. *Numerical operator calculus in higher dimensions.* Proc. Natl. Acad. Sci. USA **99** (2002) 10246–10251.

[12] G. Beylkin and M.J. Mohlenkamp. *Algorithms for numerical analysis in high dimension.* SIAM J. Scientific Computing, **26** (6) (2005) 2133-2159.

[13] G. Beylkin, M.J. Mohlenkamp and F. Pérez. *Approximating a wavefunction as an unconstrained sum of Slater determinants.* Journal of Math. Physics, **49** 032107 (2008).

[14] T. Blesgen, V. Gavini and V. Khoromskaia. *Tensor Product Approximation of the Electron Density of Large Aluminium Clusters in OFDFT.* Preprint 66/2009 MPI MIS Leipzig, 2009.

[15] D. Braess, W. Hackbusch. *Approximation of* $1/x$ *by exponential sums in* $[1, \infty)$. IMA J. Numer. Anal. 25 (2005).

[16] E. Cancés and Le Bris. *On the convergence of SCF algorithms for the Hartree-Fock equations.* ESAIM: M2AN, vol. 34/4, 2000, 749-774.

[17] J.D. Carrol and J. Chang. *Analysis of individual differences in multidimensional scaling via an* N*-way generalization of 'Eckart-Young' decomposition.* Psychometrika 35 (1970), 283-319.

[18] J.D. Carrol, S. Pruzansky, and J.B. Kruskal. *CANDELINC: A general approach to multidimensional anlysis of many-way arrays with linear constraints on parameters.* Psychometrika, 45 (1980), pp. 3-24.

[19] S.R. Chinnamsetty, M. Espig, W. Hackbusch, B.N. Khoromskij, H-J Flad, *Kronecker tensor product approximation in quantum chemistry.* Journal of Chemical Physics 127, 084110 (2007).

[20] P.G. Ciarlet and C. Le Bris, eds. *Handbook of Numerical Analysis. Vol. X, Computational Chemistry.* Elsevier, Amsterdam, 2003.

[21] L. De Lathauwer. *Signal processing based on multilinear algebra.* PhD Thesis. Katholeke Universiteit Leuven, 1997.

[22] L. De Lathauwer. *Decomposition of a higher-order tensor in block terms. Part II: Definitions and uniqueness.* Tech. Report no. 07-81, ESAT/SCD/SISTA, K.U. Leuven, Belgium, 2007.

[23] L. De Lathauwer, B. De Moor, J. Vandewalle. *On the best rank-*1 *and rank-*$(R_1, ..., R_N)$ *approximation of higher-order tensors.* SIAM J. Matrix Anal. Appl., 21 (2000) 1324-1342.

[24] L. De Lathauwer, B. De Moor, J. Vandewalle. *A multilinear singular value decomposition.* SIAM J. Matrix Anal. Appl., 21 (2000) 1253-1278.

[25] T.H. Dunning Jr. *Gaussian basis sets for use in correlated molecular calculations. I. The atoms boron through neon and hydrogen.* J. Chem. Physics, **90** (1989), 1007-1023.

[26] L. Elden and B. Savas. *A Newton-Grassmann method for computing the best multilinear rank-*(r_1, r_2, r_3) *approximation of a tensor.* SIAM J. Matrix Anal. and Appl., Volume 31, Issue 2, pp.248-271 (2009).

[27] H.-J. Flad, W. Hackbusch, B.N. Khoromskij, and R. Schneider. *Concepts of Data-Sparse Tensor-Product Approximation in Many-Particle Modeling.* In: Matrix Methods: Theory, Algorithms, Applications, (dedicated to the memory of Gene Golub) V. Olshevsky, E. Tyrtyshnikov eds., World Scientific, 2010, pp.313-347.

[28] H.-J. Flad, W. Hackbusch, and R. Schneider. *Best* N*-term approximation in electronic structure calculations: I. One-electron reduced density matrix.* ESAIM: M2AN 40, 49-61 (2006).

[29] H.-J. Flad, B.N. Khoromskij, D.V. Savostyanov, and E.E. Tyrtyshnikov. *Verification of the cross 3d algorithm on quantum chemistry data.* J. Numer. Anal. and Math. Modelling, 4 (2008), 1-16.

[30] H.-J. Flad, R. Schneider, B.-W. Schulze. *Asymptotic regularity of solutions to Hartree-Fock equations with Coulomb potential.* Math. Methods Appl. Sci., 31 (2008), no. 18, 2172-2201.

[31] S. Friedland, V. Mehrmann, A. Miedlar, and M. Nkengla. *Fast low rank approximation of matrices and tensors.* 2008, www.matheon.de/preprints/4903.

[32] V. Gavini, J. Knap, K. Bhattacharya, and M. Ortiz. *Non-periodic Finite-element formulation of orbital-free density-functional theory.* J. Mech. Phys. Solids **55(4)** (2007), 669-696.

[33] V. Gavini, K. Bhattacharya, and M. Ortiz. *Quasi-continuum orbital-free density-functional theory: A route to multi-million atom non-periodic DFT calculation.* J. Mech. Phys. Solids **55(4)** (2007), 697-718.

[34] I.P. Gavrilyuk, W. Hackbusch and B.N. Khoromskij. *Hierarchical Tensor-Product Approximation to the Inverse and Related Operators in High-Dimensional Elliptic Problems.* Computing 74 (2005), 131-157.

[35] I.P. Gavrilyuk, W. Hackbusch, and B.N. Khoromskij. *Tensor-product approximation to elliptic and parabolic solution operators in higher dimensions.* Computing **74** (2005), 131-157.

[36] I. P. Gavrilyuk, W. Hackbusch and B. N. Khoromskij. *Data-sparse approximation of a class of operator-valued functions.* Math. Comp. 74 (2005), pp. 681-708.

[37] G.H. Golub, C.F. Van Loan. *Matrix Computations.* Johns Hopkins University Press, Baltimore, MD, 1996.

[38] L. Grasedyck. *Hierarchical Singular Value Decomposition of Tensors.* SIAM J. Matrix Anal. Appl. 31:2029-2054, 2010.

[39] L. Grasedyck. *Polynomial Approximation in Hierarchical Tucker Format by Vector-Tensorization.* Preprint 43 DFG 1324, submitted to BIT.

[40] M. Griebel and J. Hamaekers. *Sparse grids for the Schroedinger equation.* M2AN, 41 (2007), pp. 215-247.

[41] W. Hackbusch. *Hierarchische Matrizen: Algorithmen und Analysis.* Springer Verlag, Berlin 2009.

[42] W. Hackbusch. *Fast and Exact Projected Convolution for Non-equidistant Grids.* Computing **80** (2007), 137-168.

[43] W. Hackbusch. *Efficient convolution with the Newton potential in d dimensions.* Numerische Mathematik, 110 (2008) 4, p. 449-489.

[44] W. Hackbusch and B.N. Khoromskij. *Low-rank Kronecker product approximation to multi-dimensional nonlocal operators. Part I. Separable approximation of multi-variate functions.* Computing **76** (2006), 177-202.

[45] W. Hackbusch and B. N. Khoromskij. *Low-rank Kronecker-product Approximation to Multi-dimensional Nonlocal Operators. Part II. HKT Representation of Certain Operators.* Computing 76 (2006), pp. 203-225.

[46] W. Hackbusch and B. N. Khoromskij. *Tensor-product Approximation to Operators and Functions in High dimension.* Journal of Complexity **23** (2007), 697-714.

[47] W. Hackbusch, B.N. Khoromskij and E.E. Tyrtyshnikov. *Hierarchical Kronecker tensor-product approximations.* J. Numer. Math. **13** (2005), 119–156.

[48] W. Hackbusch, B.N. Khoromskij and E. Tyrtyshnikov. *Approximate iteration for structured matrices.* Numer. Math., **109** (2008), 365-383.

[49] W. Hackbusch, B.N. Khoromskij, S. Sauter and E. Tyrtyshnikov. *Use of Tensor Formats in Elliptic Eigenvalue Problems.* Preprint 78, MPI MIS, Leipzig 2008, submitted.

[50] W. Hackbusch and S. Kühn. *A new scheme for the tensor representation.* J. Fourier Anal. Appl. 15 (2009), no. 5, 706-722.

[51] R.J. Harrison, G.I. Fann, T. Yanai, Z. Gan, and G. Beylkin. *Multiresolution quantum chemistry: Basic theory and initial applications.* J. of Chemical Physics, 121 (23): 11587-11598, 2004.

[52] E. Hayryan and V. Khoromskaia. *Low-rank Approximation of the Electrostatic Potential of Proteins,* 2010, (in progress).

[53] T. Helgaker, P. Jørgensen and J. Olsen. *Molecular Electronic-Structure Theory.* Wiley, New York, 1999.

[54] F.L. Hitchcock. *The expression of a tensor or a polyadic as a sum of products.* J. Math. Physics, 6 (1927), 164-189.

[55] F.L. Hitchcock. *Multiple invariants and generalized rank of a p-way matrix or tensor.* J. Math. Physics, 7 (1927), 39-79.

[56] M. Ishteva, L. De Lathauwer, P.-A. Absil and S. Van Huffel. *Differential-geometric Newton method for the best rank-*(R_1, R_2, R_3) *approximation of tensors.* Numer. Algorithms 51 (2009), no. 2, 179-194.

[57] V. Khoromskaia. *Computation of the Hartree-Fock Exchange in the Tensor-structured Format.* Computational Methods in Applied Mathematics, Vol. 10(2010), No 2, pp.204-218.

[58] V. Khoromskaia. *Multilevel Tucker Approximation of 3D Tensors.* 2010, in progress.

[59] B. N. Khoromskij. *Structured Data-sparse Approximation to High Order Tensors arising from the Deterministic Boltzmann equation.* Math. Comp. 76 (2007), pp. 1292-1315.

[60] B. N. Khoromskij. *Structured Rank-$(r_1, ..., r_d)$ Decomposition of Function-related Tensors in $\mathbb{R}^d$.* Comp. Meth. in Applied Math., **6** (2006), 2, 194-220.

[61] B. N. Khoromskij. *Fast and Accurate Tensor Approximation of Multivariate Convolution with Linear Scaling in Dimension.* J. Comp. Appl. Math., 2010, DOI:10.1016/j.cam.2010.02.004, to appear.

[62] B. N. Khoromskij. *On Tensor Approximation of Green Iterations for Kohn-Sham equations.* Computing and Visualisation in Science, (2008) 11:259-271.

[63] B.N. Khoromskij. *Tensor-Structured Preconditioners and Approximate Inverse of Elliptic Operators in $\mathbb{R}^d$.* J. Constructive Approximation, 30:599-620 (2009).

[64] B.N. Khoromskij. *$O(d \log n)$-Quantics Approximation of n-d Tensors in High-Dimensional Numerical Modeling.* Preprint MPI MIS 55/2009, Leipzig 2009; J. Constructive Approximation, accepted.

[65] B.N. Khoromskij. *An Introduction to Structured Tensor-Product Representation of Discrete Nonlocal Operators.* Lecture Notes 27, MPI MIS, Leipzig 2005.

[66] B.N. Khoromskij. *Tensors-structured Numerical Methods in Scientific Computing: Survey on Recent Advances.* Preprint MPI MIS 21/2010, Leipzig 2010 (submitted).

[67] B. N. Khoromskij and V. Khoromskaia. *Low Rank Tucker Tensor Approximation to the Classical Potentials.* Central European J. of Math., **5**(3) 2007, 1-28.

[68] B.N. Khoromskij and V. Khoromskaia. *Multigrid Tensor Approximation of Function Related Arrays.* SIAM J. on Scient. Computing, **31**(4), 3002-3026 (2009).

[69] B. N. Khoromskij, V. Khoromskaia, S. R. Chinnamsetty, H.-J. Flad. *Tensor Decomposition in Electronic Structure Calculations on 3D Cartesian Grids.* J. of Comput. Physics, 228 (2009) 5749-5762.

[70] B.N. Khoromskij, V. Khoromskaia and H.-J. Flad. *Numerical solution of the Hartree-Fock equation in multilevel tensor-structured format.* SIAM J. on Scient. Computing, **33**(1), 45-65 (2011).

[71] B.N. Khoromskij, and I. Oseledets. *Quantics-TT approximation of elliptic solution operators in higher dimensions.* Preprint MPI MiS 79/2009, Leipzig 2009, submitted.

[72] B.N. Khoromskij, and Ch. Schwab. *Tensor Approximation of Multi-parametric Elliptic Problems in SPDEs.* Preprint MPI MiS 9/2010, Leipzig 2010, SISC, accepted.

[73] T. Kolda. *Orthogonal tensor decompositions.* SIAM J. Matrix Anal. Appl. 23 (2001) 243-255.

[74] T. G. Kolda and B. W. Bader. *Tensor Decompositions and Applications.* SIAM Rev, 51(2009), no. 3, pp.455-500.

[75] D. Kressner and C. Tobler. *Krylov subspace methods for linear systems with tensor product structure.* SIAM J. Matrix Anal. Appl., 31(4):1688-1714, 2010.

[76] P.M. Kroonenberg and J. De Leeuw. *Principal component analysis of three-mode data by means of alternating least squares algorithms.* Psychometrika, 45 (1980) 69-97.

[77] J.B. Kruskal. *Three-way arrays: rank and uniqueness of trilinear decompositions, with applications to arithmetic complexity and statistics.* Linear Algebra Appl., 18 (1977) 95-138.

[78] C. Le Bris. *Computational chemistry from the perspective of numerical analysis.* Acta Numerica (2005), 363 - 444.

[79] Ch. Lubich. *On Variational Approximations in Quantum Molecular Dynamics.* Math. Comp. **74** (2005), 765-779.

[80] Ch. Lubich. *From quantum to calssical molecular dynamics: reduced models and numerical analysis.* Zurich Lectures in Advanced Mathematics, EMS, 2008.

[81] F.R. Manby, P.J. Knowles and A.W. Lloyd. *The Poisson equation in density fitting for the Kohn-Sham Coulomb problem.* J. Chem. Phys. **115** (2001), 9144-9148.

[82] K.K. Naraparaju and J. Schneider. *Generalized Cross Approximation for 3d-tensors.* Preprint 29/2010 MPI MIS, Leipzig, 2010.

[83] I.V. Oseledets. *Compact matrix form of the d-dimensional tensor decomposition.* Preprint 09-01, INM RAS, Moscow 2009.

[84] I.V. Oseledets. *Approximation of $2^d \times 2^d$ matrices by using tensor decomposition.* SIAM J. Matrix Anal., 2009, accepted.

[85] I.V. Oseledets, D.V. Savostyanov, and E.E. Tyrtyshnikov. *Tucker dimensionality reduction of three-dimensional arrays in linear time.* SIMAX, 30(3), 939-956 (2008).

[86] I. Oseledets, D. Savostyanov, E. E. Tyrtyshnikov. *Linear algebra for tensor problems.*. Computing, 85 (2009), no. 3, 169-188.

[87] I. Oseledets and E. E. Tyrtyshnikov. *Breaking the curse of dimensionality or how to use SVD in many dimensions.* SIAM J. Scient. Computing, 31 (2009), no.5, 3744-3759.

[88] I. Oseledets and E. E. Tyrtyshnikov. *TT-cross approximation for multidimensional arrays.* Linear Algebra Appl. 432 (2010), no.1, 70-88.

[89] P. Pulay. *Improved SCF convergence acceleration.* J. Comput. Chem. **3**, 556-560 (1982).

[90] R. Polly, H.-J. Werner, F. R. Manby and P. J. Knowles. *Fast Hartree-Fock theory using density fitting approximations.* Mol. Physics, **102**:2311-2321, 2004.

[91] M. Reed, and B. Simon. *Functional analysis.* Academic Press, 1972.

[92] B. Savas, L.-H. Lim. *Quasi-Newton methods on Grassmanians and multilinear approximations of tensors.* SIAM J. Scient. Computing, submitted.

[93] R. Schneider. *Analysis of the projected coupled cluster method in electronic structure calculation.* Numer. Math. 113, (2009), no. 3, 433-471.

[94] R. Schneider. *Multiscalen-Matrixkompression und Wavelet-Matrixkompression.* Tuebner Verlag, 1998.

[95] R. Schneider, Th. Rohwedder, J. Blauert, A. Neelov. *Direct minimization for calculating invariant subspaces in density functional computations of the electronic structure.* Journal of Comp. Math. 27 (2009), no. 2-3, 360-387.

[96] J. Sielk, H. F. von Horsten, F. Krüger, R. Schneider, B. Hartke. *Quantum-mechanical wavepacket propagation in a sparse, adaptive basis of interpolating Gaussians with collocation.* Physical Chemistry Chemical Physics, 2009, 11 pp.463-475.

[97] A. Smilde, R. Bro, P. Geladi. *Multi-way Analysis.* Wiley, 2004.

[98] F. Stenger. *Numerical methods based on Sinc and analytic functions.* Springer-Verlag, Heidelberg, 1993.

[99] J. Strang and G.J. Fix. *An Analysis of the Finite Element Method.* Prentice-Hall, inc. N. J., 1973.

[100] E. Süli, D. Mayers. *An introduction to Numerical Analysis.* Cambridge University Press, 2008.

[101] E. E. Tyrtyshnikov. *A Brief Introduction to Numerical Analysis.* Birkhauser, Boston, 1997.

[102] E. E. Tyrtyshnikov. *Mosaic-skeleton approximations.* Calcolo **33**, 47-57 (1996).

[103] E. E. Tyrtyshnikov. *Incomplete cross approximation in the mosaic-skeleton method.* Computing **64**, 367-380 (2000).

[104] E.E. Tyrtyshnikov. *Tensor approximations of matrices generated by asymptotically smooth functions.* Sbornik: Mathematics **194**, No. 5-6 (2003), 941–954 (translated from *Mat. Sb.* **194**, No. 6 (2003), 146–160).

[105] E.E. Tyrtyshnikov. *Kronecker-product approximations for some function-related matrices.* Linear Algebra Appl. **379** (2004), 423–437.

[106] L.R. Tucker. *Some mathematical notes on three-mode factor analysis.* Psychometrika 31 (1966) 279-311.

[107] J. VandeVondele, M. Krack, F. Mohamed, M. Parinello, Th. Chassaing, J. Hutter. *QUICKSTEP: Fast and accurate density functional calculations using a mixed gaussian and plane waves approach.* Comp. Phys. Comm., 167(2005) 103-128.

[108] H.-J. Werner, P.J. Knowles et al. *MOLPRO, version 2002.10, a package of ab initio programs for electronic structure calculations.*

[109] T. Yanai, G. Fann, Z. Gan, R. Harrison and G. Beylkin. *Multiresolution quantum chemistry: Hartree-Fock exchange.* J. Chem. Phys. 121 (14) (2004) 6680-6688.

[110] H. Yserentant. *The hyperbolic cross space approximation of electronic wavefunctions.* Numer. Math., 105 (2007) 659-690.

[111] H. Yserentant. *Regularity and Approximability of Electronic Wave Functions.* Lecture Notes in Mathematics series, Springer-Verlag, 2010, to appear.

[112] T. Zhang and G. Golub. *Rank-0ne approximation to high order tensors.* SIAM J. Matrix Anal. Appl. v. 23 (2001) 534-550.

Daten zum Autor:

Name	Venera Khoromskaia
geboren	25. August 1952, in Stadt Kazan, Russland
1969-1974	staatliche Universität Kazan, Physik Fakultät. Abschluss: Dipl.- Phys.
1974 -1995	Joint Institute for Nuclear Research, Dubna, Russland wiss. Mitarbeiter
1995 -2005	Aufenthalt in Deutschland (ohne Arbeitserlaubnis)
2001, 2002, 2003	wiss. Stipendien an der Universität Leipzig, Institut für Informatik
2006 -	Max-Planck-Institut für Mathematik in den Naturwissenschaften wiss. Mitarbeiter

Bibliographische Daten
Numerical Solution of the Hartree-Fock Equation by the Multilevel Tensor-structured Methods.
(Numerische Lösung der Hartree-Fock-Gleichung mit der Multilevel Tensor-struktur-Verfahren.)
Venera Khoromskaia
Dissertation
157 Seiten, 58 Abbildungen, 112 Referenzen

Hiermit erkläre ich, die vorliegende Dissertation selbständig und ohne unzulässige fremde Hilfe angefertigt zu haben. Ich habe keine anderen als die angeführten Quellen und Hilfsmittel benutzt und sämtliche Textstellen, die wörtlich oder sinngemäß aus veröffentlichten oder unveröffentlichten Schriften entnommen wurden, und alle Angaben, die auf mündlichen Auskünften beruhen, als solche kenntlich gemacht. Ebenfalls sind alle von anderen Personen bereitgestellten Materialien oder erbrachten Dienstleistungen als solche gekennzeichnet.

Leipzig, 21 September, 2010

.....

(Venera Khoromskaia)